Effects of dissolved polymer on the transport of colloidal particles in a microcapillary.

Citation

INFORMATION TO USERS

This manuscript has been reproduced from the microfilm master. UMI films the text directly from the original or copy submitted. Thus, some thesis and dissertation copies are in typewriter face, while others may be from any type of computer printer.

The quality of this reproduction is dependent upon the quality of the copy submitted. Broken or indistinct print, colored or poor quality illustrations and photographs, print bleedthrough, substandard margins, and improper alignment can adversely affect reproduction.

In the unlikely event that the author did not send UMI a complete manuscript and there are missing pages, these will be noted. Also, if unauthorized copyright material had to be removed, a note will indicate the deletion.

Oversize materials (e.g., maps, drawings, charts) are reproduced by sectioning the original, beginning at the upper left-hand corner and continuing from left to right in equal sections with small overlaps.

Effects of Dissolved Polymer on the Transport of Colloidal

Particles in a Microcapillary

by

Sittipong Amnuaypanich

A Dissertation

Presented to the Graduate and Research Committee

of Lehigh University

in Candidacy for the Degree of

Doctor of Philosophy

In

Chemical Engineering

Lehigh University

April 2003

UMI Number: 3086930

Copyright 2003 by
Amnuaypanich, Sittipong

All rights reserved.

UMI®

Certificate of Approval

Approved and recommended for acceptance as a dissertation in partial fulfillment

of the requirements for the degree of Doctor of Philosophy.

April 22, 2003
Date

April 24, 2003
Accepted Date

Dr. Cesar A. Silebi, Dissertation Advisor
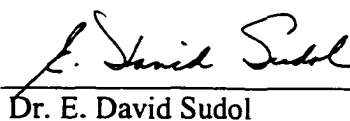
Committee Members:

Dr. Cesar A. Silebi, Chairman

Dr. Hugo S. Caram

Dr. Andrew Klein

Dr. Sudhakar Neti

Dr. E. David Sudol

ii

Acknowledgement

I would like to express my sincere gratitude to Dr. Cesar A. Silebi who served as my dissertation advisor. His guidance has been appreciated.

I am indeed grateful to: Dr. Hugo S. Caram, Dr. Andrew Klein, Dr. Sudhakar Neti and Dr. E. David Sudol for serving as my thesis committee and providing me with the valuable suggestions of this work.
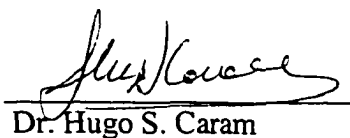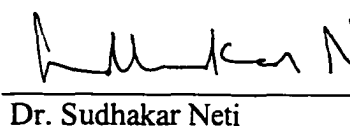
I also would like to thank Dr. Andrew D. Hollingsworth and Dr. Cesar A. Silebi for the use of their CHDF computer program.

A special gratitude goes to the Royal Thai Government for the financial support during the years of my study. My appreciation also goes to the Emulsion Polymer Institute for providing me with the necessary research facilities to complete my work.

Finally, I am indeed thankful to my parents, Supat and Anongnuch for giving me life and ambition in addition to their abundant love and support which helping go through all difficulties.

Table of Contents

v

vi

List of Figures

ix

x

List of Tables

xiii

Abstract

Effects of dissolved polymer on the transport of latex particles through a microcapillary were investigated. The capillary hydrodynamic fractionation (CHDF) experiments carried out using poly(ethylene oxide) (PEO) solutions as the eluant showed an increase in the particle separation factor as well as a decrease in the degree of axial dispersion when the molecular weight of the PEO was increased. To some extent, this separation factor enhancement effect resulted from the enlargement of the effective particle diameter due to the adsorption of PEO on particles.

The occurrence of polymer adsorption was confirmed by performing dynamic light scattering on the polystyrene (PS) latex particles dispersed in the PEO solutions. The results showed the expected increase of the particle size depending on the molecular weight of the PEO.

PEO-adsorbed particle was modeled as a composite sphere with a solid core surrounded by a permeable porous shell. The drag force was computed and related to the diffusivity of the composite particle. The CHDF dynamic simulation performed using the composite particle predicted a lower degree of axial dispersion compared to a hard sphere of the same size.

Migration of particles in PEO solutions was also investigated using CHDF. Experiments performed with PEO solutions using the latex particles pre-adsorbed with Brij35SP surfactant to prevent the change of particle size because of PEO adsorption. The results suggested that the significant increase of the separation factor arose from the viscoelastic effect of the PEO solution. The particle migration velocity due to this effect was incorporated into the CHDF model and it was found to agree well with the experimental results.

1

Chapter One

Introduction

1.1 Overview of Capillary Hydrodynamic Fractionation (CHDF)

Capillary hydrodynamic fractionation is an analytical technique for the characterization of particle size and particle size distribution of submicron colloidal dispersions. The separation of colloidal particles according to size is made possible by utilizing the parabolic velocity of the fluid flow field through a small open-bore capillary tube. As such the particles close to the capillary wall will move slower than those near the capillary center. Therefore, CHDF is based on a single liquid phase and makes use of the velocity gradient of the fluid flowing through the capillary without involving the partitioning of the fractionated species between two phases.

For normal operation in CHDF, samples of colloidal dispersions are injected into a capillary and transport with the fluid through it. The diameter of capillary in the range of 10 to 25 μm, assuring that the fluid flowing through the capillary will be in the laminar regime. Then, the colloidal particles are fractionated hydrodynamically and elute from the capillary in order of decreasing size. The optical densities of the fractionated species are measured at the capillary exit in order to determine the particle elution time and peak variance. By comparing the average elution time of unknown-particle size sample with that of the known-particle size standard, the particle size of the sample will be determined. Because of this indirect method in evaluation of particle size in CHDF, the accurate calibration and steady operating conditions are required.

1.2 Development of the Separation of Colloidal Particles Using CHDF

The fractionation of colloidal particles by a single open-bore capillary was successfully

2

developed into an analytical technique by Silebi and DosRamos [1]. Using a micron-size capillary together with a high-pressure pump and an UV detector, colloidal particles in sub-micron size range can be separated according to their sizes with a better resolution compared to the hydrodynamic chromatography technique [9]. They quantified the separation efficiency in CHDF by introducing the separation factor (R_f), which is the ratio of the average velocity of the colloidal particles to the average velocity of the fluid (eluant) phase. They showed experimentally that the separation factor can be influenced by the particle diameter of the colloidal dispersion, the capillary internal diameter, the ionic strength of the eluant, and the average velocity of the fluid phase. Moreover, a steady state CHDF mathematical model describing the separation mechanism and axial dispersion of the colloidal particles flowing through the microcapillary has been established [2,3].

Further parametric investigation of CHDF by Venkatesan [4] led to significant improvement in the separation efficiency of CHDF. He showed that the use of nonionic surfactants around their critical micelle concentration (cmc) increased the separation factor. In addition, he found that increasing the molecular weight of the surfactant could improve the separation factor. He concluded that this result is due to the steric repulsion generated by the layer of adsorbed-surfactant and the osmotic repulsion, which is caused by the difference in the surfactant concentrations between a bulk phase and interstitial areas between the particles and the capillary wall.

Later, Hollingsworth [5] studied the separation of colloidal particles in CHDF using very low ionic strength eluants. He found experimental evidence for the existence of repulsive electroviscous forces, known as electrokinetic lift, of colloidal particles in the Poiseuille flow [6]. This effect would become pronounced with decreasing conductivity, increasing particle size, and decreasing capillary internal diameter. The effect of particle concentration on the transport of

3

colloidal particles was also investigated over a range of eluant conductivity and flow rates. The negatively-skewed CHDF fractogram of the particle indicated the influence of a large particle-wall interaction energy gradient coupled with particle-particle interactions. Moreover, a dynamic CHDF mathematical model describing the evolution of colloidal particle concentration while traveling through the microcapillary has been developed.

1.3 Transport of Colloidal Particles in Microcapillary

Under laminar flow condition of the fluid in the capillary, the fluid develops a parabolic velocity profile. Therefore, colloidal particles dispersed in this moving fluid would experience different velocities within the microcapillary according to their radial positions. The relative elution times of colloidal particles in the microcapillary depends upon the particle size, the capillary internal diameter, eluant species and concentration, ionic strength of the eluant, and the fluid velocity.

Transport of colloidal particles through a microcapillary can be described as a convective-diffusion process. The fluid velocity distribution inside the capillary causes a convective effect that distorts the particle slug when it enters the flow field. This distorted slug induces a concentration gradient, which causes the diffusion of the particles mainly in the radial direction. For large elution time, the convective effect will be balanced by the diffusion process resulting in a Gaussian distribution of particle concentration. For dilute particle concentrations where particle-particle interactions are weak, the mechanism of size separation in CHDF primarily due to the interactions between particles and the capillary wall.

In the absence of external forces, the neutrally buoyant colloidal particles dispersed in the moving fluid would experience random Brownian motion. Because of their finite size, the centers of gravity are excluded from the capillary wall equal to the length of their radius (for spherical

4

particles). Since larger particles can not approach the tube wall closer than smaller ones due to their larger radius, larger particles will sample faster moving streamlines causing the large particles to elute first from the capillary. This phenomenon is known as the size exclusion principle. If the particles dispersed in the moving fluid travel through the capillary at relatively high Reynolds numbers, the inertial forces of the fluid will be strong enough to cause the particles moving away from the capillary wall and capillary axis to attain an equilibrium non-central radial position roughly at the distance of 0.6 of the tube radius measured from the tube axis. Theoretically, the onset of this inertial effect can be determined by the product of the particle Reynolds number and the Peclet number, which depends on the eluant average velocity, particle size, and capillary inner diameter [3].

Colloidal particles dispersed in the fluid are subjected to two basic interactions: one is van der Waal's attractive forces; and the other is colloidal repulsive forces. Generally, in the CHDF system, two main repulsive forces are involved i.e., electrostatic repulsion and electrokinetic lift. The electrostatic repulsion results from the existence of an electrical double layer (EDL) surrounding the colloidal particles as well as the capillary wall. The thickness of this layer is indicated in term of the Debye length ($1/\kappa_D$). The presence of electrolyte ions in the eluant phase has a strong effect on this electrostatic potential. As the ionic strength of the eluant is increased, the EDL surrounding the particles and the capillary wall are suppressed, inducing van der Waal's attractions to dominate. Consequently, the particles will have a greater probability to sample slower velocity streamlines near the wall resulting in the increase of axial dispersion and the decrease of separation efficiency. On the contrary, under low ionic strength conditions, the electrostatic repulsion is significant compared to the van der Waal's attractions. The electrokinetic lift force occurs when a charged surface and the diffuse part of the electrical double layer are made to move relative to each other in the presence of the wall. Electrical effects arise

5

solely from the deformation of the EDL by the primary fluid motion. In the CHDF system, the electrokinetic lift force would act in the radial direction toward the tube axis, repelling the particles away from the tube wall. An increased relative velocity of the particles and reduced axial dispersion would be obtained under such conditions. The electrokinetic lift would be significant under a very low ionic concentration and high viscosity of the eluant [6].

Figure 1-1 shows the schematic diagram of the aforementioned effects associated with the transport of colloidal particles through the microcapillary.

1.4 Transport of Colloidal Particles through Microcapillary in the Presence of High Molecular Weight Dissolved Polymer

In the CHDF system, surfactants are added into the eluants in order to improve the colloidal stability of the particles during the particle fractionation process. In fact, not only is the colloidal stability increased, but the separation efficiency can be improved as well. The surfactant species can adsorb both on the particle surfaces and on the capillary wall. This can be considered to be equivalent to a narrowing of the capillary diameter as well as an enlargement of the effective particle diameter due to the thickness of adsorbed surfactant layer. However, the surfactants which have been studied to date were of low molecular weights (in the range of 600 to 13,000 g/mol) in which the effect of adsorbed layer is negligible. An increase of separation efficiency arises from the alteration of other parameters such as the ionic strength of the eluant and the eluant average velocity.

As the molecular weight of polymer (surfactant species) increases, the presence of this high molecular weight polymer can provide a significant impact on the particle separation in CHDF. Obviously, a thicker adsorbed layer on the particle surface gives rise to a substantial enlargement of the particle diameter. The larger adsorbed thickness was found to depend upon the
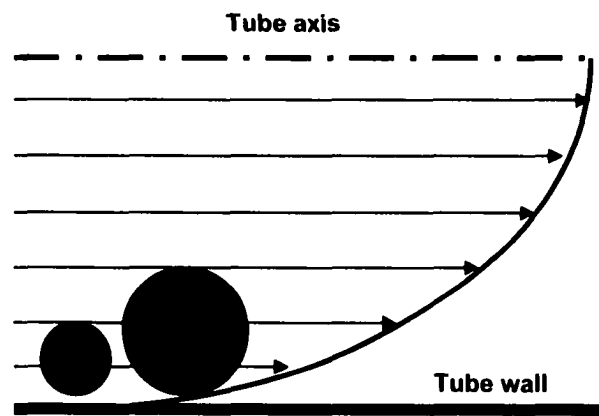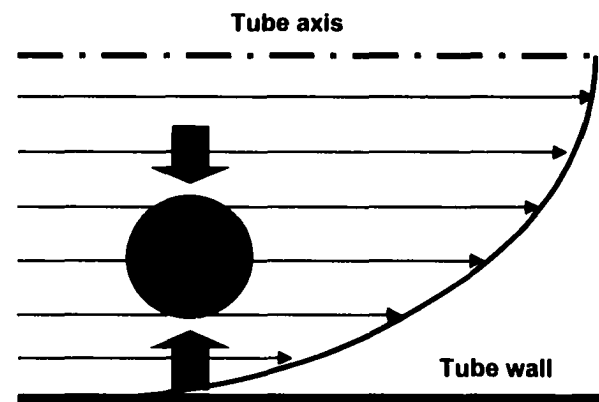
6
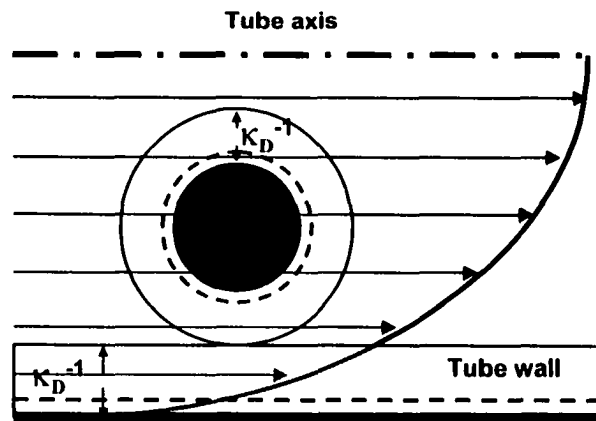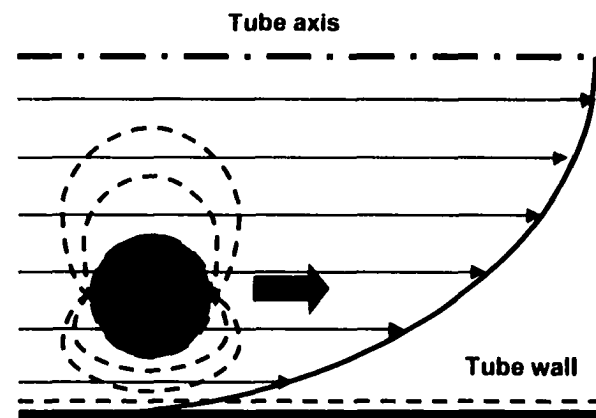
Figure 1-1: Schematic diagram of various effects associated with the transport of colloidal particles through microcapillary.

molecular weight of the polymer and is of the same magnitude as the radius of gyration of the polymer molecule in solution [7,11,12]. Hydrodynamically, a polymer-adsorbed particle will respond to the flow different than a solid particle of the same size due to the ability of the adsorbed polymer layer to allow the fluid to penetrate. The fluid drag force exerted on the polymer-adsorbed particle will be reduced compared to the rigid particle. Thus, the particle diffusivity of the polymer-adsorbed particles, which is closely related to the drag force, will be modified.

The adsorbed polymer layer on the particles not only changes the effective diameter of the particles but alters the surface charge properties as well. For adsorption of uncharged polymers on a charged surface, the surface charge density of the polymer-adsorbed surface is expected to decrease. The conductometric titration of 176 nm polystyrene (PS) standard latex particles showed a decrease in the surface charge density from -1.7 $\mu C/cm^2$ for the bare PS particles to -0.8 $\mu C/cm^2$ for the particles dispersed in poly(ethylene oxide) (PEO) solutions.

Because the surface charge density is reduced with adsorption of PEO, the zeta potential of latex particles will be decreased (less negative) as well. Using the Coulter Doppler electrophoretic light scattering analyzer (DELSA 440) with 1 mM NaCl as the background electrolyte, the zeta potential of 234 nm PS latex particles was found to change from -45 mV for bare particles to -11 mV for the PEO–coated latex. This alteration in the surface charge density as well as the zeta potential influences the electrostatic and electrokinetic properties of the particles which is important for the particle separation in CHDF using low ionic strength eluant.

The flow behavior of the polymer solution might affect the particle transport through the microcapillary. There are two surface phenomena taking place near the capillary wall (i.e., slip and adsorption) that are associated with the flow of a polymer solution [13]. The slip effect refers to the abnormally low apparent viscosities of polymer solutions in an inhomogeneous stress field

8

compared to the viscosities measured in uniform stress fields [8]. Therefore, if the capillary flow of a polymer solution is accompanied by the slip effect, the fluid flow rate will be enhanced. Unlike the flow associated with the polymer adsorption, the adsorbed layer on the capillary wall hampers the flow causing the flow rate to be reduced.

The slip effect is caused by the migration of polymer molecules from the high shear region near the capillary wall toward the low shear area around the capillary center. The polymer migration in tube flow creates a concentration gradient of polymer across the tube radius, which will result in the radial variation of polymer solution viscosity. Consequently, this change of viscosity will affect the particle transport through the microcapillary. In the case of adsorption, if the molecular weight of the polymer is high, the reduction of capillary diameter is noticeable and thus the separation of particles in the presence of adsorbed polymer on the capillary wall is expected to be improved.

Another aspect of polymer solutions that has a significant effect on the transport of particles in the capillary is the viscoelastic property. Unlike Newtonian fluid, a polymer solution is known to possess non-zero normal stresses. The normal stress of a polymer solution is believed to be responsible for the migration of particles toward the region of lower velocity gradient in low Reynolds number Couette and Poiseuille flows [14-20]. In CHDF, this normal stress of a polymer solution will cause the particles to migrate from the capillary wall toward the center which on the average, will result in faster moving particles through the capillary relative to the moving fluid.

1.5 Research Strategy

Transport of colloidal particles through the microcapillary in the presence of high molecular weight dissolved polymer is explored. Three important aspects will be studied; these are the adsorption of polymer on the particles, the surface phenomena associated with the flow of

9

polymer solution through the capillary, and the particle migration due to the viscoelastic properties of the polymer solution.

Dynamic light scattering is used to determine the effective size of the particles with an adsorbed polymer layer. In addition, CHDF experiments will be conducted using a mixture of colloidal particles in polymer solution as a sample in order to investigate the transport of polymer-adsorbed particles in CHDF. The eluant is high ionic strength NaCl solution (4 mM) in order to diminish the electrostatic and electrokinetic effects. In the experiment, the irreversibility of polymer adsorption was assumed because high molecular weight homopolymers were used; multiple attachments of the polymer chains on the adsorbing surface would be expected.

Surface phenomena in capillary flow of polymer solutions are investigated experimentally. Two surface phenomena, slip and adsorption, will be distinguished by measuring the average velocity of the flow of polymer solution through different diameter capillaries. The adsorption will be identified and the thickness of the adsorbed polymer layer on the capillary surface will be estimated.

Particle migration due to viscoelastic properties of the polymer solution will be studied using CHDF. The eluants are polymer solutions with high ionic concentration prepared by adding certain amount of NaCl into surfactant-free polymer solutions. Since polymer chains can adsorb on the particles while they are traveling through the polymer solution, low molecular weight surfactant (Brij35SP) is adsorbed on the particle surfaces to prevent polymer adsorption and keep the diameter of the particles constant.

1.5.1 Scope and Objectives

This research aims to investigate effects of polymer present in the eluant as well as the dispersed medium of the latex samples on the transport of particles in CHDF and to gain a

10

fundamental understanding of the separation mechanism. Monodisperse polystyrene (PS) latex particles were used as the model colloid system in CHDF. The particle diameters were between 109 and 794 nm as determined by transmission electron microscope. The capillary considered here has the nominal diameter of 25 μm. The eluants were aqueous solutions of poly(ethylene oxide) (PEO) and in some cases, deionized (DI) water and NaCl solutions were also used. The molecular weight of the PEO varied from 10,000 g/mol up to 1,000,000 g/mol. The concentration of PEO solutions was limited (less than 0.2 % w/w) to avoid the complication from the shear thinning effect.

The research objectives of this research are:

- To investigate particle transport through the microcapillary in the presence of high molecular weight dissolved polymer.

- To evaluate the prevailing effect arising from the presence of high molecular weight polymer on the particle separation in CHDF.

- To improve the fundamental understanding of the separation mechanism of particles in CHDF when polymer solution is used as the eluant by incorporating the effects of high molecular weight polymer in the theoretical analysis of CHDF.

1.6 Experimental

1.6.1 CHDF Experimental Setup

Figure 1-2 shows a schematic diagram of the experimental CHDF system. Eluant is delivered into the system using a positive displacement pump (Milton Roy minipump model 396) equipped with a pulse dampener. The eluant is pumped through a sample injection valve (Rheodyne model 8125), which is used to introduce colloidal dispersions into the capillary. The

11
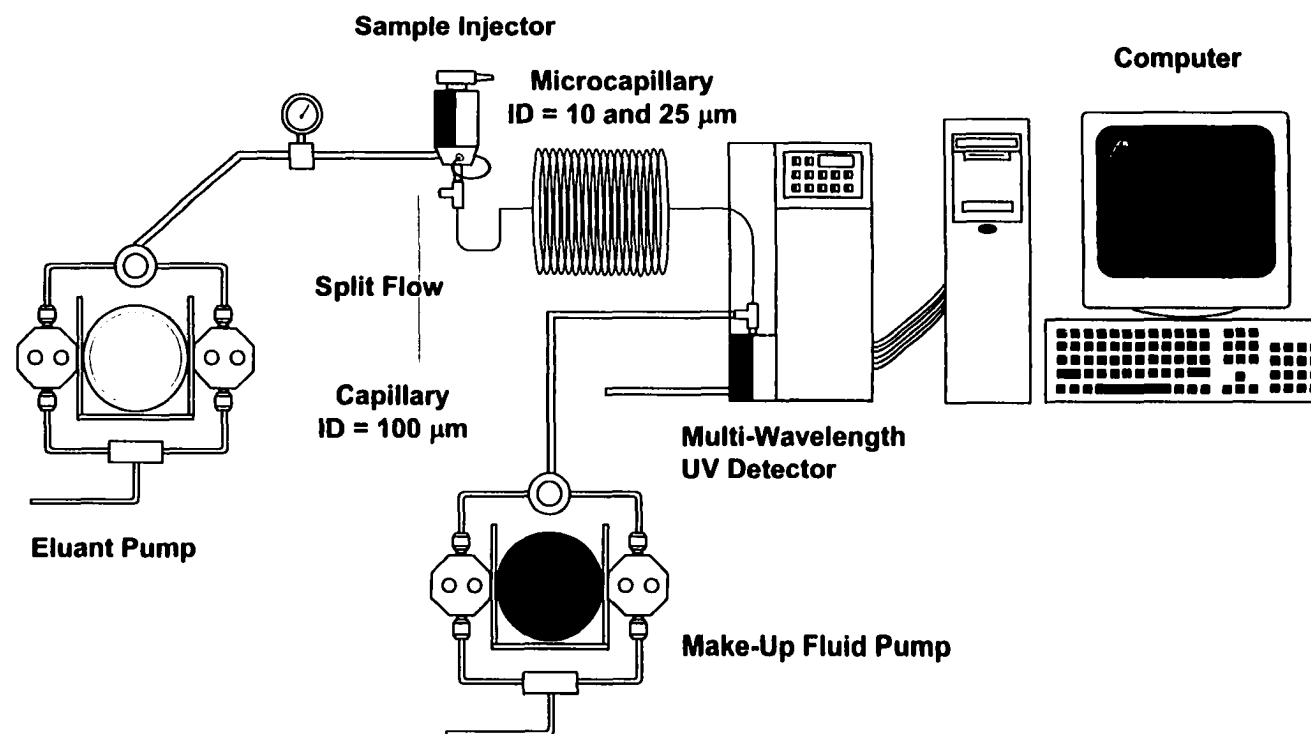
Figure 1-2: Schematic diagram of experimental capillary hydrodynamic fractionation (CHDF) system.

volumetric size of the sample for each injection is kept constant by the use of a sample loop (5 μL or 20 μL) before the sample is carried into the microcapillary column by the eluant stream. The eluant flow from the pump is divided into two streams at a T-connection before entering the capillary; one stream continues through the microcapillary, while the other is discarded. The purpose of the split flow is to minimize the volume of the eluant stream entering the capillary which in part prevents a volumetric overloading and effectively reduces the dead volume of the sample inside the sample loop. The silica-fused microcapillary purchased from Polymicro Technologies Inc., which has an approximate internal diameter of 25 μm, is connected by one end to the T-connector while the other end is attached to the detector cell of a multi wavelength UV detector. The actual average internal diameter of the microcapillary is calculated using the Hagen-Poiseuille law for fluid flowing through a cylindrical tube under laminar conditions. A UV detector is used to detect the emerging particles by measuring their optical densities. The detector output is monitored every 0.46 second at various wavelengths in the UV range and interfaced to a computer for data acquisition and analysis. Due to the small volumetric flow rate in the capillary, which would tend to generate a dead volume in the detector cell, a constant flow of DI water (make-up stream) is also passed through the detector cell.

1.6.2 Eluant Compositions and Standards

Water-soluble poly(ethylene oxide) (PEO), supplied from Aldrich, with different molecular weights were used in the eluant solutions. The molecular weights and molecular weight distributions of the PEOs determined by aqueous GPC are shown in Table 1-1. A root-mean-square end-to-end distance $\langle r^2 \rangle^{1/2}$ of the PEO molecules in water at 25 °C is determined using Peterlin's equations:

$$\left\langle r^2 \right\rangle^{1/2} = 1.21 \times 10^{-8} \left(\frac{[\eta]M}{1-a} \right)^{1/3} \tag{1.1}$$

where $[\eta]$ is the intrinsic viscosity in units of cm^3/g, M is molecular weight of the polymer, and a

is the Mark-Houwink exponent (see equation (3.46)).

The PEOs were dissolved in deionized (DI) water to prepare the eluant solutions. In order

to remove any ionic contamination in the solutions, all eluants were cleaned by passing them

through an ion-exchange resin column, followed by filtering using 1-2 μm pore size membrane.

The ion-exchange cleaning process was repeated until the conductivity of the solutions fell into

the range of 1 to 3 μS/cm. The conductivity was measured using a YSI model 32 conductance

meter with the YSI model 3403 electrode (cell constant = 1.0 cm^{-1}) at room temperature. The

conductivity of the eluant was modified by adding a certain amount of NaCl solution.

Table 1-1: Molecular Weights of PEOs

Polymer	M_n (g/mol)	M_w (g/mol)	M_v (g/mol)	PDI	$\left\langle r^2 \right\rangle^{1/2}$ (nm)
PEO1	9700	11500	11300	1.2	11.8
PEO2	27800	122200	99200	4.4	43.6
PEO3	70800	368600	308400	5.2	84.1
PEO4	248400	1217500	1061600	4.9	159.1

A series of cleaned monodisperse polystyrene (PS) latex standards, manufactured by the

Dow Chemical Co., of various particle diameters were used as the colloidal samples. Average

particle sizes and the standard deviations as determined by electron microscopy (TEM) are shown

in Table 1-2. Before injection, these latexes were diluted in the eluants to a certain concentration,

providing that the fractogram is discernable while the particle-particle interactions are minimized.

14

Then the dispersion samples were sonified for 1 minute in order to break up any aggregates that might have formed during the sample preparation.

Table 1-2: Particle Diameter and Standard Deviation of Polystyrene Latex Standards[*]

Particle Diameter (nm) measured by TEM	Standard Deviation (nm)
109	2.7
176	2.3
234	2.6
357	5.6
610	9.0
794	4.4

[*] Data obtained from the manufacturer.

1.7 Quantification of Separation Efficiency in CHDF

1.7.1 Separation Factor (R_f)

The efficiency of particle separation in CHDF can be evaluated in terms of a separation factor. The separation factor is defined by the ratio of the average particle velocity to the average fluid velocity; that is,

$$R_f = \frac{\langle v_{pz} \rangle}{\langle v_z \rangle} \qquad (1.2)$$

where $\langle v_{pz} \rangle$ and $\langle v_z \rangle$ are the average velocities of the particles and fluid, respectively. In fact, for the CHDF system where we have a constant length of the microcapillary, the separation factor can be calculated by taking the ratio of the mean elution time of the fluid to that of the particles. The mean elution time of the eluant is denoted by the average elution time of a molecular-size

15

marker species (sodium benzoate). For a symmetrical fractogram, the mean elution time corresponds to the peak elution time. In the case of an asymmetrical fractogram, the mean elution time is measured at the mean retention time at the peak's center of mass. This statistical moment can be calculated using the following formula [9]:

$$\langle t_s \rangle = \frac{\sum_i t_i S(t_i) \Delta t_i}{\sum_i S(t_i) \Delta t_i} \tag{1.3}$$

where $\langle t_s \rangle$ is the mean elution time of the sample (either the particles or the marker), $S(t_i)$ is the detector response at time t_i and Δt_i is the measuring time difference.

In CHDF, the separation factor is always greater than 1 indicating that on average, the particles move through the microcapillary faster than the eluant. In principle, the maximum value of the separation factor is 2 for a Newtonian fluid, which occurs when the particles are travelling at the center of the capillary. Nonetheless, this situation never exists because of the retarding effect of the capillary wall on the particle velocity [2].

1.7.2 Axial Dispersion

Axial dispersion of the particles takes place when a slug of colloidal particles flowing through a capillary is spread out while it is transported by the carrier phase. The axial dispersion causes a peak broadening in CHDF and is responsible for the Gaussian shape fractogram of species. In the absence of axial dispersion, the peak would appear as a sharp spike rather than a bell-like shape. In order to ensure efficient particle separation in a microcapillary, it is essential to account not only for the separation factor but also for the rate at which the peak broadens during the separation process.

An axial dispersion is quantified by the plate theory of chromatography, which is adapted

16

from the theory of distillation column. The plate theory considers a column as a series of discrete, narrow horizontal layers called theoretical plates. A movement of the solute and the carrier phase is viewed as a series of stepwise transfers from one plate to another. The efficiency of the separation process is indicated by a theoretical plate height, H_{TP}, which is the thickness of one plate in a plate series. An increase in dispersion of a solute is characterized by an increase in the effective dispersion coefficient and hence an increase in H_{TP}. The length of the total column is a product of the height of one plate and the number of theoretical plates in the column.

The axial dispersion of a solute in a microcapillary can be determined experimentally from the CHDF fractogram. The broadening of the fractogram is characterized by the axial dispersion coefficient which can be evaluated from the variance σ_t^2 of the fractogram [9]

$$\sigma_t^2 = \frac{\sum_i \left(t_i - \langle t_s \rangle\right)^2 S(t_i) \Delta t_i}{\sum_i S(t_i) \Delta t_i} \tag{1.4}$$

To express the variance in terms of a distance-based variance σ_z^2, the time-based variance is multiplied by the square of the average axial velocity; that is,

$$\sigma_z^2 = \sigma_t^2 \langle v_{pz} \rangle^2 \tag{1.5}$$

The plate height H_{TP} is defined as the distant-based variance in the peak width per unit length of axial displacement L; thus,

$$H_{TP} = \frac{\sigma_z^2}{L} \tag{1.6}$$

The distant-based variance consists of two contributions; one is the contribution to the total variance from the flow through the capillary σ_c^2 and another is the contribution to the additional variance from the nonidealities in the system σ_{n-1}^2, such as a dead volume effect. In terms of the plate height:

17

$$H_{TP} = H_c + H_{n-1} \tag{1.7}$$

The contribution due to the nonidealities of the system was calculated from the difference between the total experimental dispersion of the maker species (sodium benzoate) in CHDF and the ideal degree of axial dispersion σ_{id}^2 of this solute flowing through the microcapillary according to Taylor diffusion. Taylor's theory suggests that the ideal degree of axial dispersion can be given by [10]

$$\sigma_{id}^2 = 2D_{eff}\langle t_m \rangle \tag{1.8}$$

where D_{eff} is the effective diffusion constant, which is given by:

$$D_{eff} = D_{solute} + \frac{\langle v_z \rangle^2 R_o^2}{48 D_{solute}} \tag{1.9}$$

where D_{solute} is the diffusion coefficient of the solute and R_o is the capillary radius.

1.8 Adsorption Behavior of PEO on PS particles

For the system of colloidal particles dispersed in a high molecular weight homopolymer solution, it is generally assumed that the high molecular weight polymer, when used in dilute concentration, will tend to flocculate the particles by a bridging mechanism whereby long polymer chains extending from one particle are caught by another particle. However, at high concentration of the polymer, restabilization may occur because the high coverage of polymer chains on particle surfaces reduces the free surface area on which the bridging can take place and the dense polymer layer generates an additional steric repulsion.

To acquire a better stability for PS particles dispersed in PEO solutions, the saturated surface concentration (full coverage of PEO on particle surfaces) of each molecular weight was determined. Known concentrations of PEO solutions were mixed with the PS latex particles (234

18

nm diameter) at a particle concentration of 0.10 % w/w. The mixtures were stored for at least 12 hours to ensure that the adsorption equilibrium was reached. The mixtures were then centrifuged at 20,000 rpm for 6 hours at 25 °C. The supernatants were carefully removed with a syringe and filtered through a 5 µm pore size filter. The concentrations of free polymer in the supernatant were determined by measuring the refractive index (RI).

Figure 1-3 shows the adsorption isotherm of various molecular weight PEOs adsorbed on 234 nm PS particles. The saturated surface concentrations (mg PEO/m^2 PS) were obtained from the plateau area of the adsorption isotherm.

Figure 1-4 shows CHDF fractograms of 0.5 % w/w 109 nm PS latex particles dispersed in 0.01 % w/w and 0.1 % w/w PEO4, which correspond to surface concentrations of 0.38 and 3.8 mg PEO4/m^2 PS, respectively. This figure shows that, if the concentration of PEO4 was below the saturated concentration, the CHDF fractogram showed extra peaks that appeared at earlier elution times. This indicates that particles had flocculated and formed larger aggregates, which as expected for CHDF, larger size aggregates traveled faster and then eluted first from the capillary. This flocculation of latex particles at low PEO4 concentrations occurred probably because the long protruding parts of the polymer chains can overcome the distance of closest approach between two PS particles (due to the high particle concentration used). As the concentration of PEO4 increased above the saturation point, a single peak fractogram can be observed. At this stage, there are sufficient numbers of PEO chains in the solution for total surface coverage of PEO4 on the PS particles, thus imparting colloidal stability to the particles provided by the steric barrier of the dense adsorbed PEO4 layer.

Also displayed in Figure 1-4 is the turbidity ratio, which is the ratio of particle optical densities between two wavelengths of UV. Because the turbidity ratio has a unique value for each particle size, it can be used to follow the forming of aggregates in the CHDF system [4]. For

19
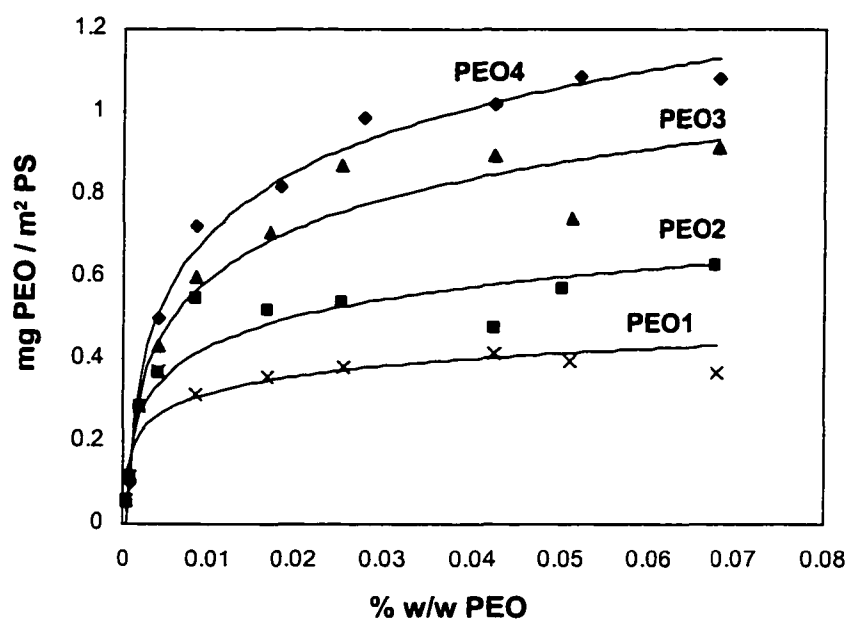
Polymer	Saturated surface concentration (mg PEO / m² PS)	Area per molecule (nm²)
PEO1	0.39 ± 0.02	48
PEO2	0.55 ± 0.06	300
PEO3	0.86 ± 0.08	596
PEO4	1.06 ± 0.04	1664

Figure 1-3: Adsorption isotherm of various molecular weight PEOs on PS latex particles.

20
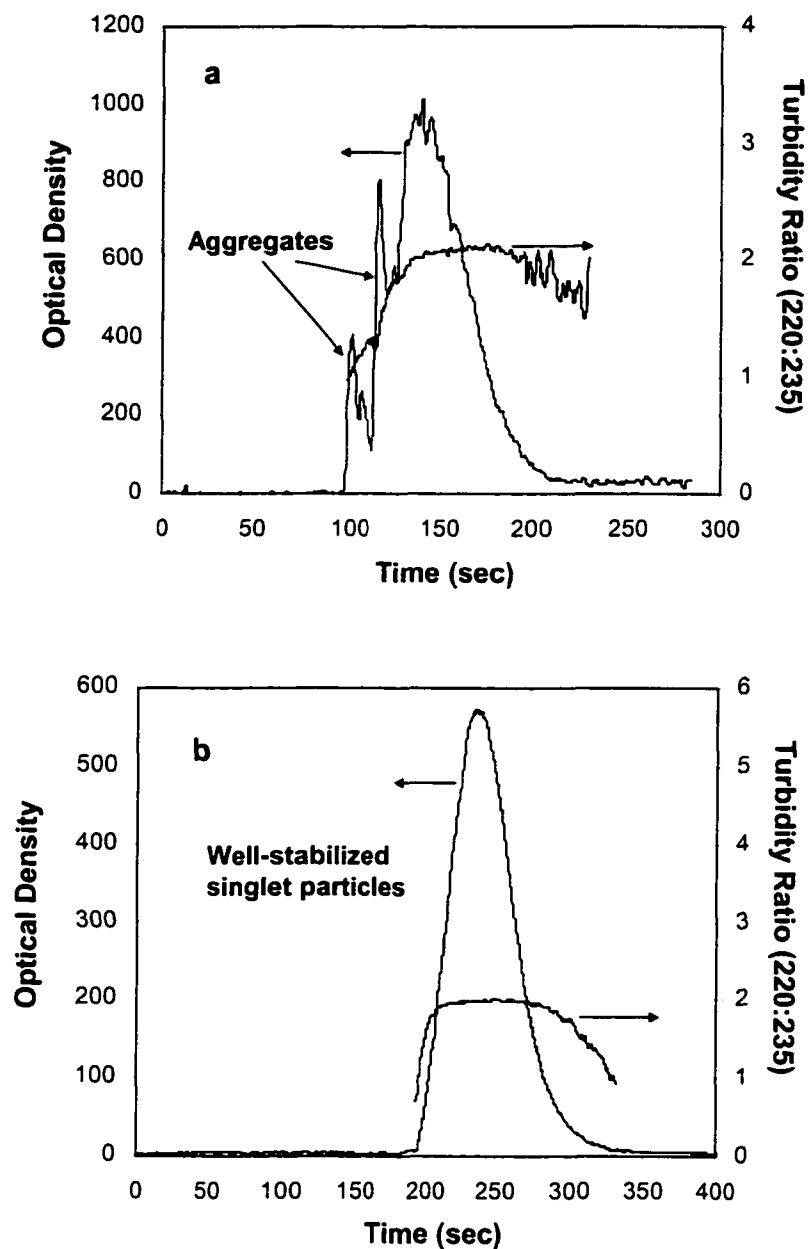
Figure 1-4: CHDF fractograms of 109 nm PS particles dispersed in: (a) 0.01 % w/w PEO4 and, (b) 0.1 % w/w PEO4; particle concentration is 0.5 % w/w.

21

particles at concentrations of PEO4 below saturation, the decreasing value of the turbidity ratio indicated that larger sizes of aggregates were formed and these correspond to the extra peaks appearing at the earlier time of the fractogram. When the PS particles were dispersed in the saturated concentration of PEO4, the turbidity showed a constant value indicating the particles were well separated from each other and no aggregates were formed.

22

Chapter Two

Effective Particle Size of PEO-Adsorbed Latex Particles

2.1 Introduction

For dispersions of polystyrene (PS) latex particles in aqueous solutions of poly(ethylene oxide) (PEO), the PEO polymer molecules can adsorb on the PS particle surfaces through hydrophobic interactions. This adsorption of PEO can have an impact on the characterization of the particles. One important effect is the enlargement of particle due to the thickness of the adsorbed polymer. The thickness of adsorbed polymer layer can be determined using hydrodynamic methods such as dynamic light scattering and capillary viscometry [21]. Using dynamic light scattering, Kato et al. [11] determined the thickness of the adsorbed PEO layer (δ) on PS latex particles. They found that adsorbed layer thickness depended upon the concentration of the PEO for very dilute PEO solutions before reaching a constant thickness at higher concentrations, which was believed to be the saturation concentration for PEO adsorption. At this saturation point, the adsorbed layer thickness will increase with the molecular weight of the PEO. Polverari and van de Ven [12] also studied the adsorption of PEO on latex particles. They observed an increase in δ for smoother particle surfaces such as PS particles with SO_4^{-2} as a functional surface group. Moreover, they also found that δ as well as the adsorbed amount will decrease as the surface densities of functional groups increased.

In the present study, the impact of the PEO adsorption on the particle size is investigated using both dynamic light scattering (DLS, Nicomp model 370) as well as CHDF. The dependency of the thickness of the adsorbed layer on the PEO molecular weight was determined experimentally and expressed in term of the power law type model. The effect of particle size on

the thickness of the adsorbed PEO also investigated using DLS. In addition, CHDF experiments with latex particles in the presence of PEO were also performed in order to investigate the effect of the size increment due to the adsorption of PEO on the transport of particles in the capillary. The effect of PEO concentration in the dispersion medium of the sample on the particle separation in CHDF was investigated along with the ionic strength and viscosity effects. A high ionic strength NaCl solution was selected as the eluant in order to eliminate the effects from electrostatic repulsion and electrokinetic lift force [1,6]. The stability of the latex samples was ensured by dispersing the PS particles in PEO solutions in which the concentration was higher than the concentration at the saturation point obtained from the plateau of the adsorption isotherm.

The CHDF dynamic model is presented here following the development of Hollingsworth and Silebi [5]. The polymer-adsorbed particle was modeled as a composite sphere containing a rigid core surrounded by a flow penetrable shell. The Brinkman-type fluid dynamic equation [21] was employed to describe the flow inside the adsorbed polymer layer. The diffusivity and local particle velocity were calculated based on the hydrodynamic model of the composite sphere.

The main objective of this study is to demonstrate experimentally and numerically how the adsorption of PEO affects the particle size of latex particles and how the PEO-adsorbed particles behave when traveling through the capillary.

2.2 Numerical Simulation of Polymer-Adsorbed Particles in CHDF

A particle having polymer adsorbed on the surface is modeled as a composite sphere consisting of a rigid core of substrate particle surrounded by a permeable shell of adsorbed polymer layer. The outer adsorbed layer of the polymer-adsorbed particle behaves somewhat like

24

a porous medium, which allows the fluid to penetrate through it causing different hydrodynamic characteristics compared to a rigid particle.

2.2.1 Hydrodynamics of a Composite Sphere in an Unbounded Fluid

In order to model the effect of adsorbed polymers on the hydrodynamic response of particles, three basic factors have to be considered: 1) a model representing the macroscopic properties of adsorbed polymers, 2) an equation of motion for the flow within the adsorbed layer and 3) solution of the fluid dynamics equations for both the interior and exterior of the adsorbed polymer layer [22].

The most commonly used equation of motion describing the fluid velocity and hydrodynamic pressure in the adsorbed layer is the Brinkman equation [21,23]. For creeping flow conditions, the Brinkman equation is defined as follows:

$$\eta^* \nabla^2 \mathbf{u}^* - \frac{\eta}{k^2} \mathbf{u}^* = \nabla p^* \tag{2.1}$$

where $\mathbf{u}^*$ and p^* are velocity vector and hydrodynamic pressure of fluid inside the porous shell. η is the viscosity of the fluid outside the adsorbed layer and η^* is the effective fluid viscosity inside the adsorbed polymer layer, which can be different from the viscosity of the surrounding fluid. However, by setting $\eta^* = \eta$, a closer agreement between the predictions and the experimental results was observed [21,24]. k represents the permeability of the adsorbed polymer layer, which depends on the volume fraction of polymer segments.

In order to obtain the velocity and pressure inside the adsorbed layer, equation (2.1) is solved along with the continuity equation for a Newtonian incompressible fluid:

$$\nabla \cdot \mathbf{u}^* = 0 \tag{2.2}$$

Outside a composite sphere, the equations describing the flow field for an incompressible

25

Newtonian creeping flow are the Stokes and continuity equations:

$$\eta \nabla^2 \mathbf{u} = \nabla p \qquad (2.3)$$

$$\nabla \cdot \mathbf{u} = 0 \qquad (2.4)$$

2.2.1.1 Method of Solution

To solve the problem of creeping flow past a stationary isolated composite sphere (see Figure 2-1), it is more convenient to employ a stream function (ψ) since the flow is two dimensional and axisymmetrical. Spherical coordinates (r, θ, ϕ) are used and the velocities are given in term of the stream function by [25]:

$$u_r = -\frac{1}{r^2 \sin\theta} \frac{\partial \psi}{\partial \theta} \qquad (2.5)$$

$$u_\theta = \frac{1}{r \sin\theta} \frac{\partial \psi}{\partial r} \qquad (2.6)$$

These velocities are chosen such that the continuity equation is satified. Taking the curl of the Stokes and Brinkman equations, one obtains, repectively [26]

$$E^4 \psi = 0 \qquad (2.7)$$

and

$$E^4 \psi^* - \frac{\eta}{\eta^*}\left(\frac{1}{k^2} E^2 \psi^* - \frac{d}{dr}\left(\frac{1}{k^2}\right)\frac{d\psi^*}{dr} \right) = 0 \qquad (2.8)$$

where

$$E^2 \equiv \frac{\partial^2}{\partial r^2} + \frac{\sin\theta}{r^2} \frac{\partial}{\partial \theta}\left(\frac{1}{\sin\theta} \frac{\partial}{\partial \theta} \right) \qquad (2.9)$$

and

$$E^4 \equiv E^2(E^2\psi) \qquad (2.10)$$

The ratio $\dfrac{\eta}{\eta^*}$ is taken as 1 and the permeability of the adsorbed polymer is assumed to vary in the

26
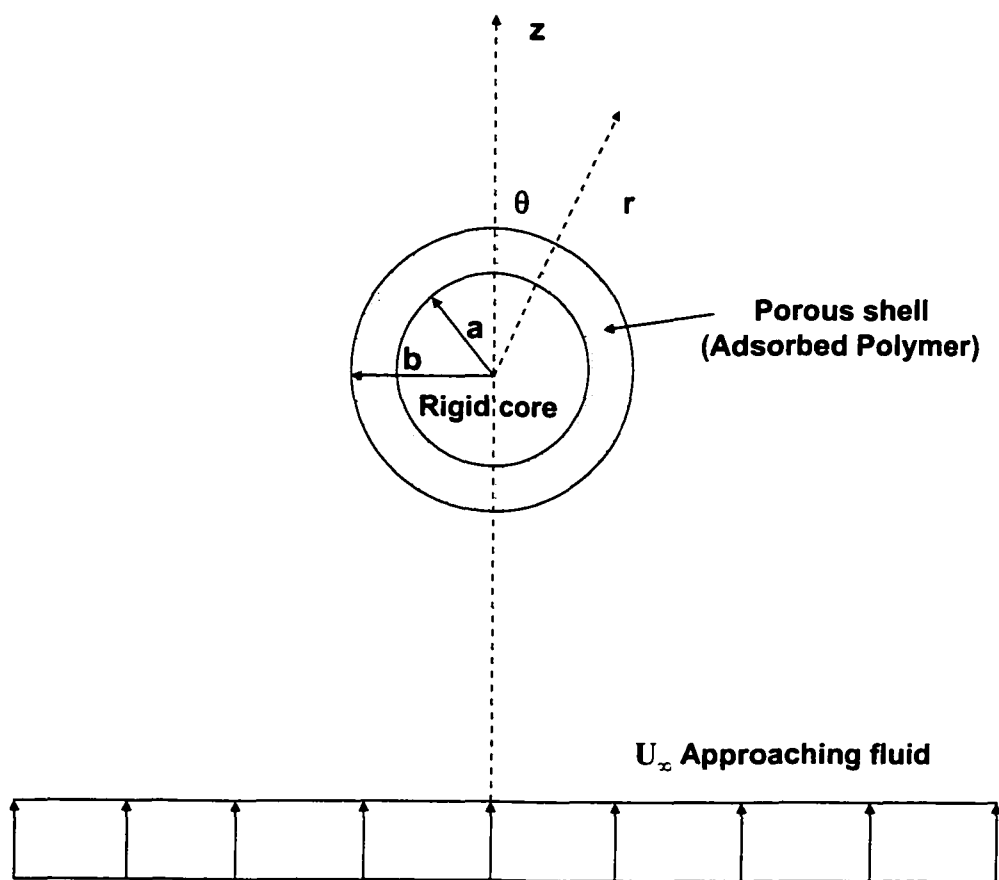
Figure 2-1: Isolated composite sphere held fixed in an unbounded fluid flow field.

27

radial direction only. The boundary conditions associated with this problem are the following:

$$r = a : \quad \mathbf{u}^* = 0 \tag{2.11}$$

$$r = b : \quad \mathbf{u}^* = \mathbf{u} \quad \text{and} \quad \tau^* = \tau \tag{2.12 and 2.13}$$

$$r \rightarrow \infty : \quad \mathbf{u} \rightarrow -\mathbf{U}_x \tag{2.14}$$

Equation (2.11) assumes a no-slip condition at the solid core surface. Equations (2.12) and (2.13) describe the continuity of the velocities and stresses at the outer edge of the porous shell. Equation (2.14) indicates that the fluid velocity resumes a uniform flow field at a position far from the sphere.

2.2.1.1.1 Analytical Solution

For the case of a constant permeability of the adsorbed polymer layer, analytical solutions to equation (2.7) and (2.8) are permitted and these have been obtained by Masliyah et al. [27]. Since the permeability is constant, equation (2.8) is transformed to:

$$E^4 \psi^* - \left(\frac{1}{k^2} E^2 \psi^* \right) = 0 \tag{2.15}$$

Analytical solutions of equations (2.7) and (2.15) are as follows:

$$\psi(\xi,\theta) = -\frac{k^2 U_x}{2} \left[\frac{A}{\xi} + B\xi + C\xi^2 + D\xi^4 \right] \sin^2 \theta \qquad \beta \leq \xi < \infty \tag{2.16}$$

$$\psi^*(\xi,\theta) = -\frac{k^2 U_x}{2} \left[\frac{E}{\xi} + F\xi + G\left(\frac{\cosh \xi}{\xi} - \sinh \xi \right) + H\left(\frac{\sinh \xi}{\xi} - \cosh \xi \right) \right] \sin^2 \theta$$

$$\alpha \leq \xi \leq \beta \tag{2.17}$$

where $\xi = \frac{r}{k}$, $\alpha = \frac{a}{k}$ and $\beta = \frac{b}{k}$.

The constants A, B, C, D, E, F, G, H are obtained from the boundary conditions and have the

28

specific values:

$$B = \frac{B_o}{2J(\alpha \sinh \beta - \cosh \alpha)} \qquad (2.18)$$

where

$$\begin{aligned}
B_o &= 3(\alpha^4 + 2\alpha\beta^3 + 3\alpha^2)\cosh \alpha \\
&\quad + 9\alpha^2(\cosh \beta - \beta \sinh \beta - \alpha \sinh \alpha) \\
&\quad + 3\cosh \Delta\left[(\alpha^3 + 2\beta^3 + 3\alpha)(\alpha\beta \sinh \beta - \alpha \cosh \beta - \beta \cosh \alpha) + 3\alpha^2\beta \sinh \alpha\right] \\
&\quad + 3\sinh \Delta\left[(\alpha^3 + 2\beta^3 + 3\alpha)\cosh \alpha + 3\alpha^2(\alpha\beta \sinh \beta - \alpha \cosh \beta - \sinh \alpha)\right]
\end{aligned} \qquad (2.19)$$

and

$$J = -6\alpha + (3\alpha + 3\beta + \alpha^3 + 2\beta^3)\cosh \Delta + 3(\alpha^2 - 1)\sinh \Delta \qquad (2.20)$$

with $\Delta = \beta - \alpha$

$$H = \frac{3(\alpha^3 + 2\beta^3)\cosh \alpha + 9\alpha(\cosh \alpha - \alpha \sinh \alpha - \cosh \beta + \beta \sinh \beta)}{J} \qquad (2.21)$$

$$G = \frac{3\alpha - (\alpha \cosh \beta - \sinh \alpha)H}{\alpha \sinh \beta - \cosh \alpha} \qquad (2.22)$$

$$F = \frac{(G \cosh \alpha + H \sinh \alpha)}{3\alpha} \qquad (2.23)$$

$$E = 2B + 2\beta^3 F \qquad (2.24)$$

$$D = 0 \qquad (2.25)$$

$$C = -1 \qquad (2.26)$$

$$A = \beta^3 - \beta^2 B + E + \beta^3 F + (\cosh \beta - \beta \sinh \beta)G + (\sinh \beta - \beta \cosh \beta)H \qquad (2.27)$$

The hydrodynamic drag force F_H acting on the composite sphere is obtained by integrating the normal and tangential stress distributions over the sphere surface; that is,

$$F_H = 2\pi b^2 \int_0^\pi [\tau_{rr} \cos\theta - \tau_{r\theta} \sin\theta]_{r=b} \sin\theta d\theta \qquad (2.28)$$

29

where τ_{rr} and $\tau_{r\theta}$ are the normal and tangential components of the stress tensor, respectively. Thus, the drag force is obtained as follows:

$$F_H = 6\pi\eta U_\infty b\Omega \tag{2.29}$$

where Ω is the correction factor taking into account the porous shell and is given by:

$$\Omega = \frac{2B}{3\beta} \tag{2.30}$$

2.2.1.1.2 Asymptotic Solution for a Thin Shell Composite Sphere

If the permeability of the adsorbed polymer is not uniform throughout the layer, equation (2.8) cannot be solved analytically. However, for a thin layer of adsorbed polymer on the particle, the approximate solution is possible using a matched asymptotic expansion [22,28]. Following Anderson and Kim [22], dimensionless variables are used in which u and u* are normalized by a characteristic velocity V, η^* by the fluid viscosity η, r by the solid core radius a, and fluid pressure p by $\mu V/a$. Hence, equation (2.8) is given in dimensionless form as:

$$\bar{\eta}^* E^4 \psi^* - \frac{1}{\lambda^2}\left(\frac{\delta^2}{k^2} E^2 \psi^* - \frac{d}{d\bar{r}}\left(\frac{\delta^2}{k^2} \right)\frac{d\psi^*}{d\bar{r}} \right) = 0 \tag{2.31}$$

and the boundary conditions become

$$\bar{r} = 0: \psi^* = \frac{\partial\psi^*}{\partial\bar{r}} = 0 \tag{2.32}$$

$$\bar{r} \to \infty: \psi \to \frac{1}{2}U_\infty \bar{r}^2 \sin^2\theta \tag{2.33}$$

where the variables with overbar denote the dimensionless form; δ is the adsorbed polymer layer length scale and λ is the ratio of the polymer layer length scale to the solid core radius.

For a sphere translating through a quiescent fluid, the drag force F_H acting on a sphere

30

surface can be calculated from [29]

$$F_{\text{H}} = \pi\eta \int_0^{\pi} \bar{r}^3 \sin^3 \theta \, \frac{\partial}{\partial \bar{r}} \left(\frac{E^2 \psi}{\bar{r}^2 \sin^2 \theta} \right) \bar{r} d\theta \tag{2.34}$$

This is equivalent to the drag force on the sphere given by Stokes' law taking into account the hydrodynamic layer thickness of the adsorbed polymer layer:

$$F_{\text{H}} = 6\pi\eta U_x (a + L_{\text{H}}) \tag{2.35}$$

where L_{H} is the hydrodynamic layer thickness of adsorbed polymer defined by:

$$L_{\text{H}} = a(A\lambda + B_{\text{T}}\lambda^2) \tag{2.36}$$

Therefore, L_{H} represents the impermeable adsorbed layer which provides an equivalent drag force as the adsorbed polymer thickness of δ. By combining equations (2.34)-(2.36) after solving equation (2.7) and (2.31) for ψ and ψ^*, one can obtain parameters A and B_{T}.

The solutions of equations (2.7) and (2.31) are obtained by the expansion in λ and then match these expansions at the outer edge of polymer layer.

The solution for the flow outside the adsorbed layer is given by:

$$\psi = \left(\frac{1}{2}\bar{r}^2 + \frac{C}{\bar{r}} + D\bar{r} \right) U_x \sin^2 \theta \tag{2.37}$$

where the constants C and D are approximated by expanding in λ:

$$C = C_0 + \lambda C_1 + \lambda^2 C_2 + ... \tag{2.38a}$$

$$D = D_0 + \lambda D_1 + \lambda^2 D_2 + ... \tag{2.38b}$$

Within the polymer adsorbed layer, a solution to equation (2.31) is sought in the form

$$\psi^* = [F_0(y) + \lambda F_1(y) + \lambda^2 F_2(y) + ...] U_x \sin^2 \theta \tag{2.39}$$

with the boundary condition at the solid core surface (no slip condition)

$$y = 0: \quad F_n = \frac{dF_n}{dy} = 0 \tag{2.40}$$

31

where a new variable is introduced as $y = \dfrac{\bar{r} - 1}{\lambda}$. Substituing equation (2.39) into equation (2.31)

and collecting terms of equal order in λ generates the equations, which must be solved for $F_n(y)$. The unknown boundary conditions for F_n at $y \to \infty$, the interface of the polymer layer and the fluid, and the constants C_n and D_n are obtained by matching equation (2.37) with equation (2.39) at equivalent order in λ according to the assumption of the continuity of the velocity and stress field, that is at the outer edge:

$$\lim_{y \to \infty} \psi^* = [\psi]_{r \to 1 + \lambda y} \tag{2.41}$$

After performing this matching, the constants are obtained as follows:

$$A = -\frac{4}{3} D_1 \tag{2.42}$$

$$B_T = \frac{D_2}{D_1} \tag{2.43}$$

$$D_0 = -\frac{3}{4} \tag{2.44}$$

$$D_1 = \frac{1}{2} \lim_{y \to \infty} \left(\frac{dF_2}{dy} - \frac{3}{2} y \right) \tag{2.45}$$

$$D_2 = \frac{1}{2} \lim_{y \to \infty} \left(F_2 + \frac{dF_3}{dy} \right) \tag{2.46}$$

$$\bar{\eta}^* \frac{d}{dy} \left(\frac{d^2 F_2}{dy^2} \right) - \frac{\delta^2}{k^2} \frac{dF_2}{dy} = 0 \tag{2.47}$$

$$y \to \infty : \frac{d^2 F_2}{dy^2} \to \frac{3}{2} \tag{2.48}$$

$$\bar{\eta}^* \frac{d}{dy} \left(\frac{d^2 F_3}{dy^2} \right) - \frac{\delta^2}{k^2} \frac{dF_3}{dy} = -\frac{3}{2} \tag{2.49}$$

32

$$y \to \infty: \quad \frac{d^2F_3}{dy^2} \to -\frac{3}{2}y - 2D_1 \qquad (2.50)$$

Equations (2.47) and (2.49) have to be solved numerically requiring that the dependence of k on y

is known. Defining the new variables: $G = -\frac{2}{3}\frac{dF_2}{dy}$ and $H = -\frac{2}{3}\frac{dF_3}{dy}$, equation (2.47) and (2.49)

are transformed to:

$$\bar{\eta} \cdot \frac{d}{dy}\left(\frac{dG}{dy}\right) - \frac{\delta^2}{k^2}G = 0 \qquad (2.51)$$

$$y = 0: \quad G = 0 \qquad (2.52)$$

$$y \to \infty: \quad \frac{dG}{dy} \to -1 \qquad (2.53)$$

$$\bar{\eta} \cdot \frac{d}{dy}\left(\frac{dH}{dy}\right) - \frac{\delta^2}{k^2}H = 1 \qquad (2.54)$$

$$y = 0: \quad H = 0 \qquad (2.55)$$

$$y \to \infty: \quad \frac{dH}{dy} \to y - A \qquad (2.56)$$

After solving for parameters G and H, A and B_T can be obtained from:

$$A = \lim_{y \to \infty}(G + y) \qquad (2.57)$$

$$B_T = \frac{1}{A}\left[\lim_{y \to \infty}\left(H - \frac{y^2}{2} + Ay\right) + \int_0^\infty (G + y - A)dy\right] \qquad (2.58)$$

Coefficient A which represents the hydrodynamic thickness of the adsorbed layer is independent of the type of flow and always positive. Whereas B_T is the coefficient that takes into account the degree of curvature of the substrate surface.

33

2.2.1.2 Hydrodynamics of a Composite Sphere in Poiseuille Flow

According to Faxen's law, if a rigid spherical particle with radius a translates with velocity v_p through an unbounded fluid which is in motion at infinity with velocity U_∞, then the hydrodynamic force on the sphere is [29]

$$\mathbf{F}_H = 6\pi\eta a([\mathbf{U}_x]_0 - \mathbf{v}_p) + \eta\pi a^3(\nabla^2\mathbf{U}_x)_0 \tag{2.59}$$

where the subscript o implies evaluation at the location of the sphere center. For a composite sphere, Anderson and Solomentsev [30] have obtained a modified version of Faxen's law that accouts for the adsorbed layer on the particle:

$$\mathbf{F}_H = 6\pi\eta a(1 + A\lambda + B_T\lambda^2)([\mathbf{U}_x]_0 - \mathbf{v}_p) + \pi\eta a^3(1 + 3A\lambda + B_Q\lambda^2)(\nabla^2\mathbf{U}_x)_0 \tag{2.60}$$

where the coefficients A is given by equation (2.57) and B_T and B_Q are given by:

$$B_T = A^2 + 2\int_0^\infty (G - A + y)dy \tag{2.61}$$

$$B_Q = 3A^2 \tag{2.62}$$

Note that B_T obtained by equation (2.61) is equivalent to the one calculated from equation (2.58). However, in equation (2.61), B_T can be calculated without having to determine a function H.

For a composite particle suspended in Poiseuille flow, the force exerted on a translating composite sphere will be:

$$F_z = 6\pi\eta a(1 + A\lambda + B_T\lambda^2)\left[2v_m\left(1 - \frac{r^2}{R_o^2}\right) - v_{pz}(r)\right] - \pi\eta a^3(1 + 3A\lambda + B_Q\lambda^2)\frac{8v_m}{R_o^2} \tag{2.63}$$

where R_o is the tube radius, v_m is the average velocity of the fluid and v_{pz} is the local axial velocity of the particle.

34

2.2.1.3 Permeability of Adsorbed Polymer Layer

An adsorbed polymer can be visualized as a porous medium of random hydrodynamically interacting obstacles of polymer segments. The permeability of an adsorbed polymer layer depends upon the conformations of the polymer chains, which for a flexible homopolymer, can be configured as loop, train, and tail as shown in Figure 2-2. The different conformations of adsorbed polymers give rise to the variation of a volume fraction of polymer segments generally in the direction normal to the adsorbing surface. Quantitatively, the permeability of the adsorbed polymer can be expressed as [31]:

$$\frac{1}{k^2} = \frac{1}{c}\phi f(\phi)$$

(2.64)

where ϕ is a local volume fraction of polymer segments and f is the function of the polymer segment volume fraction which describing the hydrodynamic interaction between the segments. Anderson and Kim [22] suggested an empirical function for f, which is the combination of a modified Brinkman equation at low ϕ and the Blake-Kozeny equation at high ϕ:

$$f = 1 + 2.121\phi^{1/2} + 0.84\phi\ln\phi + 16.45\phi \quad \text{for } \phi < 0.29$$

(2.65)

$$f = \frac{8.34\phi}{(1-\phi)^3} \quad \text{for } \phi > 0.29$$

For a free draining polymer segment, $f = 1$ which takes place for $\phi \rightarrow 0$ and $f \rightarrow \infty$ indicates a non-draining of polymer segment. c is a constant related to the size of the polymer segment. If one considers the polymer segment as a hard sphere of diameter a, c is equal to $a^2/18$ [32].

Due to the different chain conformations on the adsorbing surface, the volume fraction of polymer segments is not uniform throughout the adsorbed layer but instead it is higher close to the adsorbing surface, where most conformations are loops and trains, and decreases with the distance from the surface toward zero at the outer edge of the layer, where the chain conformation

35
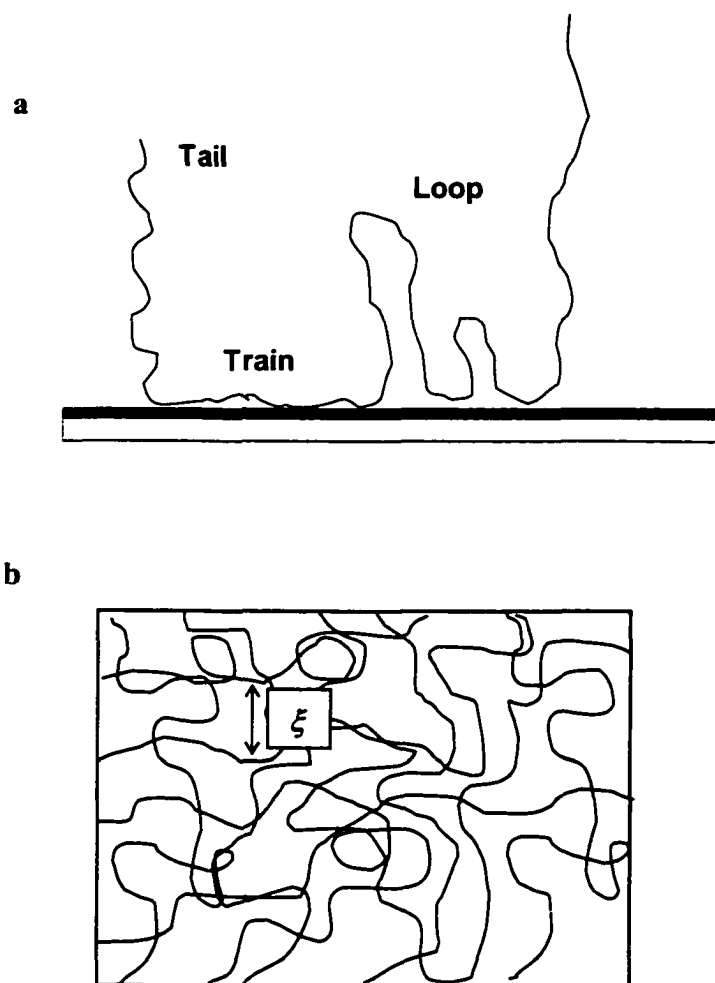
Figure 2-2: Conformations of adsorbed homopolymer (a) and characteristic mesh size (ξ) of polymer molecules in a semi-dilute polymer solution (b).

is mostly tails. For randomly adsorbed homopolymer, theoretical analysis suggested an exponential function form for the polymer segment distribution [33]. Hence, a polymer segment volume fraction profile can be represented as [34]:

$$\phi = \phi_0 \exp\left(-\frac{x}{\delta}\right)$$ (2.66)

where ϕ_0 is the volume fraction of polymer segments at the adsorbing surface, x is the normal distance from the adsorbing surface and δ is a characteristic decay length, which is comparable to an adsorbed layer thickness. The difficulty that arises with the exponential form of polymer segment volume fraction is that $\phi \to 0$ only when $x \to \infty$ but one requires that the concentration of polymer segments is zero outside the adsorbed layer. However, the parabolic function can provide a simple fit to the exponential function and yield a zero concentration of polymer segment at a finite thickness of the adsorbed layer [35,36]:

$$\phi = \phi_0 \left(1 - \frac{x}{\delta}\right)^2$$ (2.67)

The volume fraction of polymer segments at the adsorbing surface, ϕ_0, can be estimated from the adsorbed amount of polymer per unit area, Γ, which can be obtained from the adsorption isotherm; that is,

$$\Gamma = \frac{M}{NN_A} \int_0^\delta \frac{\phi}{(\pi a^3 / 6)} dx$$ (2.68)

where M is a molecular weight of polymer, N is a number of polymer segments per polymer chain and N_A is Avogadro's number. Substituting ϕ into equation (2.67), one obtains

for an exponential function of ϕ:
$$\phi_0 = \left(\frac{\Gamma NN_A}{M}\right)\left(\frac{\pi a^3}{6}\right)\left(\frac{1}{\delta[1 - \exp(-1)]}\right)$$ (2.69)

37

and for a parabolic function:

$$\phi_o = \left(\frac{\Gamma N N_A}{M}\right)\left(\frac{\pi a^3}{6}\right)\left(\frac{3}{\delta}\right)$$

(2.70)

Alternatively, if one assumes that the concentration of polymer chains in an adsorbed layer is high enough for the polymer chains to start overlapping, the adsorbed layer can be represented by a network of entangled chains, which form a porous medium with the permeability related to a characteristic mesh size ξ (see Figure 2-2) of the entangled polymer molecules in a semi-dilute regime [37]:

$$k^2 = \xi^2(\phi) f$$

(2.71)

According to the scaling theory, the characteristic mesh size ξ is given by [38]:

$$\xi = a_n \phi^{-3/4}$$

(2.72)

where a_n is a length comparable to a monomer size, which for ethylene oxide monomer is equal to 2.78 °A [39]. Note that this expression gives $k^2 \sim \phi^{-3/2}$ instead of $k^2 \sim \phi^{-1}$.

2.2.1.4 Validity of Asymptotic Solution

Since asymptotic solution allows us to estimate the drag force exerted on a polymer-adsorbed particle even if the permeability is not uniform, this solution is preferable over the analytical solution which is limited to the case of a constant permeability only. However, as pointed out by Anderson and Kim [22], the asymtotic solution is valid in the limit of $\lambda \to 0$. The validity of this solution was verified by comparing the drag force obtained from the asymptotic method to that force calculated analytically at different layer thicknesses giving a constant permeability of the adsorbed layer in a free draining limit. This is shown in Table 2-1. Surprisingly, the ratio of the drag force calculated from the asymptotic approch and analytical solution was very close to 1 even though the thickness of the adsorbed layer is comparable to the particle radius. This provides us with some confidence to employ the asymptotic method [22] in

38

the calculations dealing with the transport of polymer-adsorbed particles.

Table 2-1: Asymptotic vs. Analytical Solutions for Drag Force Past a Composite Sphere

δ/a	A	B_T	Ω	$F_{asymptotic}/F_{analytical}$
0.01	0.5353	-0.1269	0.9954	1.000
0.1	0.7309	-0.0597	0.9750	1.000
1	0.8485	-0.0154	0.9176	0.999

2.2.2 CHDF Dynamic Model

The development of the concentration of the particles dispersed in Poiseuille flow is governed by the continuity equation:

$$\frac{\partial C}{\partial t} + \nabla \cdot \mathbf{J} = 0 \tag{2.73}$$

where C is the particle concentration and $\mathbf{J}$ is a vector representing a total flux of particle. For a dilute system where there are no particle-particle interactions, this consists of a convective flux due to the fluid velocity, diffusive flux arising from the particle concentration gradient, and the force-induced flux from the interactions between the particle and boundary wall; that is,

$$\mathbf{J} = C\mathbf{v}_p + (-\mathbf{D} \cdot \nabla C) + \frac{C\mathbf{D}}{kT} \cdot \sum (\mathbf{F} - \nabla\Phi) \tag{2.74}$$

where $\mathbf{v}_p$ is a vector of the local particle velocities, $\mathbf{D}$ is a particle diffusivity tensor, $\Sigma(\mathbf{F}\text{-}\nabla\Phi)$ is the total particle-wall interaction forces, and Φ is the particle-wall interaction potential. Since the dynamic force, $\mathbf{F}$, (e.g., inertial force and electrokinetic lift force) can be described in terms of the particle velocity by equating it to the Stokes hydrodynamic drag force, it is conceivable to describe the total flux as:

$$\mathbf{J} = C\mathbf{v}_p + (-\mathbf{D} \cdot \nabla C) + \frac{C\mathbf{D}}{kT} \cdot \nabla\Phi \tag{2.75}$$

39

where Φ is the sum of the particle-wall potential and $\mathbf{v_p}$ includes the velocity of the particle due to the dynamic forces.

For the flow through a microcapillary, a cylindrical coordinate system (r, θ, z) is appropriate and thus the continuity equation is expressed as:

$$\frac{\partial C}{\partial t} + \frac{1}{r}\frac{\partial}{\partial r}\left\{ r\left[Cv_{pr} - D_r\frac{\partial C}{\partial r} + \frac{CD_r}{kT}\left(-\frac{\partial \Phi}{\partial r} \right) \right] \right\} + \frac{\partial}{\partial z}\left(Cv_{pz} - D_z\frac{\partial C}{\partial z} \right) = 0 \qquad (2.76)$$

where v_{pr} and v_{pz} are the local particle velocities in the radial and axial directions, respectively. Normally, since the axial diffusion of the particles is relatively small compared to the axial convection term, the second derivative in the z direction is neglected. Equation (2.76) is subjected to the following boundary conditions:

$$r = 0: \qquad \frac{\partial C}{\partial r} = 0 \qquad\qquad\qquad\qquad\qquad\qquad\qquad\qquad (2.77)$$

$$r = R_o - b: \qquad J_r = Cv_{pr} - D_r\frac{\partial C}{\partial r} + \frac{CD_r}{kT}\left(-\frac{\partial \Phi}{\partial r} \right) = 0 \qquad\qquad (2.78)$$

where b represents a particle radius; in the case of the composite sphere, the radius will include the thickness of the adsorbed layer. Equation (2.77) indicates the symmetry of the particle concentration at the tube center while equation (2.78) implies that the capillary wall is impermeable, therefore, there is no flux across the wall. The capillary tube is assumed to be long enough that there are no end effects. The initial concentration of the particles is zero indicating that there are no particles present in the tube at $t = 0$.

2.2.2.1 Local Particle Velocity

The axial particle velocity for a neutrally buoyant polymer-adsorbed particle in the Poiseuille flow field can be obtained by setting the force in equation (2.63) equal to zero; that is,

40

$$v_{pz}(r) = 2v_m\left(1 - \frac{r^2}{R_o^2}\right) - \frac{4}{3}v_m\kappa^2 \frac{(1 + 3A\lambda + B_Q\lambda^2)}{(1 + A\lambda + B_T\lambda^2)} \tag{2.79}$$

where the first term is the laminar unperturbed flow profile of the fluid, which has a mean velocity v_m and κ is the ratio of the particle core radius a to the capillary radius R_o. This suggests that a particle suspended in a fluid undergoing Poiseuille flow travels at a velocity less than the axial velocity of the undisturbed fluid considering at the same distance from the tube wall as the particle's center of mass.

This expression of the axial velocity of the particle assumed a negligible effect from the boundary that is in the case of κ is very small. To account for the presence of the boundary, the axial particle velocity is multiplied by the wall correction factor K_A [29]

$$K_A = \frac{1}{1 + b_1\left(\frac{\kappa}{1 - (r/R_o)}\right) + b_3\left(\frac{\kappa}{1 - (r/R_o)}\right)^3 + O\left(\frac{\kappa}{1 - (r/R_o)}\right)^4} \tag{2.80}$$

in which for a composite sphere moving parallel to a single plane wall [30]:

$$b_1 = -\frac{3}{4}C_1, \qquad b_3 = -\frac{1}{80}N^* + \frac{1}{4}C_3 \tag{2.81}$$

where

$$N^* = -5(1 + 3A\lambda + B_Q\lambda^2) \tag{2.82}$$

$$C_1 = \frac{3}{4}\left(1 + A\lambda + B_T\lambda^2\right) \tag{2.83}$$

$$C_3 = \frac{3}{4}\left[1 + 3A\lambda + (3B_T + 2b_{n1})\lambda^2\right] \tag{2.84}$$

with

$$b_{n1} = -3\int_0^\infty (G - A + y)dy \tag{2.85}$$

41

2.2.2.2 Diffusivity of Polymer-Adsorbed Particle

According to the Stokes-Einstein equation [40], the translation diffusivity of a rigid particle can be related to the hydrodynamic drag force of the fluid exerted on it. Hence, the diffusivity of a polymer-adsorbed particle can be obtained from:

$$\frac{D_{cs}}{D_{hs}} = \frac{F_{hs}}{F_{cs}} \tag{2.86}$$

where D_{cs} is the translation diffusivity of a composite sphere and D_{hs} is the translation diffusivity of a hard sphere which is defined as: $D_{hs} = \frac{k_B T}{6\pi\eta a}$ where k_B is the Boltzman's constant and T is the absolute temperature. F_{cs} is the hydrodynamic drag force exerted on the composite sphere given by equation (2.35). F_{hs} is the Stokes drag force on the hard sphere that is equal to $6\pi\eta a U_\infty$. Therefore, the translational diffusivity of the composite sphere is given as:

$$D_{cs} = \frac{aD_{hs}}{(a + L_H)} = \frac{D_{hs}}{(1 + A\lambda + B_T\lambda^2)} \tag{2.87}$$

There are two limiting cases for the diffusivity of the composite sphere: for high permeability of the adsorbed layer, $k \rightarrow \infty$, D_{cs} would be approximately D_{hs} because of a low retardation of the adsorbed layer to the flow and for low permeability, $k \rightarrow 0$, the composite sphere will behave like a hard sphere with an increased radius of $a(1+\lambda)$. This can be seen in Figure 2-3 where the ratio of D_{cs}/D_{hs} is plotted against the normalized parameter δ/k.

For a bounded fluid, the boundary effect is taken into account by divided the diffusivity of the composite sphere by the wall correction factor; that is,

$$D_r = \frac{D_{cs}}{K_A} \tag{2.88}$$

where D_r is the radial component of the particle diffusivity and K_A is calculated from equation (2.80), which for the motion perpendicular to the wall [30]:

42
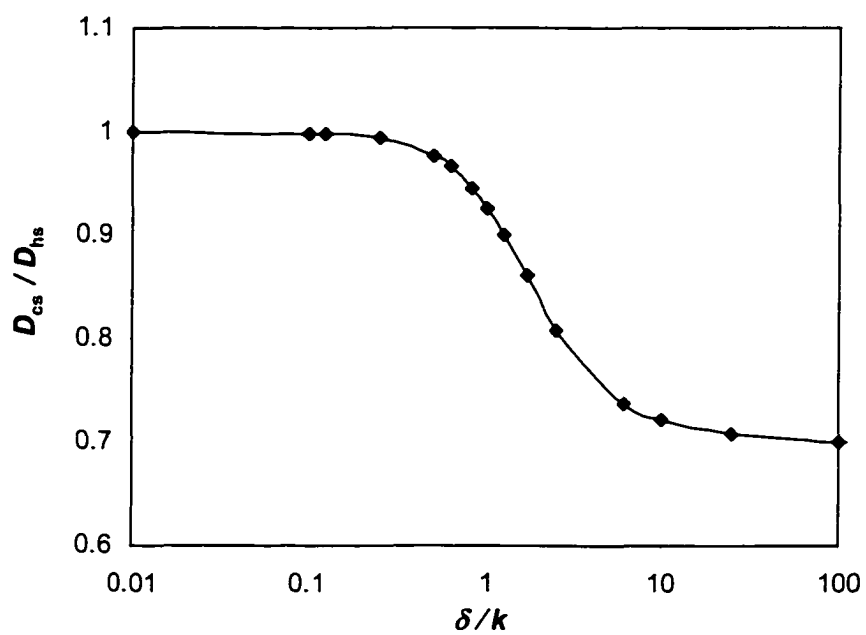
Figure 2-3: Ratio of the translational diffusivity of a composite sphere to that of a hard sphere as a function of the permeability δ/k.

$$b_1 = -\frac{3}{2}C_1, \qquad b_3 = -\frac{1}{20}N^* + C_3 \qquad\qquad (2.89)$$

2.2.2.3 Colloidal Interaction Potential

2.2.2.3.1 Electrostatic Repulsion

Electrostatic repulsion results from the existence of an electrical double layer (EDL) surrounding the particles and the capillary wall. The distance of the electrostatic interaction between two surfaces depends on the Debye length κ_D^{-1} which is strongly affected by the total molar concentration of ionic species in a medium phase C_i. For the case of a symmetric electrolyte of valence z, the Debye length is given by:

$$\kappa_D^{-1} = \left[\frac{\varepsilon_r \varepsilon_o k_B T}{2e^2 z^2 C_i N_A}\right]^{1/2} \qquad\qquad (2.90)$$

where ε_r and ε_o are the relative permittivity of the medium and the permittivity of a vacuum, respectively, e is the elementary electric charge, and N_A is Avogadro's number. Assuming a sphere-plane interaction, an approximate expression for the double layer repulsion covering small to large particle-wall separation distances has been developed by Bell et al. [41] and Ohshima et al. [42]

$$\Phi_{DL} = \frac{32(4\pi\varepsilon_r\varepsilon_o)\left(\frac{kT}{e}\right)^2 \tanh\left(\frac{e\psi_1}{4kT}\right)\tanh\left(\frac{e\psi_2}{4kT}\right) b \exp\left[-\kappa_D R_o\left(1 - \frac{r}{R_o} - \frac{b}{R_o}\right)\right]}{1 + \left[1 - \frac{2\kappa_D b + 1}{(\kappa_D b + 1)^2}\tanh^2\left(\frac{e\psi_2}{4kT}\right)\right]^{1/2}} \qquad\qquad (2.91)$$

where ψ_i is the surface potential of the capillary ($i = 1$), or the particle ($i = 2$) and b is the radius of the composite sphere.

For a particle without an adsorbed polymer layer, the surface potential ψ_{2s} is related to the surface charge density σ_s by [43]:

44

$$\psi_{2s} = \frac{2kT}{ze} \sinh^{-1}\left[\frac{\sigma_s}{\left(8\varepsilon_r\varepsilon_o kTC_iN_A\right)^{1/2}}\right]$$ (2.92)

In the case of a particle with an adsorbed polymer layer, if the thickness of the adsorbed layer is accounted for, the surface potential at the outer edge of adsorbed layer ψ_2 is required in order to calculate the electrostatic repulsion. If the particle is surrounded by an uncharged adsorbed polymer with a thickness δ and the effect of the curvature of the particle is ignored, the surface potential is given by [44]:

$$\psi_2 = \frac{2kT}{ze} \ln\left[\frac{1 + \tanh\left(\frac{ze\psi_{2s}}{4kT}\right)\exp(-\kappa_D\delta)}{1 - \tanh\left(\frac{ze\psi_{2s}}{4kT}\right)\exp(-\kappa_D\delta)}\right]$$ (2.93)

2.2.2.3.2 van der Waals Attraction

The van der Waals attractive potential between a sphere and a plane wall was originally estimated by Hamaker [45] based on the unretarded attractive energy between two atoms. To account for the retarded effect for a large surface separation, Gregory [46] has obtained a semi-empirical approximation for the retarded attractive van der Waals potential:

$$\Phi_{vw} = -\frac{A_H b}{6R_o\left(1 - \frac{r}{R_o} - \frac{b}{R_o}\right)}\left[\frac{1}{1 + 14\frac{R_o}{\lambda_o}\left(1 - \frac{r}{R_o} - \frac{b}{R_o}\right)}\right]$$ (2.94)

where A_H is Hamaker's constant and λ_o is the characteristic wavelength which is typically equal to 100 nm. Hamaker's constant can be estimated from refractive index and dielectric constant data [39]; for a body 1 (capillary wall) interacting with a body 2 (particle) across mediums 3 (solvent) and 4 (adsorbed polymer layer on a particle)

45

$$A_H = \frac{3h\nu_e}{8\sqrt{2}} \frac{(n_2^2 - n_4^2)(n_1^2 - n_3^2)}{(n_2^2 + n_4^2)^{1/2}(n_1^2 + n_3^2)^{1/2}} \left[\frac{1}{(n_2^2 + n_4^2)^{1/2} + (n_1^2 + n_3^2)^{1/2}} \right] +$$

$$\frac{3}{4} kT \frac{(\varepsilon_2 - \varepsilon_4)(\varepsilon_1 - \varepsilon_3)}{(\varepsilon_2 + \varepsilon_4)(\varepsilon_1 + \varepsilon_3)} \tag{2.95}$$

where h is Planck's constant, ν_e is the main electronic adsorption frequency which is equal to 3×10^{15} 1/s, n is the refractive index and ε is the dielectric constant. Since the polymer adsorbed layer (medium 4) contains a mixture of polymer and solvent molecules, the reflactive index and dielectric constant of this phase are estimated by:

$$n_4 = \phi_{poly}(n_{poly} - n_3) + n_3 \tag{2.96}$$

where ϕ_{poly} is the volume fraction of polymer in the adsorbed polymer layer. To calculate the dielectric constant, n in equation (2.96) is replaced by ε.

2.2.2.4 Radial Inertial Force

The radial inertial force is responsible for driving the particles toward a certain equilibrium radial position at a distance of about 60 % of the tube radius measured from the tube axis [47,48]. Since there is no rigorous theoretical analysis for a composite sphere in a flow under relatively high Reynolds numbers where the inertial effect is prominent, the well-established radial migration velocity for a rigid sphere is adopted here. Presumebly, the composite sphere behaves like the solid sphere with an increased radius of L_H (equivalent hydrodynamic thickness which provides the same hydrodynamic response as the adsorbed layer with thickness δ) .

For a freely rotating, neutrally buoyant particle suspended in tube flow, the particle radial migration velocity v_{pr} due to the inertial effect of the fluid can be calculated by [49,50]

$$v_{pr} = \frac{6\pi b}{v} \left[V_p^2 h\left(\frac{r}{R_o}\right) - V_p v_m g\left(\frac{r}{R_o}\right) + \frac{5}{9} v_m^2 \left(\frac{(a + L_H)}{R_o}\right)^2 \left(f_1\left(\frac{r}{R_o}\right) + f_2\left(\frac{r}{R_o}\right) \right) \right] \tag{2.97}$$

46

where v is the kinematic viscosity of the fluid, and V_p is the velocity of the particle relative to an undisturbed fluid. V_p is represented by the translational slip velocity of the particle in Poiseuille flow, which is equal to the second term on the right-hand size of equation (2.79) [2]. The functions h, g, f_1 and f_2 represent volume integrals containing the Green's function for creeping flow in a circular tube, which are not evaluated explicitly. However, the empirical expressions for these functions can be obtained as follows [2].

$$h = -\frac{0.207}{6\pi}\left[\left(\frac{r}{R_o}\right) - 0.53\left(\frac{r}{R_o}\right)^2\right] \tag{2.98}$$

$$g = -\frac{0.144}{6\pi}\left[\left(\frac{r}{R_o}\right) - \left(\frac{r}{R_o}\right)^6\right] \tag{2.99}$$

$$f_1 + f_2 = \frac{0.721}{\pi}\left(\frac{r}{R_o}\right)\left[0.71 - \left(\frac{r}{R_o}\right)\right]\exp\left[0.786\left(\frac{r}{R_o}\right)\right] \tag{2.100}$$

2.2.2.5 Computational Algorithm

To solve the unsteady state PDE problem of equation (2.76), the Laplace transform was applied to the time dependence term together with the initial condition, which requires a zero concentration inside the capillary. Therefore, the equation becomes:

$$v_{pz}\frac{\partial \overline{C}}{\partial z} = D_r\left[\frac{1}{r}\frac{\partial}{\partial r}\left(r\frac{\partial \overline{C}}{\partial r}\right)\right] + \left(\frac{dD_r}{dr} - v_{pr} + \frac{D_r}{kT}\frac{d\Phi}{dr}\right)\frac{\partial \overline{C}}{\partial r}$$
$$+ \overline{C}\left[-\frac{v_{pr}}{r} - \frac{dv_{pr}}{dr} + \frac{1}{kT}\left(D_r\frac{d^2\Phi}{dr^2} + \frac{D_r}{r}\frac{d\Phi}{dr} + \frac{dD_r}{dr}\frac{d\Phi}{dr}\right) - s\right] \tag{2.101}$$

where the Laplace transform of variables are denoted by an overbar and the transform s variable is a complex number.

The orthogonal collocation method was applied for approximation of spatial (radial)

47

variables [51,52]. The radial concentration was represented by a polynomial of degree N:

$$C(r) = \sum_{j=1}^{N+1} a_j r^{2(j-1)} \tag{2.102}$$

where N is the number of interior collocation points and a_1 is taken as 1. The inner collocation

points N are equal to the zeros of Jacobi polynomial of degree N; $P_N^{(\alpha,\beta)}$ with $\alpha = \beta = 0$. $P_N^{(\alpha,\beta)}$ has

N distinct, real-values zeros in the domain $[0,1]$ corresponding to $r = 0$ to $r = R_o - b$.

Considering the solution and the derivatives at the each collocation point:

$$C(r_i) = \sum_{j=1}^{N+1} r_i^{2j-2} a_j \tag{2.103}$$

$$\frac{dC(r_i)}{dr} = \sum_{j=1}^{N+1} \frac{dr_i^{2j-2}}{dr} a_j \tag{2.104}$$

$$\nabla^2 C(r_i) = \sum_{j=1}^{N+1} \nabla^2 r_i^{2j-2} a_j \tag{2.105}$$

These can be represented in matrix form, that is,

$$\mathbf{C} = \mathbf{Q} \cdot \mathbf{a} \tag{2.106}$$

$$\frac{d\mathbf{C}}{dr} = \mathbf{X} \cdot \mathbf{a} \tag{2.107}$$

$$\nabla^2 \mathbf{C} = \mathbf{Y} \cdot \mathbf{a} \tag{2.108}$$

where $Q_{ij} = r_i^{2j-2}$, $X_{ij} = \dfrac{dr_i^{2j-2}}{dr}$ and $Y_{ij} = \nabla^2 r_i^{2j-2}$. Solving for $\mathbf{a}$, the derivatives can be defined as:

$$\frac{d\mathbf{C}}{dr} = \mathbf{X}\mathbf{Q}^{-1} \cdot \mathbf{C} = \mathbf{A} \cdot \mathbf{C} \tag{2.109}$$

$$\nabla^2 \mathbf{C} = \frac{1}{r}\frac{d}{dr}\left(r\frac{d\mathbf{C}}{dr}\right) = \mathbf{Y}\mathbf{Q}^{-1} \cdot \mathbf{C} = \mathbf{B} \cdot \mathbf{C} \tag{2.110}$$

Now, equation (2.101) was discretized with respect to the radial coordinate using orthogonal

48

collocation and can be expressed as:

$$v_{pz}\frac{\partial \overline{C}_i}{\partial z} = D_{r,i}\left(\sum_{j=1}^{N+1} B_{ij}\overline{C}_j\right) + \left(\frac{dD_{r,i}}{dr} - v_{pr,i} + \frac{D_{r,i}}{kT}\frac{d\Phi_i}{dr}\right)\left(\sum_{j=1}^{N+1} A_{ij}\overline{C}_j\right)$$
$$+ \overline{C}_i\left[-\frac{v_{pr,i}}{r} - \frac{dv_{pr,i}}{dr} + \frac{1}{kT}\left(D_{r,i}\frac{d^2\Phi_i}{dr^2} + \frac{D_{r,i}}{r}\frac{d\Phi_i}{dr} + \frac{dD_{r,i}}{dr}\frac{d\Phi_i}{dr}\right) - s\right]$$

(2.111)

where for $i = 1, 2, 3,..., N+1$ represents the collocation points in the radial coordinate and A_{ij} and B_{ij} are collocation matrices which represent the first and second order derivatives, respectively.

The boundary conditions are:

$$r = 0: \qquad \sum_{j=1}^{N+1} A_{1j}\overline{C}_j = 0$$

(2.112)

$$r = R_o\text{-}b: \quad -D_{r,N+1}\left(\sum_{j=1}^{N+1} A_{N+1,j}\overline{C}_j + \frac{\overline{C}_{N+1}}{kT}\frac{\partial\Phi_{N+1}}{\partial r}\right) + v_{pr,N+1}\overline{C}_{N+1} = 0$$

(2.113)

Equation (2.113) can be solved for $\overline{C}_{N+1}$ and substituting this expression for $\overline{C}_{N+1}$ into the summation in equation (2.111), we obtained N linear, first-order ordinary differential equations:

$$\frac{\partial \overline{C}_i(z,s)}{\partial z} = \frac{D_{r,i}}{v_{pz,i}}\left[\sum_{j=1}^{N}\left(B_{ij} - \frac{B_{i,N1}A_{N1,j}}{A_{N1,N1} - \frac{v_{pr,N1}}{D_{r,N1}} + \frac{1}{kT}\frac{\partial\Phi_{N1}}{\partial r}}\right)\overline{C}_j\right]$$
$$+ \frac{1}{v_{pz,i}}\left(\frac{dD_{r,i}}{dr} - v_{pr,i} + \frac{D_{r,i}}{kT}\frac{d\Phi_i}{dr}\right)\left[\sum_{j=1}^{N}\left(A_{ij} - \frac{A_{i,N1}A_{N1,j}}{A_{N1,N1} - \frac{v_{pr,N1}}{D_{r,N1}} + \frac{1}{kT}\frac{\partial\Phi_{N1}}{\partial r}}\right)\overline{C}_j\right]$$

(2.114)

$$+ \frac{\overline{C}_i}{v_{pz,i}}\left[-\frac{v_{pr,i}}{r} - \frac{dv_{pr,i}}{dr} + \frac{1}{kT}\left(D_{r,i}\frac{d^2\Phi_i}{dr^2} + \frac{D_{r,i}}{r}\frac{d\Phi_i}{dr} + \frac{dD_{r,i}}{dr}\frac{d\Phi_i}{dr}\right) - s\right]$$

where $i = N1 \equiv N+1$, the collocation point at the boundary. Equation (2.114) can be written in matrix notation as:

49

$$\frac{d\overline{C}(z,s)}{dz} = P(s)\cdot\overline{C}(z,s) \tag{2.115}$$

The solution to this matrix equation for an arbitrary longitudinal position is given by:

$$\overline{C}(z,s) = [M(s)\exp(\Lambda(s)z)M(s)^{-1}]\overline{C}_o(s) \tag{2.116}$$

where the matrices $M(s)$ and $\Lambda(s)$ result from the diagonalization of the matrix $P(s)$:

$$P(s) = M(s)\Lambda(s)M(s)^{-1} \tag{2.117}$$

$\Lambda(s)$ is a diagonal matrix of eigenvalues of $P(s)$ and $M(s)$ is a matrix of the eigenvectors of $P(s)$.

The input signal in equation (2.116) is an initial pulse of sinusoidal waveform of length w (slug length). Its frequency was made discrete by setting $s = i\omega$ and approximating $\overline{C}_o$ as a truncated Fourier series before performing the diagonalization shown in equation (2.117). The output response at each collocation point in the time domain $C_i(z,t)$ can be obtained by performing the inverse fast Fourier transform. The cross-sectionally averaged concentration at a particular axial position was calculated and the resulting concentration profiles were superimposed to create the simulated fractogram. The average concentration of particles in the radial direction is expressed in matrix notation as:

$$\langle C \rangle = \frac{\int_0^1 Crdr}{\int_0^1 rdr} = 2W\cdot C \tag{2.118}$$

where the matrix W is defined by:

$$W = \left(\int_0^1 Qrdr\right)\cdot Q^{-1} \tag{2.119}$$

The simulated CHDF fractograms for a composite sphere with an isotropic porous shell for various permeabilities are illustrated in Figure 2-4. The low permeability of the porous shell,

50

indicated by a large δ/k, increases the retardation effect for the flow through the shell and thus the composite sphere in the flow field would behave like a rigid sphere with an increased radius. As a result, due to the larger radius, the separation factor for the low permeability composite sphere will be higher; however, the degree of axial dispersion is also larger because of the diffusivity of the particle is reduced. On the contrary, high permeability composite spheres will possess a lower separation factor and degree of axial dispersion because the low retardation effect to the flow produces the hydrodynamic response of the composite sphere toward that of rigid sphere with a smaller radius.

Figure 2-5 demonstrates the effect of a non-uniform adsorbed polymer layer. The volume fraction of polymer segments is expressed in terms of exponential, parabolic, and step functions. As evident from this figure, the concentration difference of polymer segment inside the adsorbed polymer layer does not cause a significant effect on the transport of the composite sphere. A lower concentration of polymer segments toward the outer edge of adsorbed layer as expressed by the exponential and parabolic functions creates a lower hydrodynamic drag force on the composite sphere resulting in a lower degree of axial dispersion.

2.3 Effective Size of PEO-Adsorbed PS Latex Particles

2.3.1 Dynamic Light Scattering

Following the experiments by Kato et al. [11], the thickness of the adsorbed PEO layer (δ) on standard polystyrene (PS) particles was determined experimentally using dynamic light scattering (Nicomp model 370). The thickness of the adsorbed polymer is obtained by subtracting the diameter of the bare particles from the diameter of polymer-adsorbed particles.

Standard PS latex particles were mixed with a certain concentration PEO solutions. The concentrations of the PEO were selected to fall in the plateau region of the adsorption isotherms

51
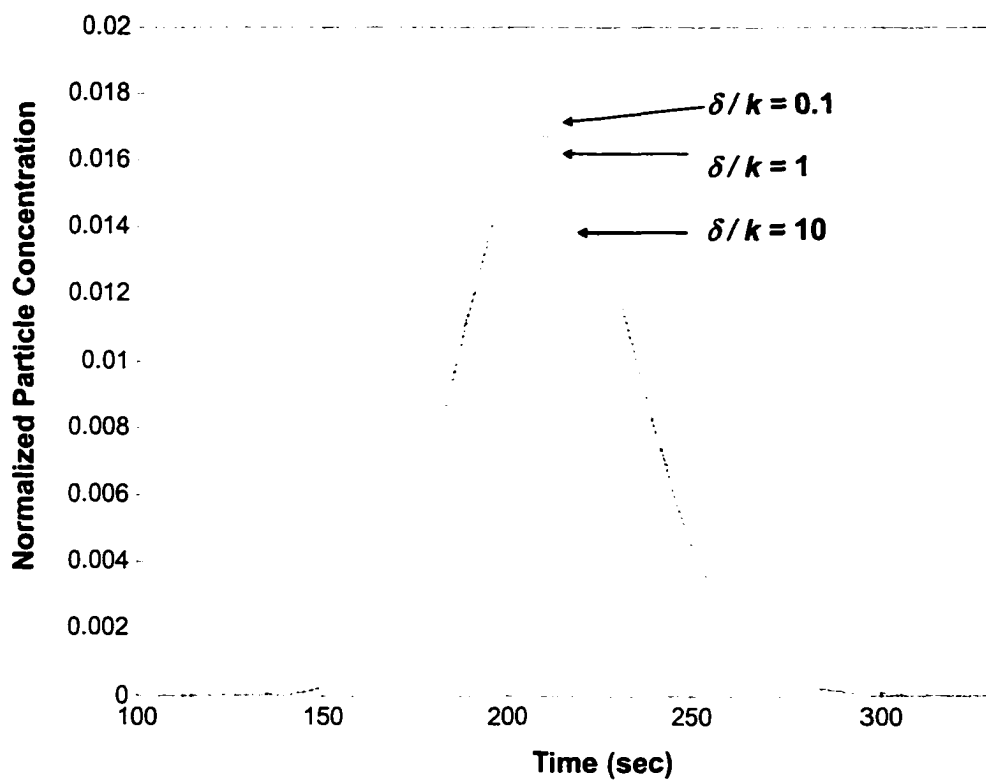
Figure 2-4: Simulated CHDF fractograms of the composite sphere for the different permeabilities; the permeability of adsorbed polymer is assumed isotropic.

52
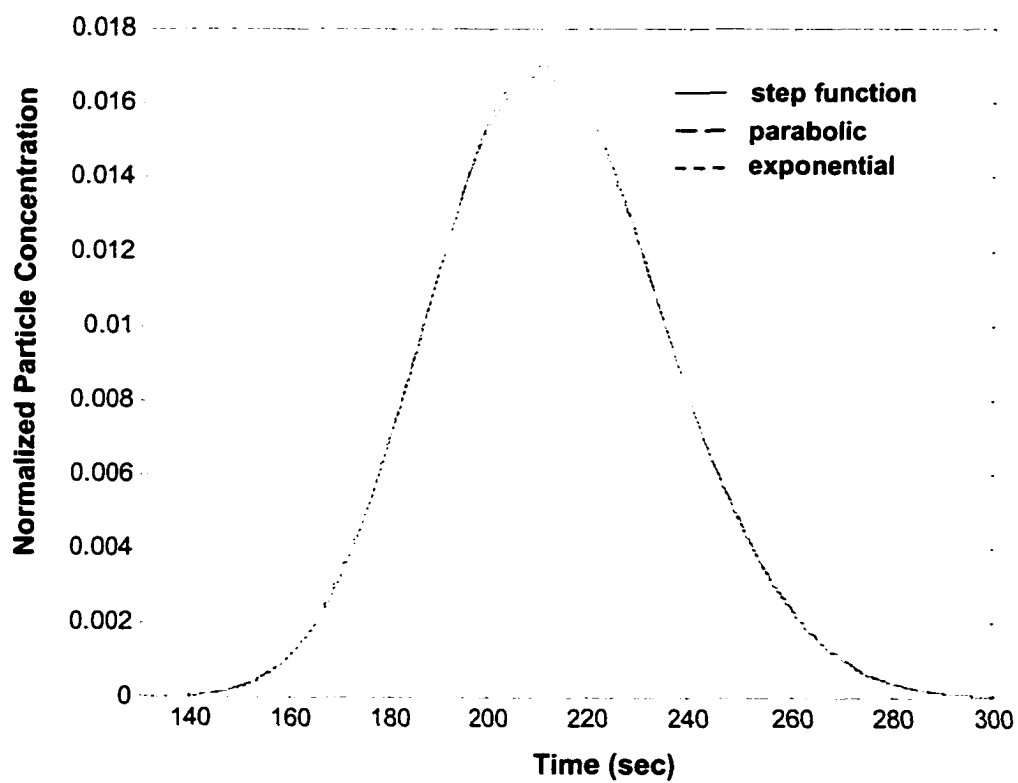
Figure 2-5: Simulated CHDF fractograms of the composite sphere with a non-uniform adsorbed layers.

53

to ensure complete coverage of PEO molecules on the particle surfaces. The mixtures were left overnight (12 hours) before performing the measurement. Since all samples must be diluted by DI water before the measurement, desorption of PEO from particle surfaces may occur. However, all the measurements conducted over a 30-minute period showed a constant diameter of the particles and a consistent particle size distribution indicating an irreversible state of polymer adsorption.

2.3.1.1 Effect of Molecular Weight of PEO

Table 2-2 reports the volume-average particle diameter (D_v) and the mean adsorbed layer thickness for adsorption of various molecular weights of PEO on 234 nm PS latex particles. The results indicate an increase of the particle diameter with the molecular weight of PEO. The dependency of molecular weight of PEO on δ was obtained by plotting $\log(M_w)$ versus $\log(\delta)$. The plot showed a linear relationship as illustrated in Figure 2-6 suggesting a power-law type dependency of δ on the molecular weight of PEO:

$$\delta \propto M_w^a \tag{2.120}$$

Table 2-2: Volume-Average Diameter (D_v) and Mean Adsorbed Layer Thickness (δ) for Adsorption of PEO on PS Latex Particles as Determined by Dynamic Light Scattering

Dispersed Phase	D_v (nm)	δ (nm)
DI Water	256.6 ± 25.4	-
0.1 wt% PEO1	261.6 ± 35.1	2.5
0.1 wt% PEO2	284.1 ± 39.3	13.7
0.1 wt% PEO3	298.6 ± 62.9	21.0
0.1 wt% PEO4	353.5 ± 106.3	48.4

54
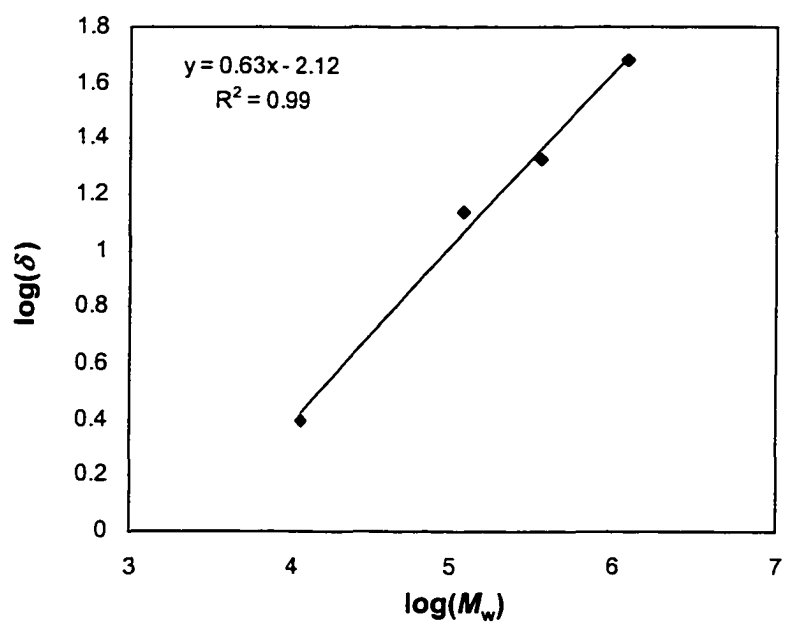
Figure 2-6: Plot of log(δ) vs. log(M_w) for PEO-adsorbed PS particles as determined by dynamic light scattering.

The dependence of δ on the molecular weight of PEO is $M_w^{0.63}$. This power-law relationship between δ and molecular weight of PEO can be used to estimate the size of the PEO-adsorbed particles for other molecular weight of PEO.

Previously, there have been several attempts to determine the exponent a. Experimentally, Baker and Berg [53] obtained the molecular weight dependence of $M_w^{0.43}$ for an adsorbed PEO layer thickness on PS particles while Polverari and van de Ven [12] found the dependence ranging from $M_w^{0.27}$ to $M_w^{0.52}$. As predicted by Flory's theory [54,55] an isolated homopolymer in a θ–solvent and a good solvent have a molecular weight dependence of $M_w^{0.5}$ and $M_w^{0.6}$, respectively (see also equation (2.121)). Therefore, they concluded that the lower molecular weight dependence of the layer thickness is due to a flatter configuration of the adsorbed polymer chain compared to the free random coil of polymer molecule in solvent [12,53]. Killmann et al. [56] used light scattering technique to determine the δ of PEO adsorbed on silica particles. Their result showed a dependence of $M_w^{0.49}$ which is similar to the value of $M_w^{0.56}$ obtained by Kato [11]. However, the higher value of $a = 0.8$ has also been found by Cosgrove et al. [57] and Cohen-Stuart et al. [31].

A large standard deviation on the particle size measurements for the PS particles in PEO3 and PEO4 solutions raised the uncertainty of the results. This deviation may have resulted from the free (unadsorbed) PEO chains and the aggregation of PEO in aqueous solution. If the molecular weight of PEO is high, the coil size of PEO chains in water is comparable to the particle size and can interfere with the light scattering experiment. If one envisages a polymer coil as a rigid sphere with a hydrodynamic radius of R_D, the size of a polymer chain is given by [58]:

$$R_D = \left(\frac{3\pi}{128}\right)^{1/2} \langle r^2 \rangle^{1/2} \tag{2.121}$$

where $\langle r^2 \rangle^{1/2}$ is a root-mean-square end-to-end distance of a polymer molecule. R_D of PEO2

56

calculated from equation (2.121) is equal to 9.7 nm while for PEO4 it is equal to 87.8 nm. Evidently, the coil size of PEO4 polymer chain is comparable to the probe particle size and can be detected by light scattering.

Moreover, PEO can form aggregates in aqueous solution, which can have a molecular weight as high as 50 times the nominal molecular weight of a single molecule [59]. Boils and Hair [60] have shown that PEO aggregates (clusters) can be formed even for very monodisperse PEO samples. Using dynamic light scattering and gel permeation chromatography, Polverari and van de Ven [61] found that PEO clusters diameter were in the range of 0.45 to 0.90 μm independent of the molecular weight.

2.3.1.2 Effect of Particle Size

The hydrodynamic layer thickness of PEO on PS latex particles is also affected by the degree of the curvature. Garvey et al. [62] measured the adsorbed layer thickness for various molecular weights of 88% hydrolyzed poly(vinyl alcohol) adsorbed on PS latex particles. They found that the volume occupied by the adsorbed polymer is the same as that occupied in bulk solution. If the surface area occupied by the polymer molecule is independent of the radius of curvature of the particle [63], then the adsorbed polymer layer must decrease as the particle size decreases. An equivalent thickness can then be calculated:

$$\bar{d} = \frac{\frac{4}{3}\pi(a+\delta)^3 - \frac{4}{3}\pi a^3}{4\pi a^2} \qquad (2.122)$$

where $\bar{d}$ and δ corresponds to the adsorbed layer on a flat surface and partice surface, respectively. The effect of particle size on δ can be seen from Table 2-3 which shows the layer thickness of adsorbed PEO4 on various particle sizes of PS latexes obtained from DLS and the corresponding adsorbed layer thickness on a flat surface calculated from equation (2.122). The

57

concentration of PEO4 used in the experiment was several folds higher than the saturation concentration of PEO on PS particles. The DLS results revealed the increasing thickness of the adsorbed PEO as the particle size of the PS particles increased suggesting the effect of surface curvature on the adsorption of PEO.

Table 2-3: Comparison of Mean Layer Thickness (δ) of Adsorbed PEO4 on Various Particle Sizes of PS Latex Particles Obtained from Dynamic Light Scattering and Values of Adsorbed PEO4 Layer on Flat Surface ($\bar{d}$) Calculated from Equation (2.122)

Particle Radius (nm)	δ (nm)	$\bar{d}$ (nm)
59.5	18.1	24.2
93.6	47.4	75.5
128.3	48.4	68.9
194.5	52.1	67.3

The calculated $\bar{d}$ approached the constant values as particle size increased. This indicates that the effect of curvature is less important when particle being larger. However, the experiment by Greenwood et. al. [64] have suggested that effect of curvature on adsorbed polymer could not be explained fully by conventional geometric arguments in which the volume available to the polymer for a small particle is greater than that for a larger particle. Baker and coworkers [65,66] studied the effect of particle size on the δ of PEO and PEO-poly(propylene) copolymers. Even though they found that δ decreased with particle radius, equation (2.122) was not sufficient to explain the trend which may be due to the specific interactions between polymer and particles.

58

2.3.2 Transport of PEO-Adsorbed Latex Particles in CHDF

As observed from the light scattering measurement, the adsorption of PEO on PS latex particles can cause the enlargement of the latex particles. Apparently, it is expected that this enlarged particle will affect the transport as well as the separation efficiency of the particles in CHDF. It has been shown experimentally that large particles travel faster through a microcapillary compared to the smaller ones because their longer radius excludes them from slower moving fluid near the capillary wall [1]. Due to the thickness of polymer adsorbed layer, PEO-adsorbed latex particles in CHDF should yield greater separation factors compared to particles without PEO adsorbed. However, size exclusion will be in effect only if there is no interaction between the particles and the capillary wall so that the particles can actually transport in close proximity to the wall. The particle-wall repulsions, especially the long range interactions in a low ionic strength eluant i.e., the electrostatic repulsion and the electrokinetic lift force [6], are responsible for repelling the particles away from the wall; therefore the effect of size exclusion might not be prevailing. In order to diminish these long range interactions, high ionic strength NaCl solution (4 mM) was selected as the eluant.

CHDF experiments were performed using 234 nm PS latex particles dispersed in 0.1 % w/w PEO solutions as the samples. Once again, this concentration of PEO was selected to provide full surface coverage of PEO molecules on the particles establishing the stability of the colloidal dispersions. The mixtures of latex particles and 0.1 % w/w PEO solutions were left for at least 12 hours in order to ensure an equilibrium state of the adsorption. Note that, PEO solutions were not used as the eluants in order to eliminate an additional effect due to the viscoelasticity of the polymer solutions.

An irreversible adsorption of PEO was assumed in this experiment because the rate of desorption of PEO from the particle surfaces is very slow in comparison to the rate of particle

59

transport through the microcapillary. High shear inside the capillary may promote the desorption of polymer chains from the particle surfaces, however as the molecular weight increased, the polymer chains make multiple attachments on the surfaces, which make the disengagement of the contacts difficult [67].

Figure 2-7 illustrates the CHDF fractograms of the 234 nm PS latex particles dispersed in 0.1 % w/w solutions of PEO1, PEO2, PEO3 and PEO4. The corresponding values of separation factor (R_f) and theoretical plate height (H_{TP}) are also provided in the figure. The experimental results show a dependency of R_f and H_{TP} on the molecular weight of PEO. Increasing the molecular weight of PEO enhances R_f and decreases H_{TP}. Under conditions of a weak particle-wall interaction, R_f will increase with particle size due to the effect of size exclusion. However, H_{TP} will also increase because of the lower particle diffusivity as the particle size increases. This is in contrast to the experimental results which suggest that as the molecular weight of PEO is increased, increasing R_f and decreasing H_{TP} are due to the migration of particles closer to the center of the capillary.

Since the latex particles were dispersed in mediums (PEO solutions) which have relatively low ionic strength compared to that of the eluant (NaCl solution), we speculated that this low ionic strength of the medium might cause the enhancement of the separation factors. We confirmed this by conducting another CHDF experiment with bare 234 nm particles dispersed in DI water (ionic strength ~ 1×10^{-3} mM) and used the high ionic strength of 4 mM NaCl as eluant. The experimental results are shown in Figure 2-8 which is the plot of separation factor as a function of fluid velocity.

The R_f of PS particles in DI water had values lower than that of PS particles in PEO4 solution indicating that the difference in the ionic strength between the dispersed medium of the latex sample and the eluant is not responsible for the enhancement of the separation factor of the

60
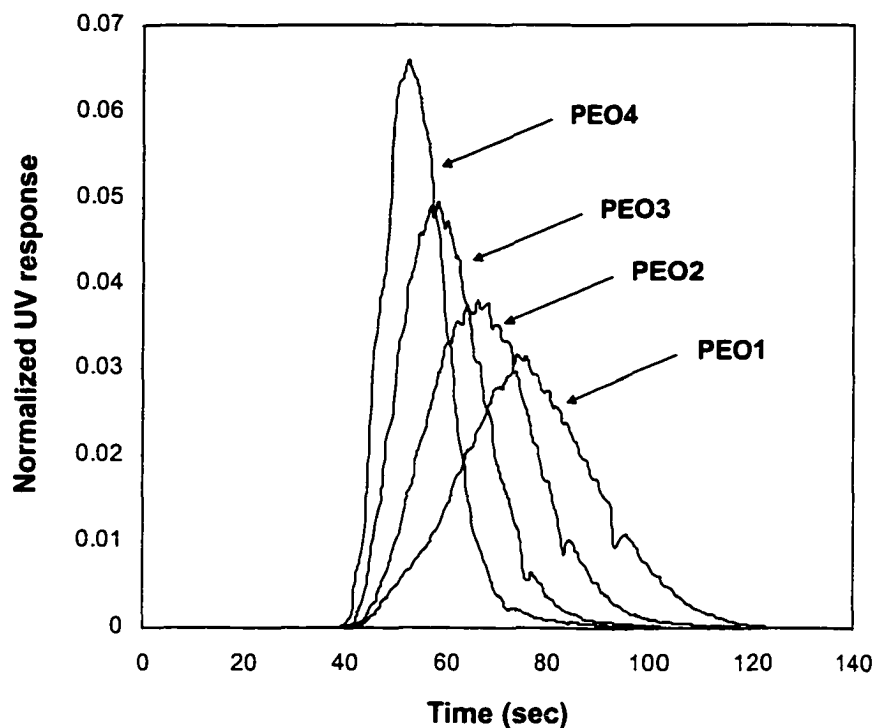
Dispersed Phase of Latex Samples	R_f	H_{TP} (cm)
PEO1	0.98 ± 0.02	11.89 ± 0.21
PEO2	1.09 ± 0.00	9.53 ± 0.52
PEO3	1.27 ± 0.03	7.55 ± 0.19
PEO4	1.39 ± 0.04	5.57 ± 0.90

Figure 2-7: Experimental CHDF fractograms of 234 nm PS latex particles dispersed in 0.1 % w/w PEO1, 0.1 % w/w PEO2, 0.1 % w/w PEO3 and 0.1 % w/w PEO4 solutions; capillary ID = 21.0 µm and length = 402.0 cm, eluant = 4 mM NaCl (conductivity K = 450 µS/cm) and the average velocity = 5.3 cm/s.

61
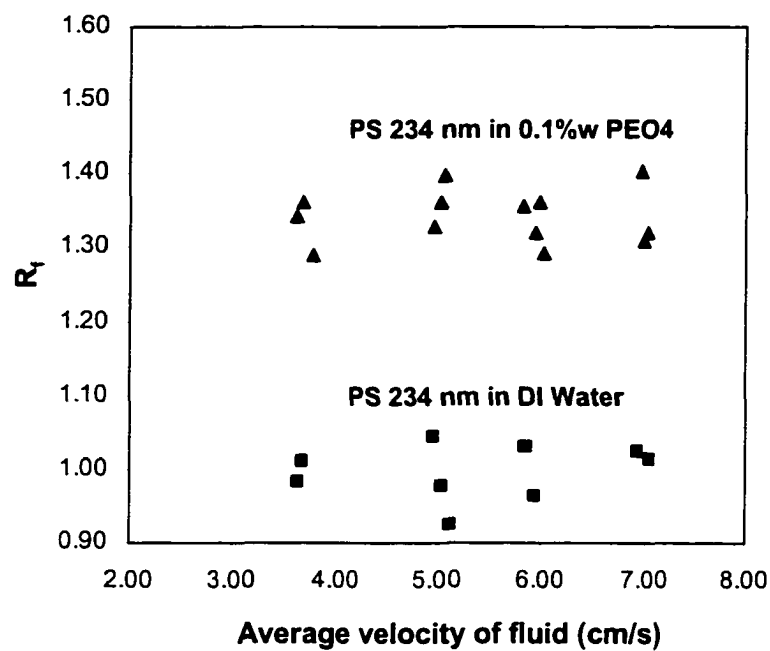
Figure 2-8: CHDF separation factors vs. average fluid velocity for 234 nm PS latex particles dispersed in DI water and 0.1 % w/w PEO4; capillary ID = 21.0 μm and length = 402.0 cm, and eluant = 4 mM NaCl (K = 450 μS/cm).

62

latex particles in PEO solutions. In addition, this provides us with the fact that the diffusion of salt ion species from the eluant into the sample slug is very fast relative to the traveling time of the particles through the capillary.

Another possibility for the separation factor enhancement is the aggregation of the particles due to bridging flocculation. Because the polymer-adsorbed particles will experience a high shear rate ($\sim 10,000$ s^{-1}) while traveling through the microcapillary, the adsorbed polymer molecules might be desorbed from the particle surfaces causing some nonuniformity of the polymer-adsorbed particles. This can lead to the bridging of the polymer chains between the particles resulting in flocculation. In order to prove that the enhancement in the separation efficiency is not due to the aggregation of the particles, the turbidity ratio of the particles was determined. As suggested by Venketesan [4], a well-separated singlet particle will show a constant turbidity ratio with the value depending on its particle size. If the aggregates are formed, a decrease in the turbidity ratio will be detected. In addition, if there is no aggregation, the value of the turbidity ratio should be equal to the value obtained from a well-stabilized system such as PS particles dispersed in Brij35SP surfactant.

The plot of turbidity ratio of PS latex particles in Brij35SP as a function of particle size is shown in Figure 2-9. Although, the particles with adsorbed PEO have a larger effective particle size compared to the particles with adsorbed Brij35SP surfactant, the same value of the turbidity ratio is expected because the adsorbed layer of PEO will not be detected by UV, and thus the adsorbed-PEO particles will appear as a bare particle. The turbidity ratios of 234 nm PS latex particles dispersed in PEO4 solutions showed a constant value of 1.2 as shown in Figure 2-10 which is identical to the value obtained for the 234 nm PS latex particles in Brij35SP. This indicated that the increase in the separation factor and decrease in the axial dispersion of the particles in the presence of PEO were not due to aggregation. Additionally, a single peak with

63
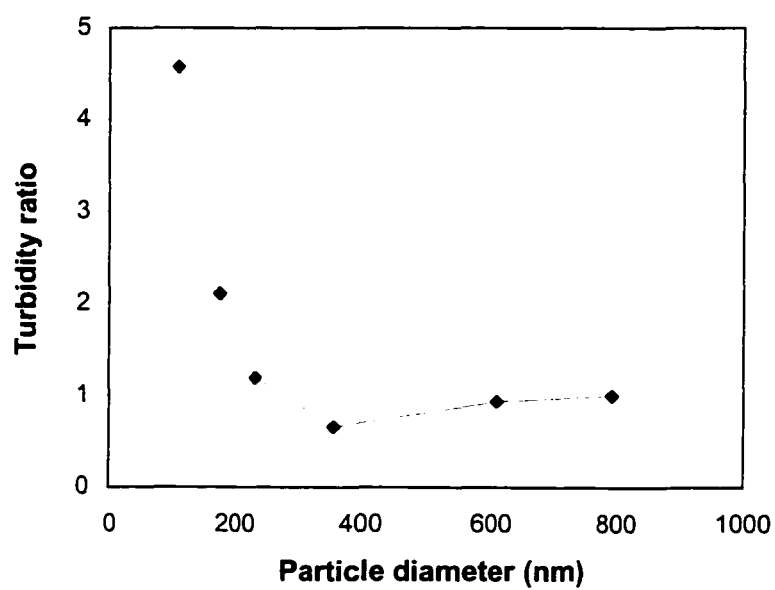
Figure 2-9: Turbidity ratios of 220:254 nm UV wavelengths for PS latex particles dispersed Brij35SP surfactant as a function of particle size.

64
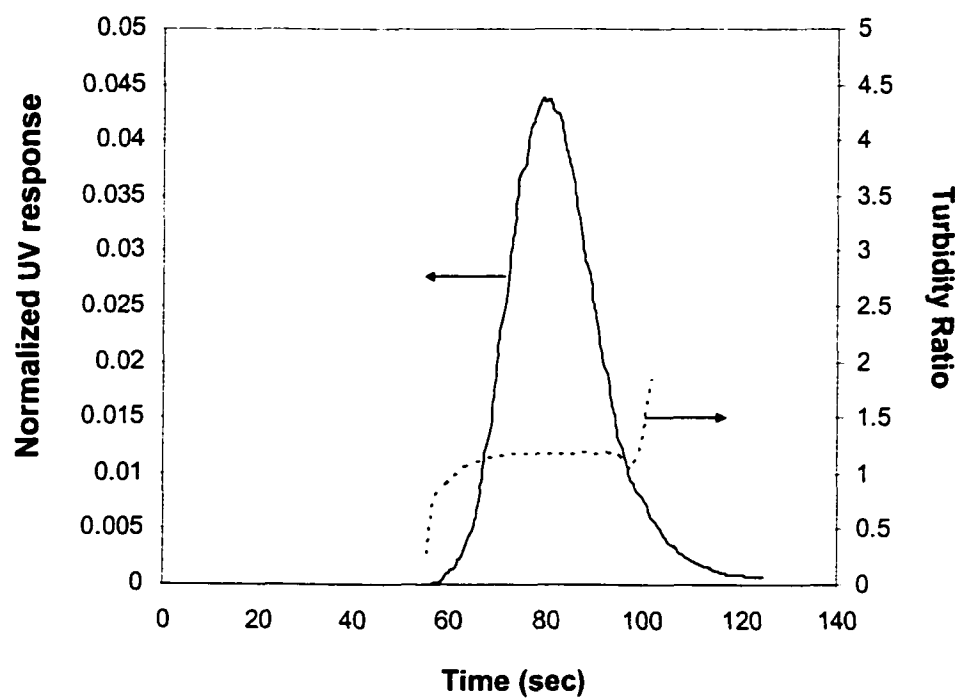
Figure 2-10: CHDF Fractogram and Turbidity ratios of 220:254 nm UV wavelengths for 234 nm PS latex particles dispersed in 0.1 %w/w PEO4 solutions.

65

Gaussian distribution profile also confirmed the non-aggregation of latex particles in PEO solutions.

In order to determine whether the enhancement of the separation factor is because of the increase in the particle size, the CHDF dynamic simulation was performed by varying the particle size only. A hard sphere particle was assumed which corresponds to a very low permeability of an adsorbed polymer layer. The effects from the electrostatic repulsion will be neglected, since the CHDF was operated at a high ionic strength (~ 4 mM). The Debye length for 4 mM ionic strength is about 4 nm. Besides the size increment, the other effect included in the simulation is the inertial effect of the fluid in order to cope with the flow rate dependency. However this effect is expected to be insignificant because of a small particle Reynolds number.

Figure 2-11 illustrates the comparison between the experimental and simulated CHDF fractograms generated using the core diameter of 234 nm plus 2 times the adsorbed layer thickness as determined by the power law relationship (2.120).

The simulation can predict the experimental results fairly well for bare latex particles (dispersed in DI water) indicating the absence of the electrokinetic lift force and electrostatic repulsion when 4mM NaCl was used as the eluant. However, the model fails to predict the fractograms of particles in the presence of PEOs and the discrepancy increases with the molecular weight. Even though, the inertial force was included because of the high fluid velocity, it did not have much impact on the enhancement of the separation factor. As the particle size increased, the dynamic model predicted the higher degree of axial dispersion (peak broadening) because the particle diffusivities were reduced due to the larger particle size providing a more prominent effect of the convection from the fluid velocity.

The effective particle size used in the simulation was based on the DLS measurement which can be different from the apparent particle size experienced by CHDF due to the effect of

66
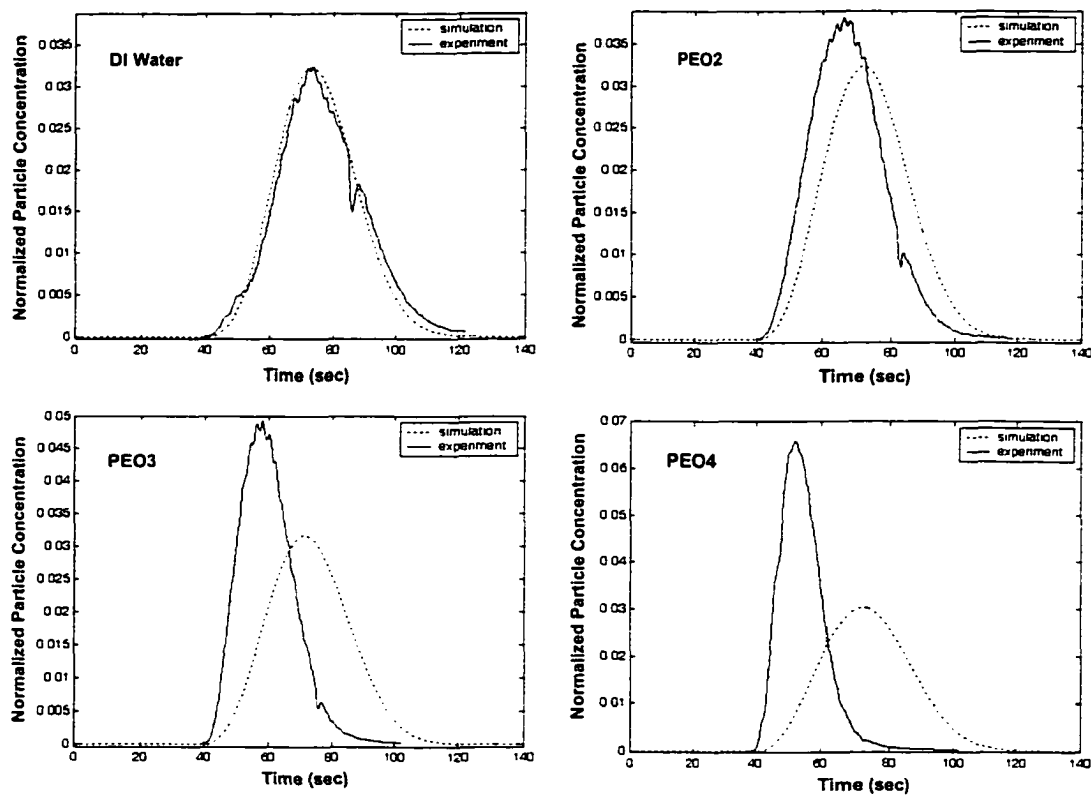
Figure 2-11: Simulated vs. experimental CHDF fractograms of 234 nm PS latex particles dispersed in DI water, 0.1% w/w PEO2, 0.1% w/w PEO3 and 0.1 % w/w PEO4 solutions; capillary ID = 21.0 μm and length = 402.0 cm, eluant = 4 mM NaCl (K = 450 μS/cm) and the average velocity = 5.3 cm/s. The electrostatic repulsion is not included in the simulation.

67

high shear. As a first attempt, the particle size was further increased in order to match the experimental results and this is shown in Figure 2-12. By increasing the particle size, CHDF simulation predicted the increasing R_f and decreasing H_{TP}. However, the experimental results for PEO3 and PEO4 which were represented by the dotted lines showed a greater values of the separation factor which cannot be predicted only by using the effect of size exclusion. Therefore, the assumption that the enhancement of the separation efficiency in CHDF is the result of the enlargement of the effective particle size was not entirely correct. One can further increase the particle size trying to match the experimental separation factor, however this would be to no avail because eventually, the simulated H_{TP} will be too small to be predicted correctly.

Since the enhancement of the experimental separation factors in the presence of PEO is not solely induced by the increase in the effective diameter as proved by the dynamic simulation, the only possibility is the effect of free (unadsorbed) PEO which is present in the samples. Recall that we simply prepared the samples by adding latex particles into PEO solutions at a certain concentration, which are normally several fold higher than the saturation concentration. Therefore, after adsorption, there would be some portion of the polymer chains left as free molecules. The experiment was performed by varying the concentration of PEO in the dispersed phase of the latex samples. Figure 2-13 shows the plot of the separation factor of 234 nm PS latex particles dispersed in PEO4 solutions as a function of weight percent of free PEO4 in the dispersed medium of the samples. The excess amount of PEO after adsorption was calculated based on the adsorbed amount of PEO4 on PS latex particles at saturation (the plateau region of the adsorption isotherm). The plot indicates that the separation factor of the particles in the presence of PEO4 depends on the concentration of free PEO4 in the dispersed phase of the samples. This effect caused the discrepancy between the predicted and experimental separation factor at high concentrations of PEO.

68
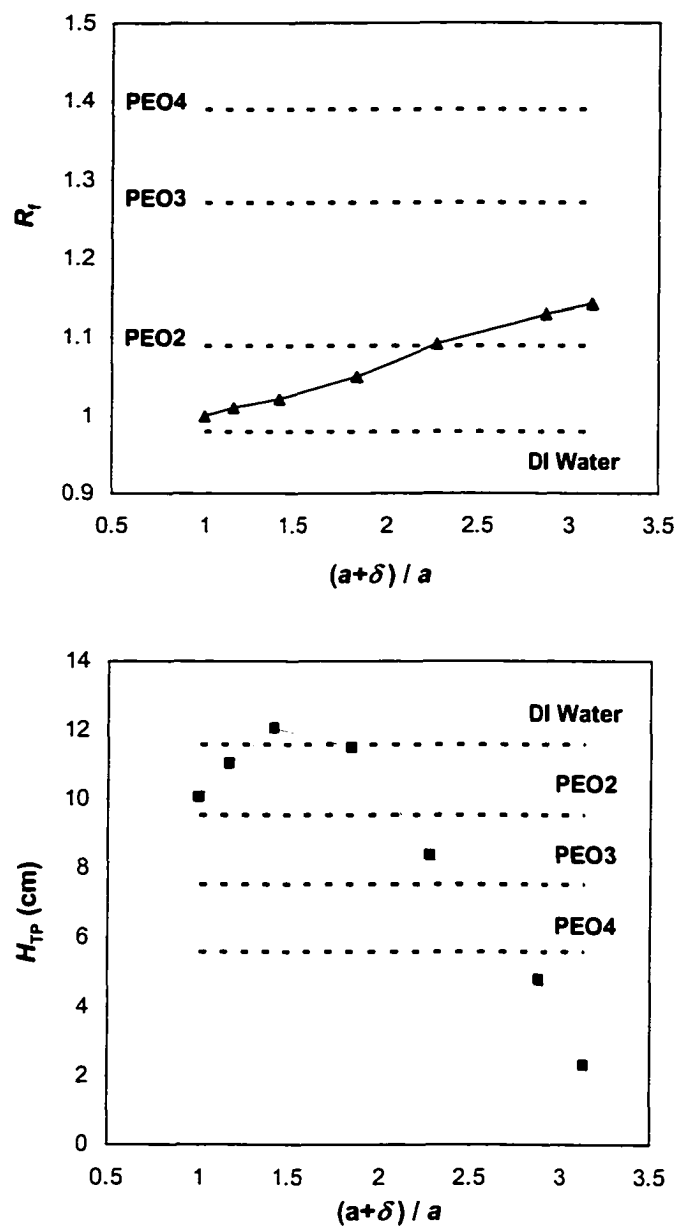
Figure 2-12: Simulated (line and closed symbol) vs. experimental (dotted lines) R_f and H_{TP} of 234 nm PS latex particles dispersed in DI water, 0.1 % w/w PEO2, 0.1 % w/w PEO3 and 0.1 % w/w PEO4 solutions as a function of the ratio of effective particle size to bare particle size; capillary ID = 21.0 μm and length = 402.0 cm, eluant = 4 mM NaCl (K = 450 μS/cm) and the average velocity = 5.3 cm/s. The electrostatic repulsion is not included in the simulation.

69

Because the presence of PEO can contribute to a viscosity increase of the sample, experiments using glycerin solutions were also conducted in order to investigate the viscosity effect as illustrated in Figure 2-14. It is evident that an increase in the viscosity of the dispersed phase of the sample does not contribute to the enhancement of the separation factor as well. Note that the viscosity of 0.1 %w PEO4 is 1.4 cP that is equivalent to the viscosity of 19.9 % w/w glycerin. Both solutions show Newtonian behaviors.

As proved experimentally, the enhancement of the separation factor of PS latex particles in the presence of PEO in the dispersed medium is dependent on the amount of excess PEO (unadsorbed). The viscosity and the ionic strength of the dispersed phase are not responsible for the enhancement. We believed that the viscoelasticity (normal stress) of the PEO solution which used as the medium plays a role in causing the migration of the particles from the wall (besides the inertial effect). This effect will be explored in the next chapter.

When the mixture of PS particles and PEO is injected into the CHDF system, the particles as well as the polymer chains travel together through the capillary. Since the diffusivity of high molecular weight PEO is comparable to the particles ($\sim 10^{-7}$ to 10^{-8} cm^2/s), the particles are most likely to be surrounded by the polymer solution instead of high ionic strength eluant. Therefore, the particles will experience the presence of PEO solution which can cause the migration of particles toward the capillary center resulting in the higher R_f and lower H_{TP}.

2.3.3 Evidence of Size Increment due to PEO-Adsorbed Layer

To minimize the effect of the unadsorbed PEO in the sample dispersion medium, the concentration of PEO was limited to the vicinity of the saturation point based on the adsorption isotherm. By using the concentration of PEO at the saturation point, the particles will be fully covered with PEO, which imparts stability to the particles and the amount of free PEO will be

70
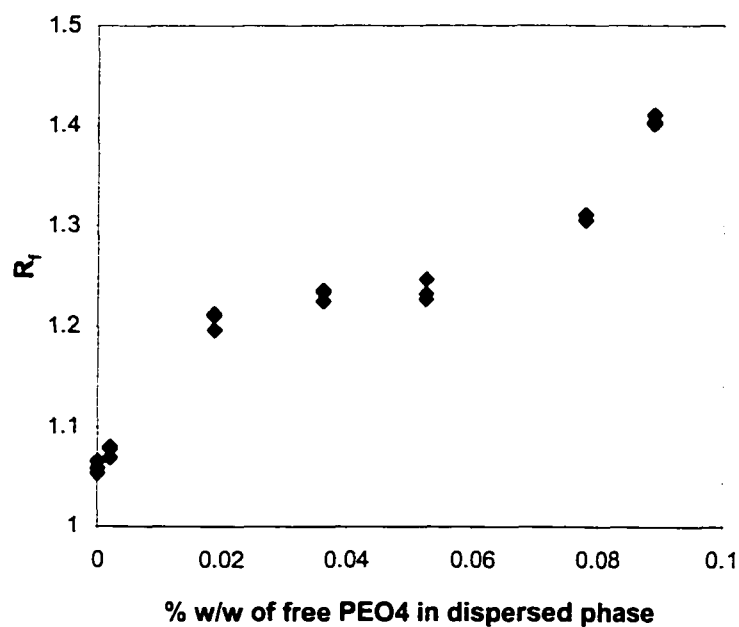
Figure 2-13: Separation factor of 234 nm PS latex particles dispersed in PEO4 solutions as a function of weight percent of free (unadsorbed) PEO4 in the dispersed phase of the samples; capillary ID = 24.0 μm and length = 655.0 cm, eluant = 4 mM NaCl (K = 450 μS/cm) and the average velocity = 3.0 cm/s.

71
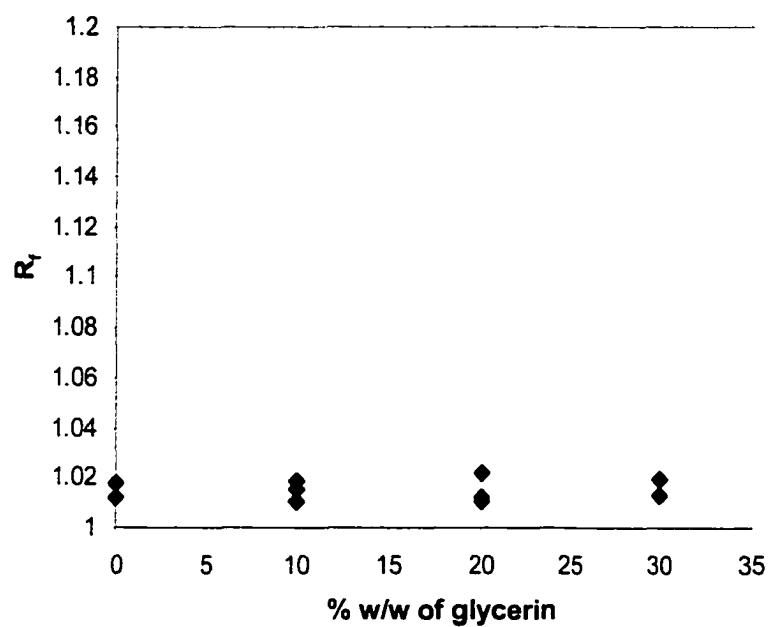
Figure 2-14: Separation factor of 234 nm PS latex particles dispersed in glycerin solutions as a function of weight percent of glycerin; capillary ID = 24.0 μm and length = 655.0 cm, eluant = 4 mM NaCl (K = 450 μS/cm) and the average velocity = 3.0 cm/s.

72

eliminated.

Figure 2-15 illustrates R_f and H_{TP} of 234 nm PS particles as a function of the average fluid velocity in the presence and absence of PEO. The PEO concentration was 0.0098 % w/w which is about 10 % higher than the saturation concentration for the particle concentration of 0.25 % w/w.

PS particles in the presence of PEO showed an increase in the separation factor compared to PS particles without PEO especially at relatively high velocities of the fluid indicating a size increment due to the adsorbed layer of PEO. In addition, as the particle size increases, the diffusivity of the particles will decrease, which gives rise to a more prominent effect from convection due to the fluid velocity resulting in a higher degree of particle axial dispersion. This can be seen as theoretical plate heights of PS particles increased in the presence of PEO.

The dynamic simulation was performed for the 234 nm latex particles in PEO4 solution at the saturation concentration and compared to the experimental fractograms. This is shown in Figure 2-16 for two different fluid velocities. The PEO-adsorbed layer thickness (δ) was adjusted until the best match was obtained between simulated and experimental fractograms. The PEO-adsorbed particle was modeled as a composite sphere with the polymer segment concentration in the adsorbed layer represented by an exponential function. Also displayed in the figure is the simulated fractogram of particles using the hard sphere model.

For the composite sphere model, the predicted adsorbed PEO4 layer of 50 nm provided a good agreement with the experiments. However, the hard sphere of the same size seemed to predict a broader fractogram, which is due to the higher resistance to the flow compared to the composite sphere.

The agreement between the prediction and the experimental results indicated that the adsorption of PEO occurred and caused an increased in the particle size resulting in the

73
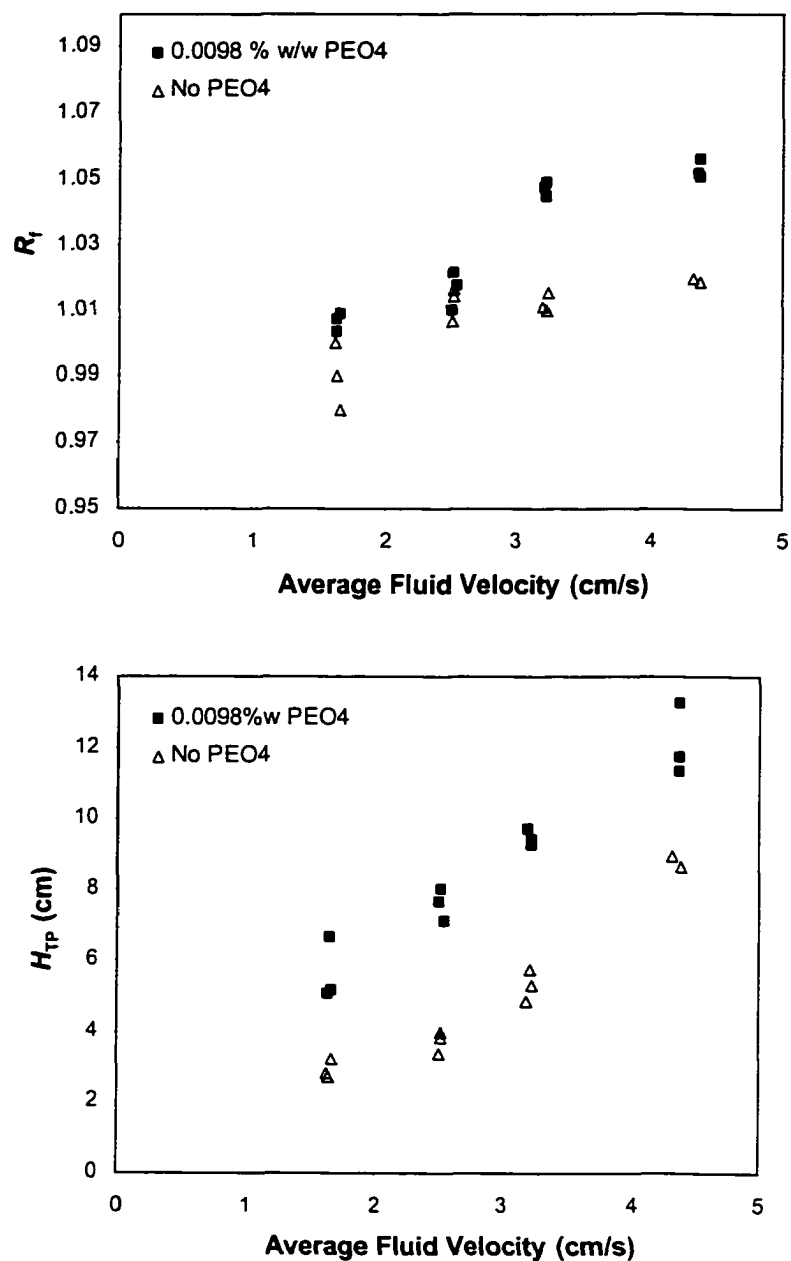
Figure 2-15: R_f and H_{TP} of 234 nm PS latex particles dispersed in 0.0098 % w/w PEO4 (saturated concentration) compared to PS particles dispersed in DI water; capillary ID = 24.0 μm and length = 655.0 cm, eluant = 4 mM NaCl (K = 450 μS/cm) and particle concentration is 0.25 % w/w.

74
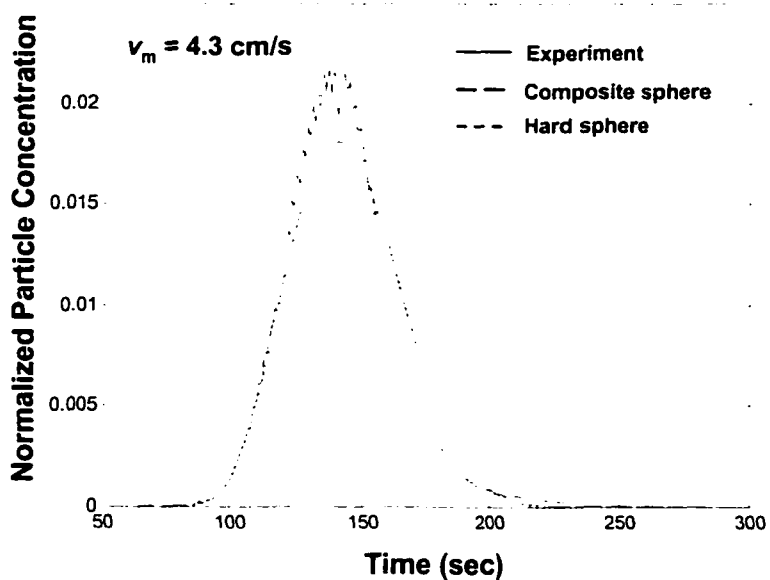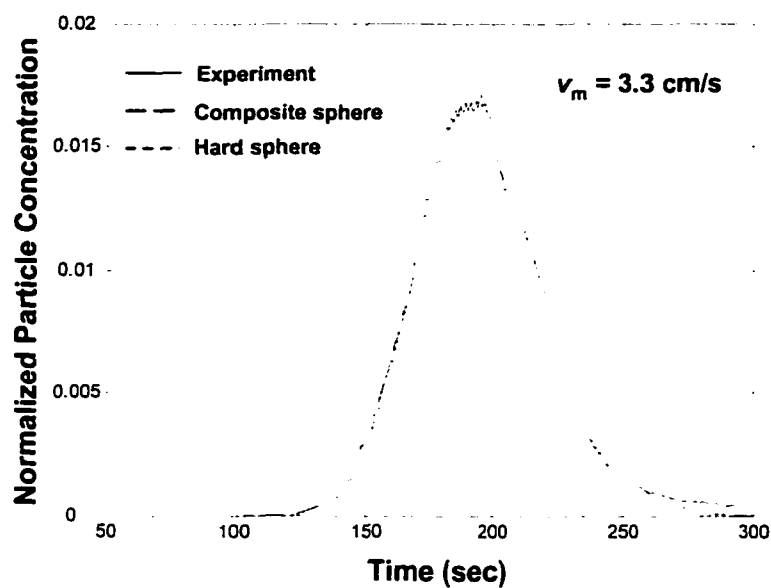
Figure 2-16: Comparison between experimental and simulated CHDF fractograms of PEO4-adsorbed particles using composite sphere and hard sphere models; capillary ID = 24.0 μm and length = 655.0 cm, eluant = 4 mM NaCl (K = 450 μS/cm).

enhancement of the separation factor and an increase of the degree of axial dispersion. This simulation was also confirmed the assumption of diminishing of the particle-wall electrostatic repulsion for a high ionic strength of the eluant.

2.4 Conclusions

Dynamic light scattering revealed that the adsorption of PEO on PS latex particles caused an increase of the effective particle size. The adsorbed layer thickness depended upon the molecular weight and the dependency can be expressed by the power-law relationship $\delta \propto M_w^{0.63}$. The size of the probe latex particle was also found to affect the thickness of the PEO-adsorbed layer. The adsorbed polymer layer was observed to decrease as the particle size decreased.

The CHDF experimental results for PS latex particles dispersed in PEO solutions using 4 mM NaCl as the eluant showed an increase in the separation factor with the molecular weight of PEO. However, the enhancement in the separation factor can not be explained by an increasing size due to the PEO adsorption as revealed by the dynamic simulation. It was found that the particle separation factor depends upon the concentration of PEO in the dispersion medium of the sample. The effect of particle size increase due to the adsorption of PEO could be observed in CHDF when the concentration of PEO used to disperse the particles was close to the saturation concentration as evidenced by the increasing separation factor and the theoretical plate height.

The comparison of the experimental fractogram with the CHDF simulation revealed a better prediction using the composite sphere model compared to the rigid sphere model of the same particle diameter. The simulated adsorbed PEO4 layer on 234 nm PS particles was 50 nm which is similar to the thickness of the adsorbed PEO4 obtained from dynamic light scattering measurements.

76

Chapter Three

Evaluation of Particle Transport in CHDF Associated with the

Flow of Polymer Solution

3.1 Introduction

Transport of latex particles in a microcapillary was studied in the presence of PEO solution. The CHDF experiments were performed using PEO solutions as the eluants. Then, the experimental results were compared with the CHDF dynamic model introduced in the previous chapter in order to predict the separation of latex particles in CHDF under the influence of PEO. Many characteristics of the PEO solution are considered. The surface phenomena associated with the flow of PEO solutions (i.e., slip effect and adsorption) were investigated experimentally. The polymer migration, which will affect the radial distribution of polymer concentration and cause the slip in the capillary flow, was also considered. Finally, the migration of particles in the polymer solution due to the viscoelasticity was examined.

In order to avoid the complication of the shear thinning effect, PEO solutions were diluted enough to exhibit Newtonian behaviors. For the largest molecular weight of PEO in our study (PEO4, $M_w \sim 1,000,000$ g/mol), the polymer solution showed a constant viscosity for concentration up to 0.2 % w/w.

The laminar flow of a polymer solution through the microcapillary can be associated with two phenomena: adsorption and apparent slip. The apparent slip refers to the abnormally low apparent viscosities of polymer solutions in an inhomogeneous stress field compared to the viscosities measured in uniform stress fields. Therefore, the flow rate will be enhanced for the

77

capillary flow of a polymer solution with an apparent slip effect. Unlike the flow accompanied by adsorption, the adsorbed layer on the capillary wall hampers the flow causing the flow rate to be reduced.

The adsorption of PEO takes place on the capillary wall because the oxygen atom in the PEO polymer molecules can form a hydrogen bond with a silanol group on the fused silica surface of the capillary [68]. The retardation effect of adsorbed polymer in the capillary flow depends upon the thickness as well as the permeability of the adsorbed layer which is a function of molecular weight and surface concentration of polymer. The presence of the adsorbed layer causes the reduction not only to the flow but also the effective diameter of the capillary. The particles traveling through the capillary associated with adsorbed polymer will experience a narrower diameter.

The slip flow of a polymer solution is the result of the polymer migration. When the shear flow has a characteristic time of flow comparable to the molecular relaxation time of the polymer, the polymer molecules in the flow field will start to deform. Since this deformed state is thermodynamically unfavored, polymer molecules will migrate from a high shear region toward the low shear area. Therefore, in capillary flow, the polymer will migrate from the tube wall toward the center line creating a concentration gradient in the radial direction. Because the viscosity of a polymer solution is a function of the polymer concentration, the polymer migration will generate an area of low viscosity near the tube wall and higher viscosity close to the center line. The change of viscosity due to the polymer migration will result in the alteration of the polymer diffusivity and thus will affect the transport of particles in the polymer solution.

The viscoelastic effect of PEO solutions was also explored. In capillary flow, the lateral migration of particles in polymer solution takes place due to the gradient of normal stress. Unlike a Newtonian fluid, the migration of particle is strictly due to the inertia of the fluid. The particle

78

migration velocity in a second-order fluid, derived by Ho and Leal [69,] was incorporated into the CHDF model in order to take into account the effect of the viscoelasticity of the PEO solution.

3.2 Transport of Colloidal Particles through a Microcapillary in the Presence of PEO Solution

The CHDF experiments were conducted using high ionic strength PEO solutions as the eluants. A small amount of NaCl was added to the PEO solutions to adjust the ionic strength. The reason for using high ionic strength eluant is to diminish the effect of the electrostatic repulsion and the electrokinetic lift. Since PEO is an uncharged polymer, the salt content was expected to have no relevant effect on the viscosity of the PEO solution.

The measured size of latex particles may be increased if we simply inject the bare latex particles into the CHDF when PEO solution is used as the eluant because adsorption can take place while the particles are traveling through the microcapillary. To prevent the adsorption of PEO, the latex particles were pre-adsorbed with a low molecular weight nonionic surfactant. The steric barrier created by the adsorbed surfactant can deter the PEO molecules from coming in contact with the particle surfaces. Ullmann et al. [34] suggested Triton X-100 as the pre-adsorbed surfactant. However, Triton X-100 contains a phenol group which is UV-absorbing. Since our CHDF equipment uses a UV detector to measure the optical density of the eluting colloidal particles, any UV-absorbing surfactant such as Triton X-100 will interfere with the measurement. To avoid such complications using Triton X-100, Brij35SP (polyoxyethylene lauryl ether with M_w = 1,198 g/mol manufactured by ICI America Inc.) was used in our experiments, instead. The ability of Brij35SP to prevent PEO adsorption was tested by performing dynamic light scattering (DLS) measurements (NICOMP model C370). Latex particles were added into the Brij35SP solution before dispersing into the PEO solutions. The concentration of Brij35SP was above the

79

critical micelle concentration (CMC), which is about 0.0072 % w/w. Then, the mixture of pre-adsorbed latex particles and PEO was diluted in deionized water before performing DLS measurements. The experimental results are illustrated in Table 3-1. The results showed the expected constant particle diameter for all PEO solutions. This indicated the effectiveness of Brij35SP in shielding the PS surfaces from PEO.

From the results of these DLS experiments, latex particles used in CHDF experiments were mixed with Brij35SP before being injected into the system. Moreover, Brij35SP was also dissolved in the PEO solutions that were used as the eluants in order to prevent the desoprtion of Brij35SP from the particle surfaces. Also, the concentration of Brij35SP in the eluant was selected to be slightly above its CMC. Fortunately, adding Brij35SP to the PEO solutions did not cause an increase in viscosity because of its low molecular weight and concentration.

Table 3-1: Volume-Average Particle Diameter of 234 nm PS Latex Particles with Pre-Adsorbed Brij35SP Present and Dispersed in PEO Solutions as Determined by Dynamic Light Scattering[*]

Dispersed Phase	D_v (nm)	Std. Deviation (nm)
Brij35SP	253	25.0
PEO2	257	14.8
PEO3	256	39.0
PEO4	255	26.7

* Before the measurement, all the samples were diluted in DI water

Figure 3-1 shows the separation factor R_f and theoretical plate height H_{TP} for various size PS latex particles in different concentrations of PEO4 solutions. The presence of PEO can improve the separation efficiency of CHDF as evident from the increasing R_f and decreasing H_{TP}.

80

The degree of improvement was enhanced with the concentration of PEO4.

At 0.01 % w/w PEO4, R_f of the small particle sizes were indistinguishable from the case of no PEO. As the particle size increased, the effect of PEO was noticed as R_f increased dramatically. H_{TP} for 0.01 % w/w PEO4 exhibited slightly larger values compared to H_{TP} in the absence of PEO. For the higher concentration of PEO4 (0.1 % w/w), R_f showed significant enhancement especially for small particles before leveling off as the particle size increased. The degree of axial dispersion also showed the improvement as H_{TP} reduced rapidly with the particle size. However, for small size particles (109 nm and 176 nm), H_{TP} was higher than that obtained for particles in 0.01 % w PEO4 and DI water. This is most likely due to the increase of eluant viscosity as the concentration of PEO increased. The significant enhancement of R_f and dramatic reduction of H_{TP} implies that the migration of particles from the capillary wall toward the center occurred when PEO4 is present in the eluant. In addition, the rate of migration was intensified as the concentration of PEO4 increased.

3.3 Adsorbed Layer Thickness of PEO on the Capillary Wall

The experiment to distinguish the slip and adsorption effects using the microcapillary was performed to allow the determination of the adsorbed layer thickness of PEO on the capillary wall.

The adsorption and apparent slip in tube flow can be indicated through the sign of the effective velocity at the wall (u_w). In the case of the apparent slip, u_w will yield a positive sign indicating an increase of the velocity near the wall. A negative u_w occurs when there is an adsorbed layer in the vicinity of the wall [70]. To determine u_w, the expression of the apparent slip in circular tubes proposed by Mooney is employed [71]:
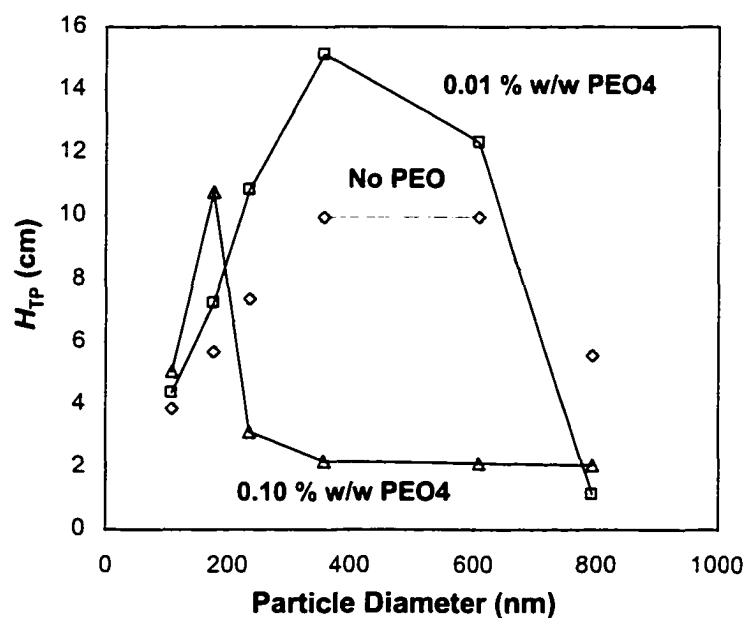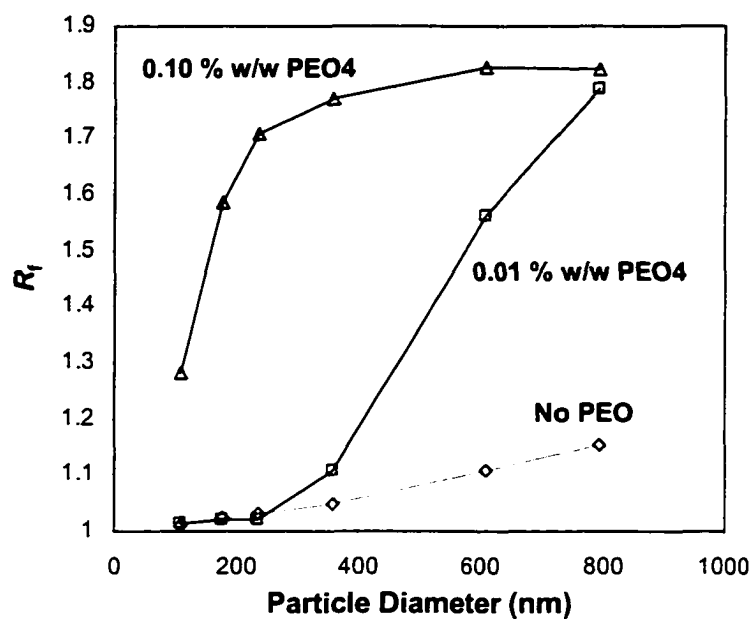
Figure 3-1: Experimental separation factor (R_f) and theoretical plate height (H_{TP}) of various sizes PS latex particles pre-adsorbed with Brij35SP in the presence of PEO4 solutions at different concentrations; capillary ID = 24.1 μm and length = 655.0 cm; eluants = 4 mM NaCl and 0.01 % w/w, and 0.1 % w/w PEO4 with 4 mM NaCl; average fluid velocity = 2.8 cm/s.

82

$$\frac{32Q}{\pi D^3} = \frac{4}{\tau_w^3} \int_0^{\tau_w} \tau^2 f(\tau) d\tau + \frac{8u_w}{D} \qquad (3.1)$$

where Q is the total volumetric flow rate, D is the capillary diameter, τ_w is the wall shear stress and $f(\tau)$ is the corresponding shear rate. Since the volumetric flow rate through the microcapillary is very small, it is more convenient to define the equation in terms of the average velocity of the fluid [72]

$$\frac{8v_m}{D} = \frac{4}{\tau_w^3} \int_0^{\tau_w} \tau^2 f(\tau) d\tau + \frac{8u_w}{D} \qquad (3.2)$$

where v_m is the average velocity of the fluid through the capillary. In fact, the term on the left hand size of the above equation is equal to twice the average shear rate $\dot{\gamma}_{ave}$. Differentiating equation (3.2) with respect to $1/D$ at constant wall shear stress yields:

$$\frac{\partial(8v_m/D)}{\partial(1/D)}\bigg|_{\tau_w} = 8u_w \qquad (3.3)$$

Therefore, a plot of $8v_m/D$ versus $1/D$ at a constant wall shear stress should yield straight lines with the slope equal to $8u_w$.

Figure 3-2 illustrates such a plot for PEO1, PEO2, PEO3 and PEO4 at 0.1 % w/w and wall shear stress equal to 15 Pa. Straight lines were obtained for all the PEO solutions. As expected, DI water showed a straight line with a zero slope because neither apparent slip nor adsorption took place. PEO1 and PEO2 showed positive slopes, which indicated the occurrence of the apparent slip effect for capillary flow of these low molecular weight PEO solutions. The higher slope of PEO1 compared to PEO2 implied that the rate of polymer migration was stronger for low molecular weight PEO1. However, this is in contrast to the theory of polymer migration which suggests the increasing rate of polymer migration with the molecular weight of polymer. We believed that this is due to the simultaneous effect of polymer adsorption. Actually, the flow

83

of polymer solutions through the capillary is more complicated because it involves both surface effects which implies that the experimental u_w is the combination of the positive u_w from apparent slip and the negative u_w from adsorption [13]. Therefore, in the case of PEO1 and PEO2 solutions, we expected that the adsorption did take place but it is moderated by the more dominant effect from apparent slip. Due to the lower molecular weight of PEO1, the effect of adsorption which provides a negative slip velocity on the u_w is less prevailing compared to the adsorption of PEO2. In addition, the low molecular weight is more susceptible to the shear causing increased disengagement of the polymer chains from the surface.

The dominant role of adsorption can be evident from the negative slopes of PEO3 and PEO4. The line representing PEO4 displays a more negative slope than PEO3. This is because the higher molecular weight of PEO4 which provides a greater adsorbed polymer layer thickness, causing a more significant decrease in the flow rate.

u_w as a function of the wall shear stress is illustrated in Figure 3-3. The effective wall velocity increased linearly with the wall shear stress. This indicates that at low concentrations of PEO (0.1 % w/w), all molecular weight PEOs showed the Newtonian behaviors. In a Newtonian fluid, the linear relationship between the shear stress and shear rate suggests that by increasing the shear stress, the shear rate also increases linearly with the magnitude depending on the viscosity of the solution. Thus, because of the linear function between the average shear rate and the effective velocity at the wall, a linear relation of u_w with the shear stress was observed.

For the case of PEO3 and PEO4, the thickness of the adsorbed polymer layer δ can be estimated from the following expressions [70]:

$$\delta = -\frac{u_w \eta_w}{\tau_w} \tag{3.4}$$

where η_w is the viscosity of the bulk solution evaluated at the wall shear stress.

84
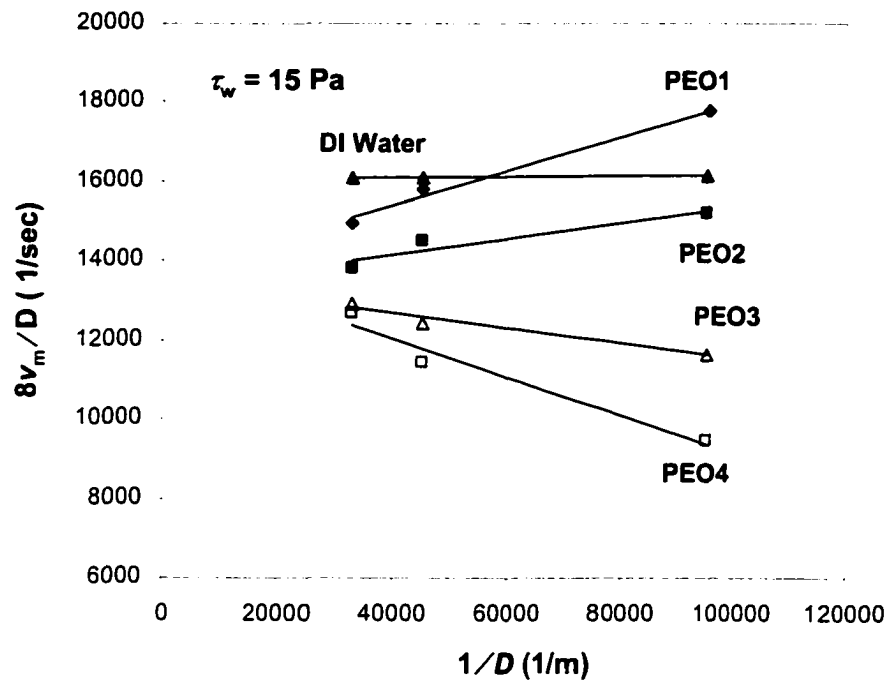
Figure 3-2: Plot of $8v_m/D$ vs. $1/D$ for flow of 0.1 % w/w PEO1, PEO2, PEO3, PEO4 and DI water through the microcapillary at the wall shear stress (τ_w) of 15 Pa.

PEO	Slope	R^2
PEO1	0.043	0.99
PEO2	0.019	0.89
PEO3	-0.019	0.96
PEO4	-0.048	0.96

85
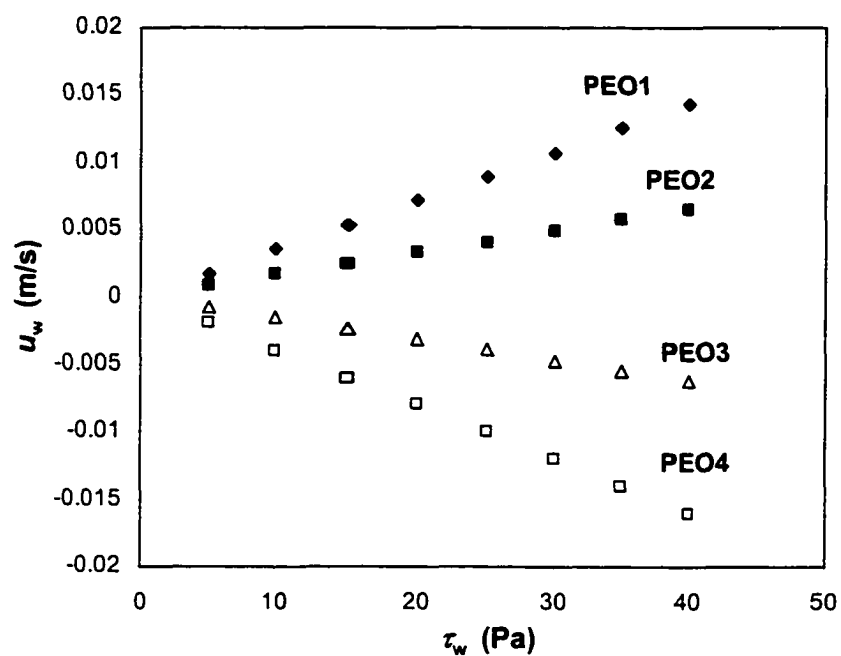
Figure 3-3: Plot of effective wall velocity (u_w) vs. wall shear stress (τ_w) for flow of 0.1 % w/w PEO1, PEO2, PEO3, PEO4 and DI water through the microcapillary.

86

Figure 3-4 shows a plot of PEO adsorbed layer thickness on the capillary surface for 0.1 % w/w PEO3 and PEO4 as a function of wall shear stress. The wall shear stress in the plot corresponds to a pressure drop from 1000 to 3000 psig which is in the range of the pressure drop usually encountered in our CHDF experiments. From the plot, it is evident that the thickness of the adsorbed layer on the capillary wall depends negligibly on the wall shear stress. Clearly, the thickness of the adsorbed layer depends upon the molecular weight of the PEO such that a higher molecular weight provides a greater layer thickness.

It has been found that the thickness of the adsorbed polymer is on the order of the hydrodynamic size of free polymer molecules in solvent [73]. Our estimation of δ is larger than the root-mean-square end-to-end distance of the PEO molecule by almost a factor of 5 for PEO4 and a factor of 2 for PEO3. Our results are also larger than the results obtained previously for flow experiments in capillary tubes [75,76]. Nonetheless, Cohen and Metzner [74] have obtained similar results to ours. They found a much larger adsorbed layer thickness compared to the root-mean-square end-to-end distance of free polymer molecules in solvent for the flow of aqueous polyacrylamide in stainless steel capillary tubes. They concluded that the discrepancy is due to the difference in the determination method. The method that was previously employed to determine δ is to compare the flow behavior of the solvent before and after the flow of polymer solution and then the extra resistance to the flow of the solvent is defined as the effective thickness of the adsorbed layer. The layer thickness obtained by this technique usually is the same order of the molecular size of the polymer molecule because it measures only the residue irreversibly adsorbed layer. The desorption of adsorbed polymer into the solvent stream might be taking place during the second flow of solvent. On the other hand, the method used by us and Cohen and Metzner [74] is to measure the adsorbed layer thickness from the flow behavior of the polymer solution. Since the capillary wall is in contact with the polymer throughout the whole

87
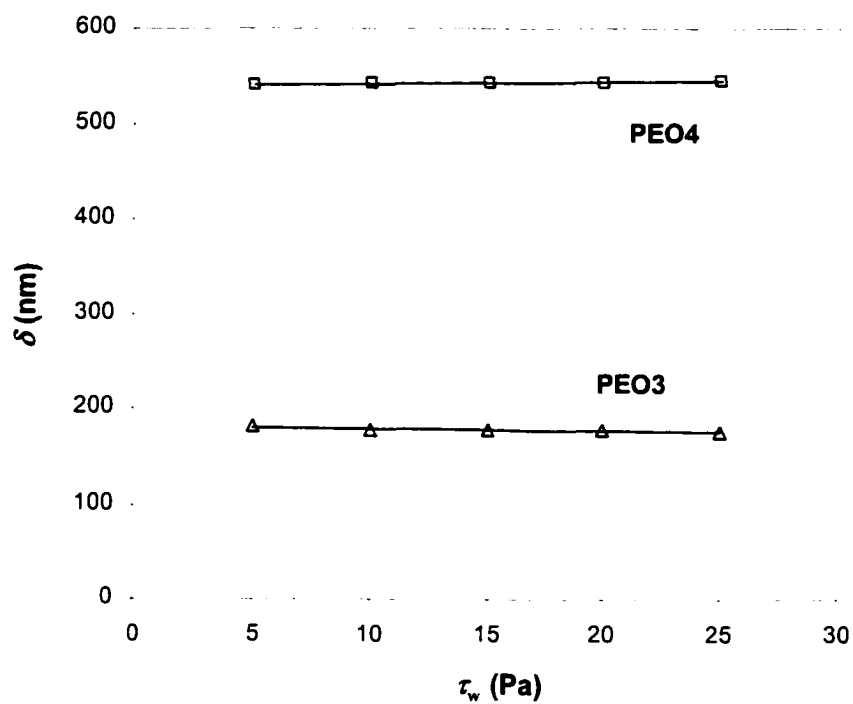
Figure 3-4: Adsorbed layer thickness (δ) of PEO3 and PEO4 on the capillary wall as a function of wall shear stress.

88

course of the measurement, the desorption of polymer molecules can be avoided.

3.3.1 Flow Inside the Polymer-Adsorbed Layer

Because adsorbed polymer retards the flow, the fluid velocity near the wall will be smaller compared to the velocity of the fluid without the layer of adsorbed polymer. This results in the reduction of the average velocity of the fluid. The change of the average velocity associated with adsorbed polymer can be calculated if the velocity profile inside the adsorbed layer is known. If the length scale of an adsorbed polymer layer is small relative to the length scale relevant to the flow about the solid, i.e., the adsorbed layer is thin compared to the diameter of the capillary, the curvature effect can be neglected and the flow inside the adsorbed layer is one dimensional.

For a thin adsorbed polymer layer δ relative to the capillary radius R_o; that is $\delta/R_o \equiv \lambda \rightarrow 0$, Anderson et al. [77] have obtained the velocity distribution inside the adsorbed layer based on the match asymptotic method. The governing equation describing the flow inside the adsorbed polymer layer is the Brinkman equation (cf. equation 2.1):

$$\frac{\partial \mathbf{u}^{\bullet}}{\partial \bar{y}} - \frac{\delta^2}{k^2}\mathbf{u}^{\bullet} = 0 \tag{3.5}$$

with the boundary conditions

$$\bar{y} = 0: \quad \mathbf{u}^{\bullet} = 0 \tag{3.6}$$

$$\bar{y} \rightarrow \infty: \quad \mathbf{u}^{\bullet} \rightarrow \mathbf{a} + \mathbf{b}\,\bar{y} \tag{3.7}$$

where $\mathbf{u}^{\bullet}$ is the fluid velocity vector tangent to the surface and $\bar{y}$ is the distance normal to the adsorbing surface which is scaled with an adsorbed polymer thickness δ. Unknown constants $\mathbf{a}$ and $\mathbf{b}$ are determined by solving equation (3.5) subject to the boundary conditions and matching $\mathbf{u}^{\bullet}$ with the external velocity field. Since the exterior flow presumably has no effect on the

89

adsorbed polymer layer, the interior velocity can be expressed in terms of a material property of the polymer layer. Thus, Anderson et al. [77] defined a scalar function G such that:

$$\mathbf{u}^* = -G\,\mathbf{n}\cdot(\nabla\mathbf{v})_0 \tag{3.8}$$

where $\mathbf{n}$ is the unit normal vector and $\mathbf{v}$ is the external fluid velocity. Subscript 0 indicates that the variable is evaluated at the wall surface. The Brinkman equation and the boundary conditions then become:

$$\frac{\partial^2 G}{\partial \bar{y}^2} - \frac{\delta^2}{k^2}G = 0 \tag{3.9}$$

$$\bar{y} = 0: \quad G = 0 \tag{3.10}$$

$$\bar{y} \to \infty: \quad \frac{dG}{d\bar{y}} \to -1 \tag{3.11}$$

The velocity gradient at the wall is given as:

$$\mathbf{n}\cdot(\nabla\mathbf{v})_0 = \frac{\tau_w}{\eta_w} \tag{3.12}$$

If the permeabilty function k is known, the velocity distribution inside the adsorbed layer is easily obtained by solving equation (3.9) for G and using equation (3.12) and (3.8) to determine $\mathbf{u}^*$. In fact, this solution of the Brinkman equation is similar to the one derived in chapter 2 for equation (2.51). The hydrodynamic layer thickness L_H is defined in the same way except in this case the effect of curvature is neglected; that is,

$$L_H = A\delta \tag{3.13}$$

where parameter A is determined from equation (2.57). L_H is equivalent to the thickness of a totally impermeable layer that gives the same hydrodynamic effect as the adsorbed polymer layer δ. Since the effect of external flow is not accounted for, L_H depends only on the permeability of adsorbed polymer layer.

90

Figure 3-5 shows the velocity distribution (scaled with the average velocity of the fluid v_m) inside the adsorbed polymer layer for different permeabilities. The permeability is assumed constant throughout the layer. Evidently, the flow of the fluid near the capillary wall was reduced due to the presence of the adsorbed polymer layer. The retardation effect is dependent on the permeability of the adsorbed layer such that high permeability allows the solvent to penetrate easily into the adsorbed layer causing a faster moving fluid through the layer. Note that for infinitely high permeability, the velocity of the fluid inside the adsorbed layer will be equivalent to the velocity in the absence of the adsorbed layer. On the contrary, low permeability of adsorbed layer caused a more prominent retardation effect resulting in the slower fluid velocity inside the adsorbed layer. The velocity of the fluid inside the adsorbed layer will approach zero for the layer with zero permeability.

Figure 3-6 shows the effect of a non-uniform polymer segment concentration on the velocity inside the adsorbed layer. The variation of the polymer segment concentration inside the adsorbed layer obviously altered the distribution of fluid velocity. The step profile (constant permeability) that roughly represents the compact conformation of adsorbed diblock copolymers provided the most retardation to the flow while less impact took place for the exponential and parabolic profiles. The exponential function is suitable for the diffuse structure of adsorbed homopolymer. The decreasing exponential concentration profile of polymer segments created the increasing permeability of adsorbed layer from the surface toward the edge of adsorbed layer and thus reducing the flow retardation effect. Nonetheless, the concentration predicted from the exponential function becomes zero at the infinite distance from the surface; that is why this function provided a lower permeability than that obtained from the parabolic function where the polymer segment concentration is zero at the edge of the adsorbed layer.

The so-called wall slip velocity can be related to the L_H by [77]:

91

$$\delta / k \quad = \qquad 10 \qquad 5 \qquad\qquad\qquad\qquad 1 \qquad 0.5 \ 0$$

[Figure: plot with y-axis labeled y / δ ranging from 0 to 1, and x-axis labeled $u^{\cdot}/ v_m$ ranging from 0 to 0.18]

y-axis (y / δ): 1, 0.9, 0.8, 0.7, 0.6, 0.5, 0.4, 0.3, 0.2, 0.1, 0

x-axis ($u^{\cdot}/ v_m$): 0, 0.02, 0.04, 0.06, 0.08, 0.1, 0.12, 0.14, 0.16, 0.18
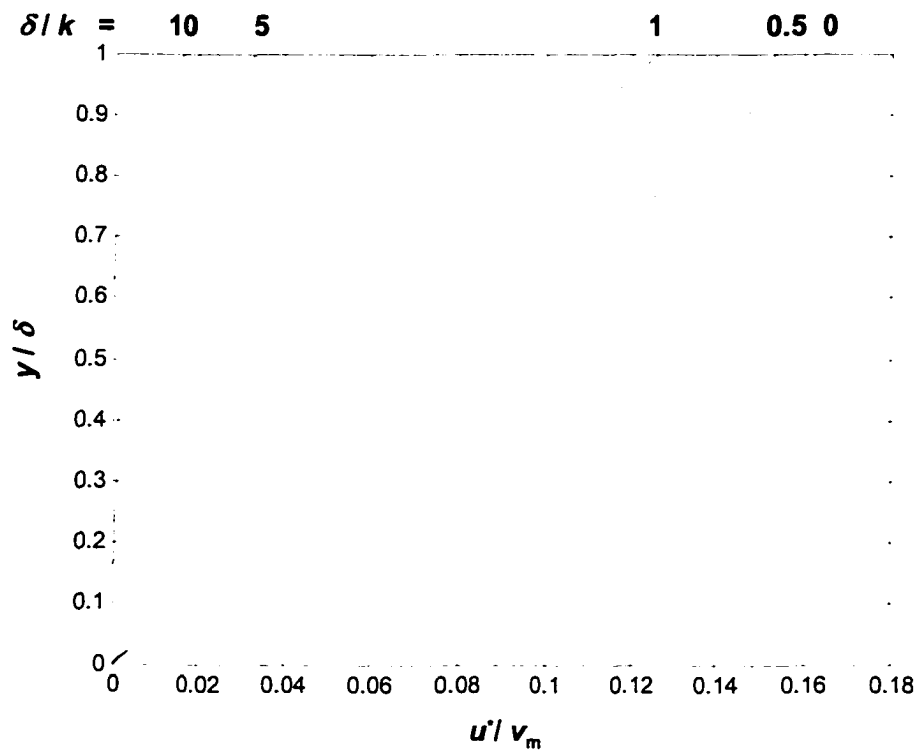
Figure 3-5: Normalized velocity distribution ($u^{\cdot}/v_m$) of fluid flowing inside the adsorbed polymer layer as a function of permeability (δ/k).
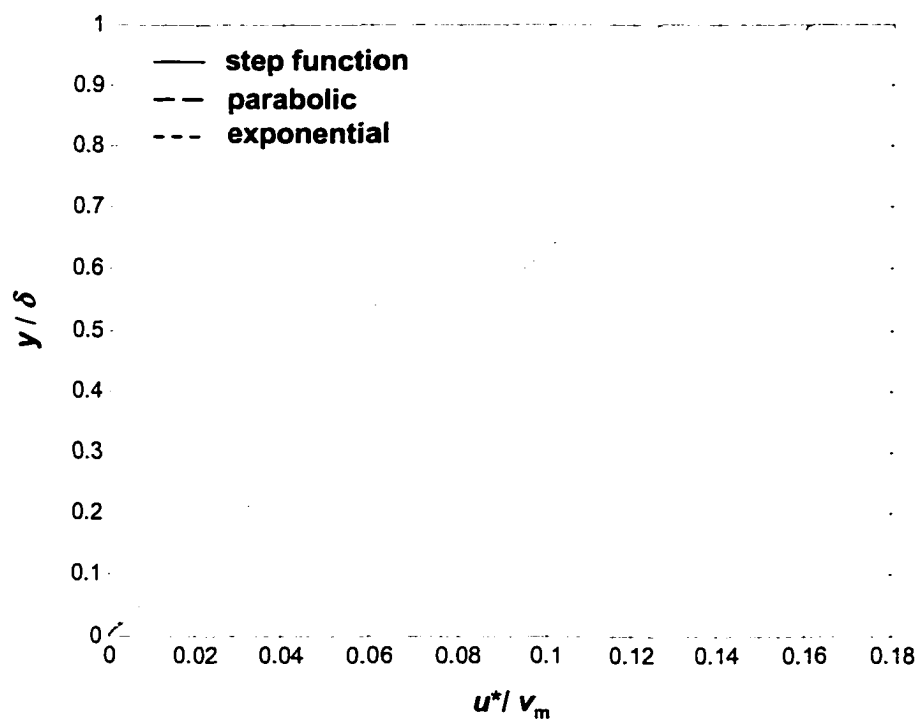
Figure 3-6: Normalized velocity distribution (u^*/v_m) of fluid flowing inside the adsorbed polymer layer for different function of polymer segment concentration.

93

$$u_s = -L_H \frac{\tau_w}{\eta_w} \tag{3.14}$$

This slip velocity is equivalent to the difference between the external velocity v_z and the internal one u_z^* at the distance L_H from the surface. Subscript z represents the axial direction. To calculate the external flow associated with L_H, the boundary condition at the surface can be used in two ways; the slip condition at the adsorbing surface in which the velocity at the wall is equal to the wall slip velocity, or the non-slip condition where the no-slip surface is moved from the capillary wall to the distance L_H. Using the no-slip condition at the L_H, the average velocity can be computed from the simple relation:

$$v_m = \frac{\int_0^{R_o - L_H} v_z r \, dr}{\int_0^{R_o} r \, dr} \tag{3.15}$$

Performing the integration, the ratio of the average velocity in the presence of adsorbed polymer to the average velocity of the fluid without polymer adsorption can be expressed as:

$$\frac{(v_m)_{adsorb}}{v_m} = \frac{2(R_o - L_H)^2}{R_o^2} \left[1 - \frac{(R_o - L_H)^2}{2R_o^2} \right] \tag{3.16}$$

Figure 3-7 shows the ratio of the average velocity of the fluid through the capillary in the presence of an adsorbed polymer layer to the average velocity without an adsorbed polymer layer as a function of L_H / R_o. The plot indicates a small impact of the adsorbed polymer layer on the average fluid velocity. The average velocity drops less than 5 percent for a micron thick adsorbed polymer layer in a 25 μm diameter capillary.

94
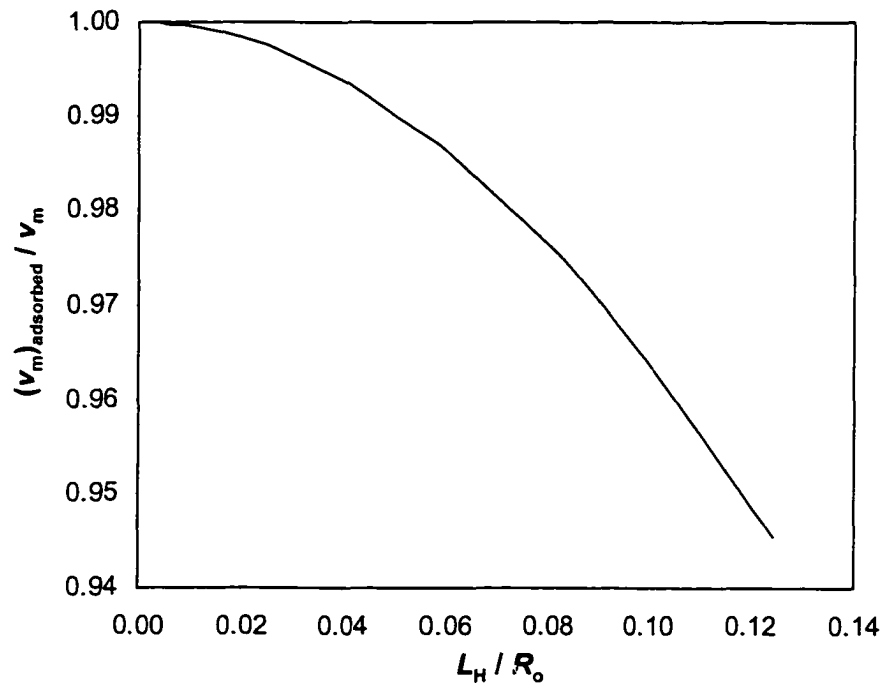
Figure 3-7: Reduction of the average fluid velocity for the fluid flow inside the microcapillary associated with the polymer adsorption.

95

3.3.2 Separation of Latex Particles in CHDF Associated with PEO-Adsorbed Layer on the Capillary Wall

The PEO adsorption on the capillary not only causes the reduction of the fluid velocity but the capillary diameter will be reduced as well. The presence of an adsorbed PEO layer generates the steric barrier which excludes the particles from approaching the capillary wall. Therefore, the particles will stay closer to the center of the capillary compared to the capillary without adsorbed PEO.

Figure 3-8 shows simulated CHDF fractograms for the transport of 234 nm particles through the capillary with different degrees of diameter reduction due to the PEO3 and PEO4 adsorption. The reduced average velocity was calculated from equation (3.16). The adsorbed layer was assumed isotropic with the permeability calculated from equation (2.71). Obviously, the presence of adsorbed PEO layer improved the separation of particles in the microcapillary. High molecular weight PEO provides a thicker adsorbed layer which limits the probability of the particles staying near the capillary wall. The particles will experience the narrower capillary diameter which result in a higher separation factor and lower degree of axial dispersion

3.3.2.1 Comparison with CHDF Experiments

The experimental R_f and H_{TP} for latex particles in 0.1 % w/w PEO4 were compared with the predicted results from CHDF dynamic model as shown in Figure 3-9. In the simulation, the reduction of the average velocity as well as the capillary diameter due to the PEO4 adsorption were included. Evidently, the experimental R_f increased at a higher rate than the simulation could anticipate. The model predicted slight change of R_f specifically for small particles but the experimental results revealed a sharp increase for small particles before leveling off as the particle size became larger.

96
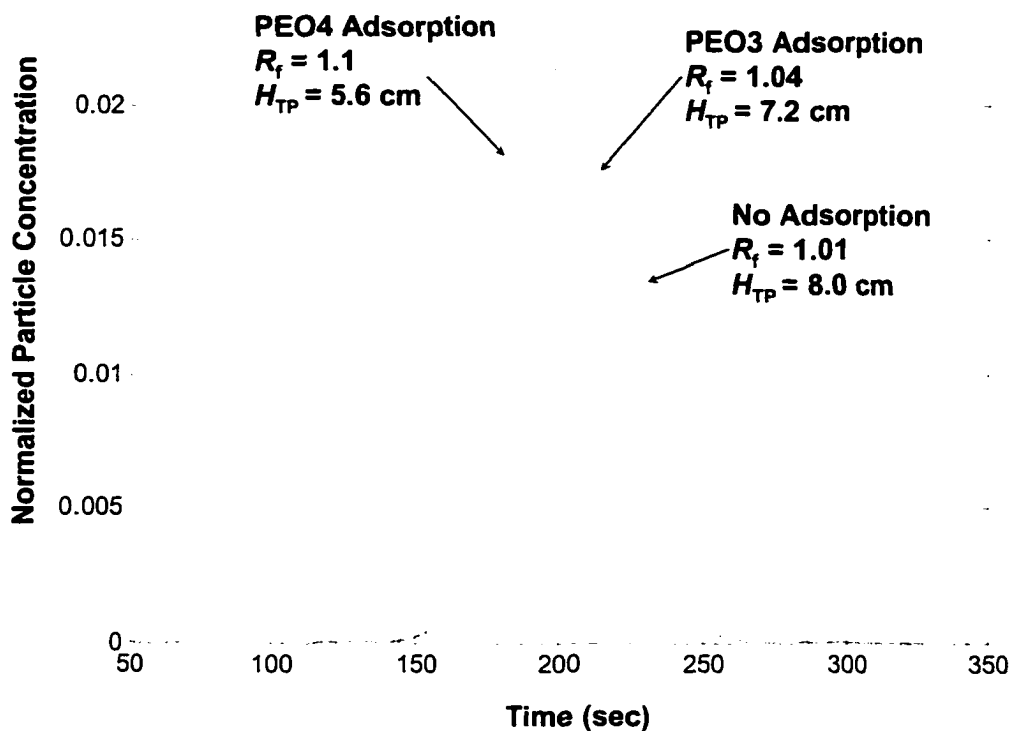
Figure 3-8: Simulated CHDF fractograms for the transport of 234 nm PS latex particles through the microcapillary associated with the adsorption of PEO; capillary = 24.1 μm and length = 655.0 cm; average velocity of the fluid without adsorption = 3.0 cm/s; adsorbed layer thickness of PEO3 = 180 nm and PEO4 = 540 nm; assumed isotropic adsorbed layer with permeability of PEO3 = 27.1 nm and PEO4 = 52.9 nm.
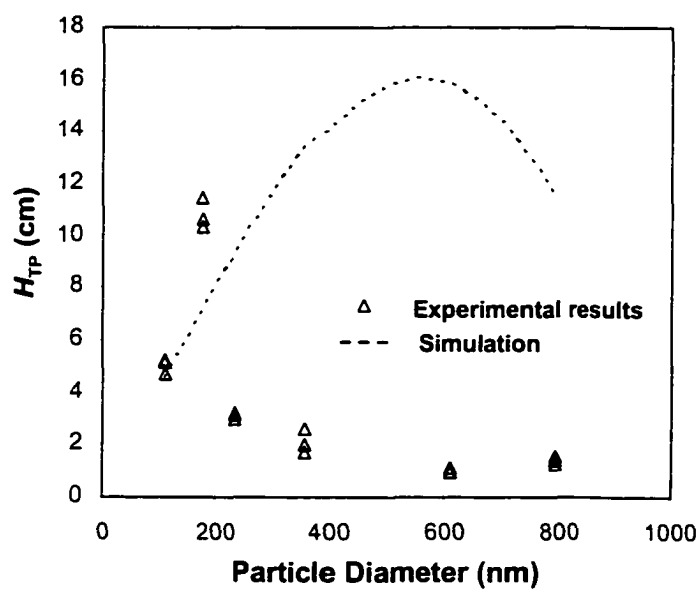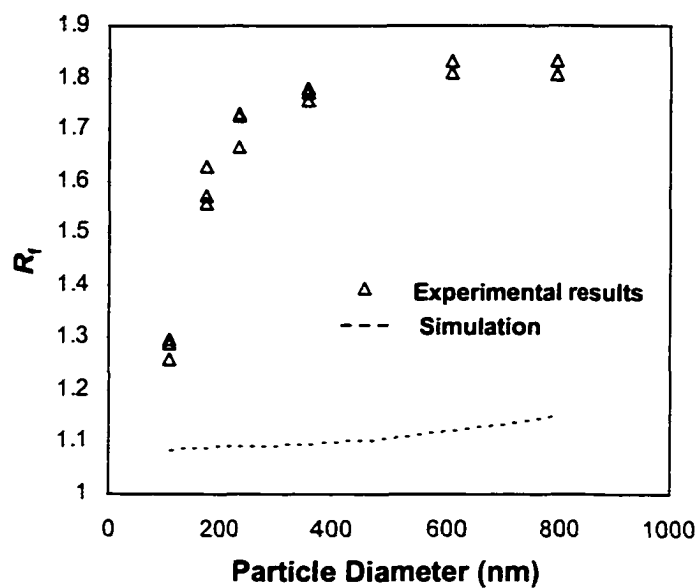
Figure 3-9: Experimental vs. simulated R_f and H_{TP} as a function of particle size associated with the adsorption of PEO4; capillary = 24.1 μm and length = 655.0 cm; average velocity of the fluid = 2.8 cm/s; adsorbed layer thickness of PEO4 = 540 nm; assumed isotropic adsorbed layer with permeability of PEO4 = 52.9 nm.

98

Also with the prediction of H_{TP}, the CHDF model, which takes into account the adsorbed PEO4 layer could not deal with the rapid decrease of experimental H_{TP}. The model predicted an increase of H_{TP} as the particle size increase due to the lower particle diffusivity before reaching a maximum and decreasing for larger particles. The reduction of the predicted H_{TP} was due to the effect of the inertia force, which was more prominent when the particle size became larger. The experimental H_{TP} showed much lower values than predicted indicating that besides the inertia force, there was another effect involved in the migration of particles toward the capillary center.

3.4 Polymer Migration in the Microcapillary

A pressure-driven flow of fluid through a microcapillary exhibits a parabolic velocity profile, indicating an inhomogeneous stress field of the flow. For a Newtonian fluid, the shear stress is strongest at the wall then decreases linearly toward the center of the tube. High shear in the vicinity of the wall might cause a deformation of the polymer molecules, providing a limited number of chain configurations compared to the polymer molecules close to the center where the polymers adopt a random coil configuration. Thermodynamically, the deformed polymer molecules close to the wall possess a lower entropy than the ones near the center of the tube and this will create the entropy difference along the radial direction. Since the higher entropy is in favor of the polymer molecules, the polymers will migrate from the low entropy region near the capillary wall towards the higher entropy region around the center of the capillary [78-80].

Cohen and Metzner [78] have derived the constitutive diffusion equation to describe the polymer migration in an inhomogeneous stress field based on the entropic driving force argument. For the steady-state laminar shear flow without external body force, the flux of polymer in the solvent can be described as:

$$\mathbf{J} = -\mathbf{D}(\phi \nabla C + C \nabla f) \qquad (3.17)$$

99

where C is the polymer concentration and **D** is the translational diffusivity of the polymer molecule. Function ϕ accounts for the concentration dependence of polymer diffusivity and can be expressed as a linear function of polymer concentration [81]:

$$\phi = 1 + k_\mathrm{D} C \tag{3.18}$$

The experiment by Scholtan [82] has confirmed this linear relationship of polymer diffusivity on the polymer concentration. He found that k_D is a strong function of polymer molecular weight especially at higher values. If the polymer molecule is modeled as a rigid sphere (non-draining), k_D is approximately equal to 1.45 [83]. Nevertheless, for a dilute solution, ϕ can be reasonably assumed as 1 indicating a negligible concentration dependence of the polymer diffusivity.

The potential function f is estimated based on a linear elastic dumbbell model of the polymer molecule or the Hookean dumbbell as shown in Figure 3-10 [78,84]:

$$f = (\lambda_\mathrm{H} \dot{\gamma})^2 - \frac{1}{2} \ln[1 + 2(\lambda_\mathrm{H} \dot{\gamma})] \tag{3.19}$$

where λ_H is the intrinsic relaxation time of the polymer molecule and $\dot{\gamma}$ is the local shear rate. The product term of $\lambda_\mathrm{H} \dot{\gamma}$ is called the Weisenburg number (We) which compares the characteristic time of flow to the time for a polymer molecule to resume a random coil state. Hence, the deformation of a polymer molecule due to the shear flow will start to take place if We ≥ 1. The molecular relaxation time of the Hookean dumbbell is given by [85]:

$$\lambda_\mathrm{H} = \frac{\zeta}{4H} \tag{3.20}$$

where ζ is the friction coefficient of the bead and H is the spring constant which is equal to $\frac{3kT}{\langle r^2 \rangle_\mathrm{o}}$ where $\langle r^2 \rangle_\mathrm{o}$ is the mean-square unperturbed end-to-end distance of the polymer molecule. These parameters can be estimated based on the molecular weight and molecular

100
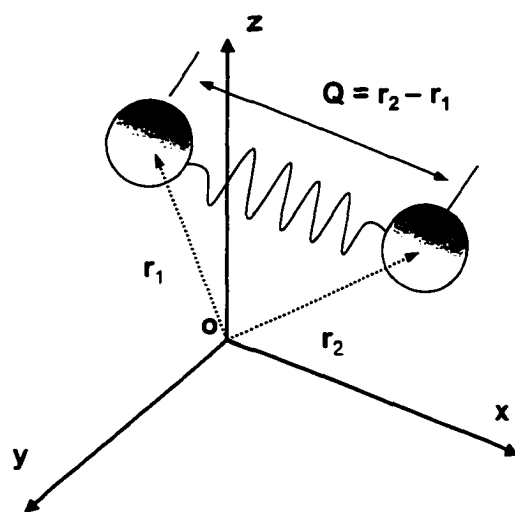
Figure 3-10: Polymer molecule modeled as a linear elastic dumbbell which consists of two equal size beads connected by a linear spring.

101

weight distribution of polymer as will be demonstrated in the next section.

To determine the concentration gradient of polymer in the capillary flow, the flux is substituted into the continuity equation:

$$\frac{\partial C}{\partial t} + \nabla \cdot C\mathbf{v} = -\nabla \cdot \mathbf{J} \tag{3.21}$$

where $\mathbf{v}$ is a local fluid velocity vector. Applying the cylindrical coordinates (z, r, θ) and taking into account the symmetry of the capillary tube, the continuity equation is transformed to:

$$\frac{\partial C}{\partial t} + \frac{\partial}{\partial z}(Cv_z) + \frac{1}{r}\frac{\partial}{\partial r}(rCv_r) = -\left[\frac{\partial J_z}{\partial z} + \frac{1}{r}\frac{\partial}{\partial r}(rJ_r)\right] \tag{3.22}$$

Since the radial component of the velocity v_r is negligible compared to the axial velocity v_z and the axial flux J_z is assumed to be much smaller than the radial flux J_r due to the slow axial diffusion compared to the convection, terms containing v_r and J_z will be neglected. Substituting the flux term equation (3.17) into the continuity equation, one obtains the convective-diffusion equation describing the polymer concentration in tube flow associated with polymer migration:

$$\frac{\partial C}{\partial t} + v_z\frac{\partial C}{\partial z} = D_r\left[\frac{1}{r}\frac{\partial}{\partial r}\left(r\frac{\partial C}{\partial r}\right)\right] + \frac{\partial C}{\partial r}\left(D_r\frac{\partial f}{\partial r} + \frac{\partial D_r}{\partial r}\right) + C\left(\frac{D_r}{r}\frac{\partial f}{\partial r} + D_r\frac{\partial^2 f}{\partial r^2} + \frac{\partial f}{\partial r}\frac{\partial D_r}{\partial r}\right) \tag{3.23}$$

This equation is subjected to the following initial and boundary conditions:

Initial condition: $t = 0$, $C = 0$; no polymer in the tube $\tag{3.24}$

Boundary conditions:

$z = 0$, $C = C_{zo}$; where C_{zo} is the polymer concentration at the capillary entrance $\tag{3.25}$

$r = 0$, $\dfrac{\partial C}{\partial r} = 0$; the symmetry at the tube center $\tag{3.26}$

$r = R_o$, $J_r = \dfrac{\partial C}{\partial r} + C\dfrac{\partial f}{\partial r} = 0$; no flux across the tube wall $\tag{3.27}$

102

3.4.1 Diffusivity of Polymer Molecule in Dilute Solution

Translational diffusivity of a polymer molecule through a solvent is determined based on the linear elastic dumbbell model. In this model, a polymer molecule is depicted as two equal size beads connected by a linear spring with a spring constant H (see Figure 3-10). In dilute solution, where interactions between polymer molecules are neglected, the forces which the polymer molecule will experience are the hydrodynamic drag force of the solvent on the beads, the Brownian force due to the bombardment of the solvent molecules and the hydrodynamic interaction force caused by the perturbation of one bead onto another [85]. This hydrodynamic interaction of a polymer molecule can be related to the draining factor of the polymer. For a free-draining molecule, there is no hydrodynamic interaction between two beads whereas a non-draining polymer refers to a molecule with infinite hydrodynamic interaction. As such the non-draining polymer will behave as a solid sphere. In the free-draining case, polymer diffusivity can be described by the classical Stokes-Einstein relation:

$$D = \frac{kT}{2\zeta} \tag{3.28}$$

where k is the Boltzmann constant, T is the absolute temperature. If the hydrodynamic interaction is accounted for, the polymer diffusivity can no longer be fully described by the scalar function but rather by the tensor quantity. This polymer diffusivity tensor is expressed as [86]:

$$\mathbf{D} = \frac{kT}{2\zeta}\left(\delta + \zeta\langle\Omega\rangle\right) \tag{3.29}$$

where δ is the unit tensor and Ω is the hydrodynamic interaction tensor expressed in analogous fashion to the Oseen tensor which described the hydrodynamic interaction of point particles in creeping flow [85].

$$\Omega = \frac{1}{8\pi\eta_s Q}\left(\delta + \frac{\mathbf{QQ}}{Q^2}\right) \tag{3.30}$$

103

where $\mathbf{Q}$ is the connection vector between two beads and Q^2 is equal to $\mathbf{Q} \cdot \mathbf{Q}$. In solvent, the polymer molecules are subjected to Brownian forces which causes a random motion of the molecules. As a result, the connector vector $\mathbf{Q}$ changes stochastically and thus Ω has to be averaged over all the polymer configurations (ensemble average); that is,

$$\langle \Omega \rangle = \int \Omega \Psi d\mathbf{Q} \tag{3.31}$$

where Ψ is the configuration distribution function of the polymer molecule. For the Hookean dumbbell with hydrodynamic interaction suspended in a homogeneous flow of an incompressible Newtonian fluid, the configuration distribution function is determined from the diffusion equation for a polymer in configuration space [85]:

$$\frac{\partial \psi}{\partial t} = -\frac{\partial}{\partial \mathbf{Q}}(\mathbf{\kappa} \cdot \mathbf{Q})\psi + \frac{\partial}{\partial \mathbf{Q}}\left[\frac{2H}{\zeta}(\delta - \zeta\Omega) \cdot \mathbf{Q}\right]\psi + \frac{2kT}{\zeta}\frac{\partial}{\partial \mathbf{Q}}(\delta - \zeta\Omega)\frac{\partial \psi}{\partial \mathbf{Q}} \tag{3.32}$$

The first term on the right hand side of the equation represents the hydrodynamic force due to the homogeneous flow and $\mathbf{\kappa}$ is the rate of strain tensor that is a function of time only. The second and third terms express the force due to the spring connector and the Brownian motion force, respectively.

To determine the ensemble average of the hydrodynamic interaction tensor, Kirkwood and Riseman [87] used the preaveraging method in which the equilibrium distribution function (ψ_{eq}) is assumed in the averaging process. The equilibrium distribution function is obtained from the diffusion equation described above with the conditions of no flow and steady state [85]:

$$\psi_{eq} = \left(\frac{H}{2\pi kT}\right)^{3/2} \exp\left(-\frac{HQ^2}{2kT}\right) \tag{3.33}$$

The diffusion tensor obtained by this preaveraging method is as follows:

$$\mathbf{D} = \frac{kT}{2\zeta}\left(1 + \sqrt{2}h^*\right)\delta \tag{3.34}$$

104

where h^* is the hydrodynamic interaction parameter defined by $\dfrac{\zeta}{\eta_s}\sqrt{\dfrac{H}{36\pi^3 kT}}$. This diffusion

tensor is isotropic and independent of the flow field due to the assumption of no flow in

determining ψ_{eq}. In order to take into account the effect of flow, the hydrodynamic interaction

tensor has to be averaged with the nonequilibrium distribution function. Öttinger and

Wedgewood introduced two new approximations to determine the hydrodynamic interaction

namely, the consistent averaging [88] and the Gaussian approximation [89,90]. These methods

lead to the Gaussian distribution of the distribution function ψ

$$\psi(\mathbf{Q},t) = \left[\left(\frac{2\pi kT}{H}\right)^3 \det\alpha(t)\right]^{-1/2} \exp\left[-\frac{H}{2kT}(\mathbf{Q}\cdot\alpha^{-1}(t)\cdot\mathbf{Q})\right] \tag{3.35}$$

The diffusion tensor determined by these methods becomes:

$$\mathbf{D} = \frac{kT}{2\zeta}\left(\delta + \sqrt{2}h^*\mathbf{H}\right) \tag{3.36}$$

where the flow field dependency of the diffusivity is introduced through the hydrodynamic

interaction function $\mathbf{H}$.

$$\mathbf{H} = \frac{3}{16\pi}(\det\alpha)^{-1/2}\int\frac{1}{\mathbf{x}}\left(\delta + \frac{\mathbf{xx}}{x^2}\right)\exp\left(-\frac{1}{2}\alpha^{-1}:\mathbf{xx}\right)d\mathbf{x} \tag{3.37}$$

where α is the covariance of the Gaussian distribution equation (3.35) which is equal

to $\dfrac{H}{kT}\langle\mathbf{QQ}\rangle$. This diffusion tensor contains an anisotropic part which indicates the flow rate

dependence.

By depicting the molecular shape of a Hookean dumbbell with hydrodynamic interaction

in a homogeneous flow as the ellipsoid, Prakash and Mashelkar [86] showed that $\mathbf{D}$ could be

decomposed into isotropic and anisotropic parts

105

$$\mathbf{D} = \frac{kT}{2\zeta}\left(1+\sqrt{2}h^{*}\right)\left(\frac{1}{1+\sqrt{2}h^{*}}\delta + \frac{\sqrt{2}h^{*}}{1+\sqrt{2}h^{*}}\mathbf{D}^{*}\right)$$ (3.38)

where $\mathbf{D}^{*}$ is related to the diffusivity of the ellipsoid, which describes the average spatial extent of the dumbbell when it is subjected to hydrodynamic and Brownian forces. Prakash and Mashelkar [91] obtained the analytical approximation of $\mathbf{D}^{*}$ by estimating the size and orientation of the ellipsoid and calculating the Stokes drag on this approximate ellipsoid. Described in terms of the flow principal axes of the ellipsoid, D_i^{*} where (i = 1, 2, 3), the analytic approximate of $\mathbf{D}^{*}$, are

$$D_1^{*} = \frac{3}{8}\left[\frac{(2\alpha_1 - 1)\chi^{*} - 2\sqrt{\alpha_1}}{(\alpha_1 - 1)}\right]$$ (3.39)

and

$$D_2^{*} = D_3^{*} = \frac{3}{8}\left[\frac{(2\alpha_1 - 3)\chi^{*} + 2\sqrt{\alpha_1}}{2(\alpha_1 - 1)}\right]$$ (3.40)

where

$$\chi^{*} = \frac{2}{\sqrt{\alpha_1 - 1}}\ln\left(\sqrt{\alpha_1} + \sqrt{\alpha_1 - 1}\right)$$ (3.41)

and

$$\alpha_1 = \frac{1}{1 - \cos 2\phi}, \qquad \alpha_2 = \frac{1}{1 + \cos 2\phi}, \qquad \alpha_3 = 1$$ (3.42a, 3.42b, 3.42c)

$$\tan 2\phi = \frac{1 - \sqrt{2}h^{*}}{\lambda_H \dot{\gamma}}$$ (3.43)

The translational diffusion coefficient of polymer through the solvent in simple shear flow is equal to one-third of the trace of the diffusion tensor. Even though the flow through the microcapillary is not homogeneous, we assume that this analytical approximation of the diffusion tensor in simple shear flow can be applied to our system because the molecular scale of the polymer is relatively small compared to the scale of the flow field. On the other hand, the local shear field around the polymer molecule can be approximated by the linear shear flow. In addition, Aubert and Tirrell [92] have shown that the configuration distribution function of a linear elastic dumbbell obtained in a parabolic inhomogeneous flow is identical to that obtained in

106

a homogeneous simple shear flow with the same shear rate as that at the center of mass.

3.4.2 Molecular Characteristics of Linear Elastic Dumbbell

Under the theta condition, polymer molecules will be in the unperturbed state. To find the end-to-end distance of a polymer molecule in the theta state, the Stockmayer-Fixman equation is employed [93]:

$$\frac{[\eta]}{\sqrt{M_n}} = K_\theta + 0.51\Phi B \sqrt{M_n} \tag{3.44}$$

where $[\eta]$ is the intrinsic viscosity and M_n is the number-average molecular weight of the polymer. The plot of $\frac{[\eta]}{\sqrt{M_n}}$ versus $\sqrt{M_n}$ should yield a straight line with intercept equal to K_θ and this term is defined as:

$$K_\theta = \Phi_o \left(\frac{\langle r^2 \rangle_o}{M} \right)^{3/2} \tag{3.45}$$

where Φ_o is the universal constant, which is equal to 2.1×10^{23} for a broad molecular weight distribution. The intrinsic viscosity is in units of cm^3/g and can be obtained experimentally. Alternatively, since we know the molecular weight and molecular weight distribution of PEO as determined by gel permeation chromatography (GPC), the intrinsic viscosity can be easily obtained from the Mark-Houwink equation expressed for PEO in water at 25 °C as [11]:

$$[\eta] = K_w M_w^a = 5.94 \times 10^{-4} M_w^{0.657} \tag{3.46}$$

where K_w is the Mark-Houwink coefficient based on the weight-average molecular weight and M_w is the weight-average molecular weight. Since the molecular weight of PEO from GPC indicated a broad distribution of molecular weights, the K coefficient has to be corrected for a high polydispersity using the method suggested by Kurata and Tsunashima [94]

107

$$K'_n = K_n \left(\frac{M_w}{M_n}\right)^{0.5a(1+a)}$$ (3.47)

$$K'_w = K_w \left(\frac{M_w}{M_n}\right)^{0.5a(a-1)}$$ (3.48)

where K' and K are the corrected and experimental Mark-Houwink coefficients, respectively.

Figure 3-11 shows the plot of $\dfrac{[\eta]}{\sqrt{M_n}}$ vs. $\sqrt{M_n}$ in which a linear relationship was

obtained as predicted by the Stockmayer-Fixman equation. K_θ, the y-intercept of the straight line

shown in the plot, is equal to 0.545 cm^3/g and this has to be corrected for polydispersity of the

molecular weight as well. For a Gaussian molecular weight distribution, the corrected K'_θ may be

approximated as:

$$K'_0 = K_\theta \left(\frac{M_w}{M_n}\right)$$ (3.49)

Finally, the unperturbed end-to-end distance of a polymer molecule can be calculated from

equation (3.45).

The friction coefficient of the bead for a linear elastic dumbbell can be estimated from

[95]:

$$2\zeta = \frac{6[\eta]_\theta \eta_s M}{N_A \langle S^2 \rangle_o}$$ (3.50)

where $[\eta]_\theta$ is the intrinsic viscosity of polymer solution at the theta state, which is equal to $K_\theta M^{1/2}$

and $\langle S^2 \rangle_o$ is the mean square unperturbed radius of gyration. For a linear flexible polymer, this is

equal to one-sixth of the mean square unperturbed end-to-end distance.

Table 3-2 shows the root mean square end-to-end distance of an unperturbed polymer

chain, the spring constant, the friction coefficient of a bead and the intrinsic relaxation time of a

108
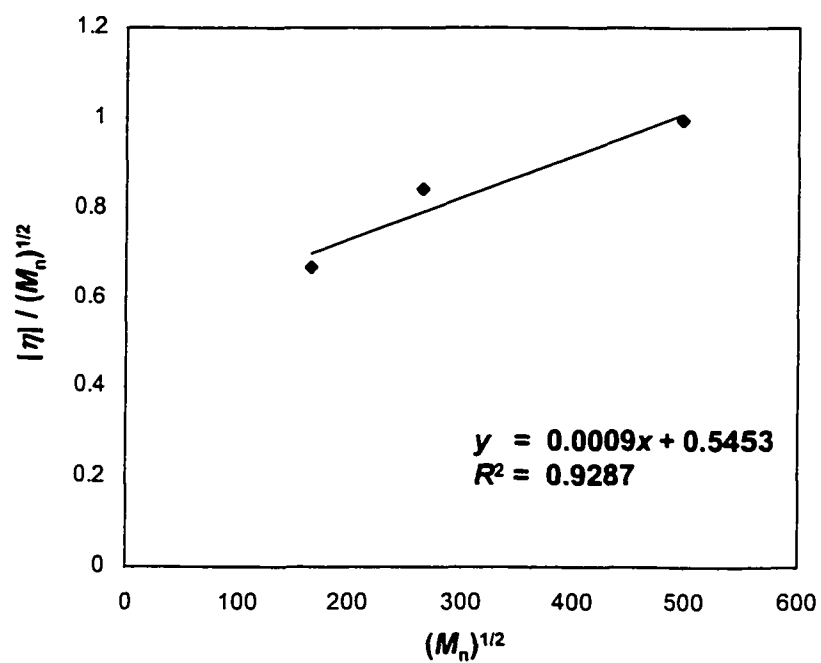
Figure 3-11: Plot of $\dfrac{[\eta]}{\sqrt{M_n}}$ vs. $\sqrt{M_n}$ for PEO in water at 25 °C.

The plot shows $[\eta]/(M_n)^{1/2}$ on the y-axis versus $(M_n)^{1/2}$ on the x-axis, with the fitted line equation:

$$y = 0.0009x + 0.5453$$
$$R^2 = 0.9287$$

Table 3-2: Root-Mean-Square End-to-End Distance of Unperturbed PEO Molecule $\langle r^2 \rangle_o^{1/2}$, Spring Constant H, Friction Coefficient of a Bead ζ and Intrinsic Relaxation Time λ_H

PEO	$\langle r^2 \rangle_o^{1/2}$ (nm)	H (ergs/cm)	ζ (g/s)	λ_H (s)
PEO1	14.3	6.00×10^{-2}	9.04×10^{-8}	3.77×10^{-7}
PEO2	37.5	8.76×10^{-2}	2.35×10^{-7}	6.71×10^{-6}
PEO3	63.4	3.07×10^{-3}	3.97×10^{-7}	3.23×10^{-5}
PEO4	116.4	9.11×10^{-4}	7.28×10^{-7}	1.99×10^{-4}

110

polymer chain based on the Hookean dumbbell model for various molecular weight of PEO.

3.4.3 Numerical Results

Due to the similarity of equation (3.23) and equation (2.76), the numerical scheme for dynamic CHDF model as demonstrated in chapter 2 is used here to solve for the dispersion of polymer molecules through the microcapillary. The slug of polymer solution with concentration C_{zo} is delivered to the parabolic flow field of the solvent and undergoes the dispersion process inside the capillary. The concentration of polymer in the slug is assumed to be dilute and contributes negligibly to the change of fluid viscosity.

Figure 3-12 shows the fractograms of PEO solutions of various molecular weights along with the values of their separation factors. The model predicted that at the same shear rate, as the molecular weight of PEO increased, the rate of polymer migration would increase. The higher separation factor and narrower distribution of PEO compared to the case of no polymer migration indicated that the PEO polymer molecules were excluded from the wall and moved toward the center of the capillary. The migration takes place when the characteristic time of flow, which is indicated by the reciprocal of shear rate, is comparable to or shorter than the relaxation time of the polymer molecules to resume the random coil states. For the case of PEO1 and PEO2, even though PEO2 has a molecular weight an order of magnitude higher than PEO1, the rate of migration of PEO2 was the same as that of PEO1. This is because in this particular flow condition, both PEO1 and PEO2 exhibited a weak response to the shear (We is much less than 1). However, with the lower diffusivity of PEO2 because of its higher molecular weight, the degree of axial dispersion was promoted, which resulted in the decreasing of average velocity of PEO2.

The effect of shear rate is illustrated in Figure 3-13 which is the plot of the separation factor as a function of wall We. The rate of migration increased with the degree of shear. For the

111
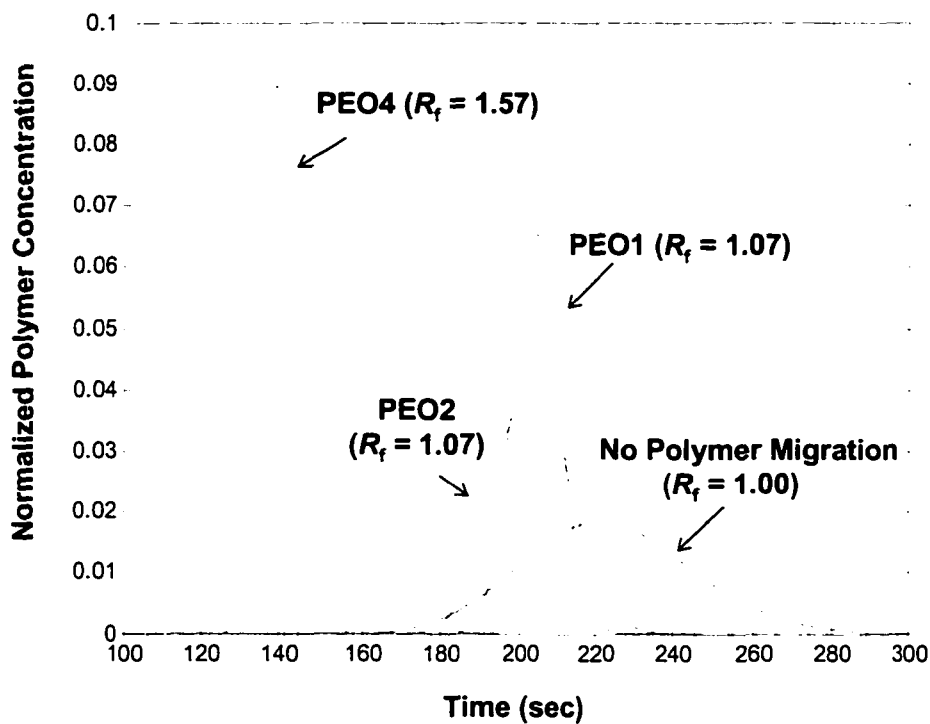
Figure 3-12: Simulated fractograms of transport of PEO through the microcapillary associated with the polymer migration; capillary ID = 24.1 μm and length = 655.0 cm; average velocity of fluid = 3.0 cm/s.
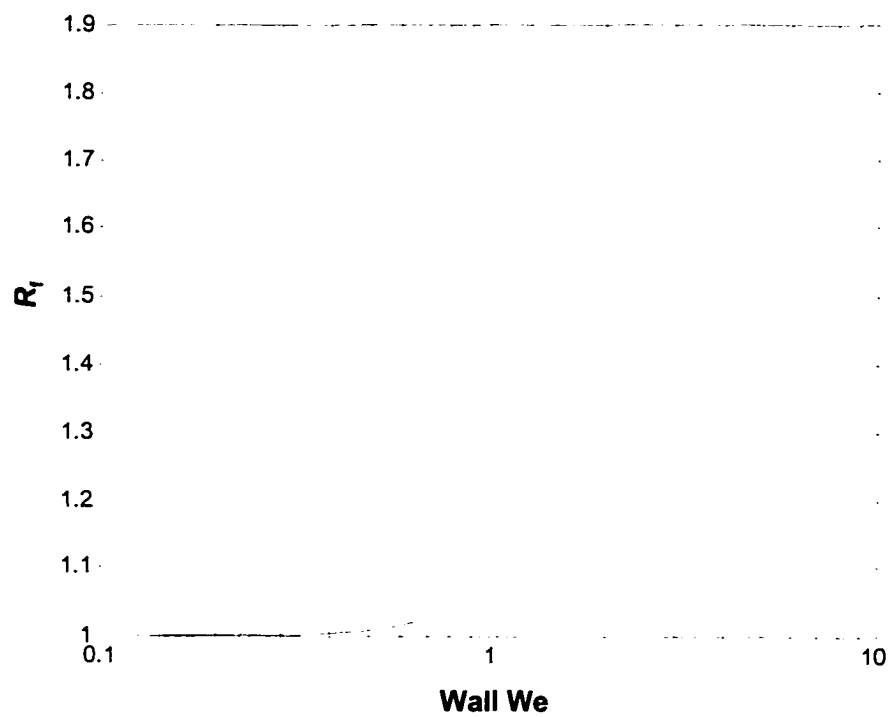
Figure 3-13: Simulated separation factor of polymer transport through the microcapillary associated with the polymer migration as a function of wall We.

113

weak flow condition in which We < 1, there was almost no polymer migration because the characteristic time of flow is much longer than the molecular relaxation time of the polymer, therefore the polymer molecules appeared in the flow field as they were in the equilibrium state of a random coil. At high shear rate, the characteristic time of flow became shorter until it became less than the relaxation time. Under this condition, polymer molecules started to deform, which would induce a higher entropic potential across the tube radius resulting in a higher rate of migration of polymer molecules toward the tube center.

3.4.4 Effect of Polymer Migration on Fully-Developed Concentration Profile of the Capillary Flow of Dilute Polymer Solutions

The flow of dilute polymer solution through a microcapillary associated with radial migration of polymer molecules is simulated by assuming that the concentration of polymer is fully developed. Therefore, the polymer concentration in the capillary is a spatial function varying only in the radial direction. At full development of polymer concentration, the flux due to polymer migration is balanced by the radial diffusive flux, therefore the net flux J_r is zero. From equation (3.17), the fully-developed polymer concentration can be obtained from the following equation:

$$\frac{dC}{dr} = -\frac{C}{\phi}\frac{df}{dr} \tag{3.51}$$

Since f is a function of λ_H and shear rate while the shear rate depends upon the polymer concentration which is varied along the radial direction, equation (3.51) can be expressed as [18]

$$\frac{dC}{dr} = -\frac{C\dfrac{\partial f}{\partial \dot{\gamma}}\dfrac{\partial \dot{\gamma}}{\partial r}}{\phi + C\dfrac{\partial f}{\partial \dot{\gamma}}\dfrac{\partial \dot{\gamma}}{\partial C}} \tag{3.52}$$

114

The Newtonian behavior of this polymer solution is assumed because the considered solution is so dilute. Thus the shear stress τ and shear rate $\dot{\gamma}$ of the solution in tube flow are related by:

$$\dot{\gamma}(C) = -\frac{dv_z}{dr} = \left(\frac{r}{R_o}\right)\left(\frac{\tau_w}{\eta(C)}\right) \tag{3.53}$$

where τ_w is the wall shear stress and η is the polymer viscosity, which is dependent upon the polymer concentration.

The concentration dependence of polymer solution viscosity is expressed in term of the stretched-exponential function [96]; that is,

$$\eta = \eta_s \exp(\alpha C^\upsilon) \tag{3.54}$$

where η_s is the solvent viscosity. The exponent prefactor α and the stretched-exponent υ are obtained experimentally by measuring the viscosity of polymer solutions as a function of concentration. Figure 3-14 shows the plot of viscosity of PEO as a function of concentration and a fit by the stretched-exponential function. Note that the concentrations of PEO shown in Figure 3-14 were dilute enough to presume a Newtonian behavior. The viscosities of polymer solutions at various concentrations were measured as a function of shear rate using the Bohlin viscometer with a cone and plate geometry.

To solve equation (3.52), the concentration of polymer at the tube center C_{ro} is assumed and then it is solved numerically over the entire cross-section. Then, the solution is checked so that the mass balance across any cross-section is satisfied. The mass balance through any cross-section is expressed as [97]

$$2\pi \int_0^{R_0} v_z(r)C(r)r\,dr = \pi R_o^2 C_{zo} \int_0^{R_0} v_z(r)r\,dr \tag{3.55}$$

If the condition is not satisfied then C_{ro} is adjusted and the iteration process continues until equation (3.55) is satisfied. After the concentration profile is known, the velocity field can be

115
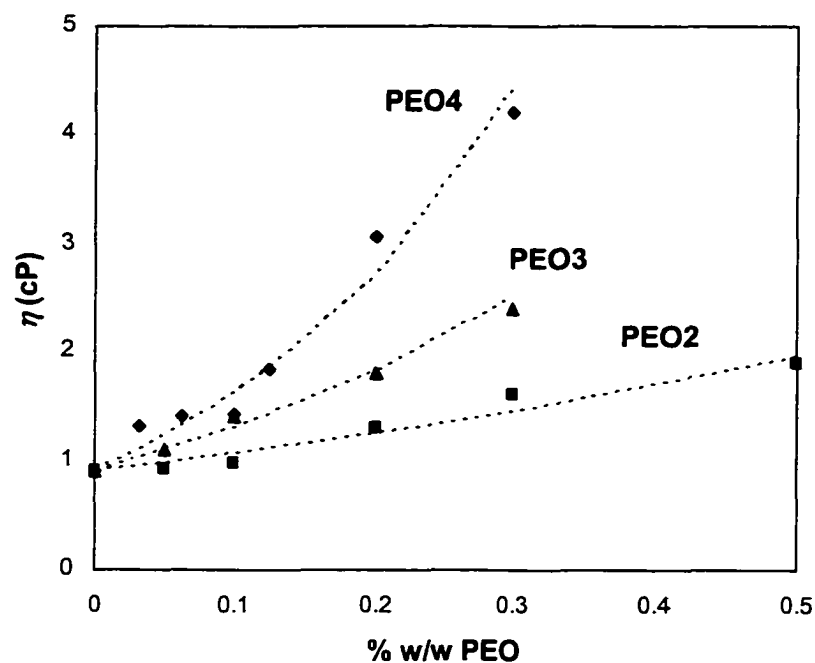
PEO	α	v
PEO2	1.5	0.95
PEO3	3.1	0.92
PEO4	4.7	0.90

Figure 3-14: plot of viscosity of PEO for various molecular weights as a function of concentration and a fit by the stretched-exponential function; closed symbols represent experimental viscosity and dashed-lines represent the functional fit.

116

obtained by integrating the shear rate equation (3.53).

Figure 3-15 shows the normalized radial concentration of PEO4 solution for different wall shear stresses. The numerical results predict the increase of the polymer concentration around the tube center. This is because polymer molecules migrate from a high shear rate region near the wall to the center of the tube where the shear rate is lower. As indicated by the higher concentration of PEO4, the polymer migration was enhanced as the wall shear stress increased. Due to the migration of polymer molecules from the capillary wall toward the center, the viscosity of polymer solution, which depends upon the polymer concentration, was also varied along the radial direction. The increasing viscosity of the fluid near the center caused the fluid velocity to decrease relative to the velocity of the fluid without the polymer migration. This is illustrated in Figure 3-16 where the velocity distribution of the polymer solution in the capillary associated with the polymer migration revealed a flatter profile compared to the one without migration. As the wall shear stress increased, the fluid velocity developed a flatter profile because of higher viscosity due to the greater rate of polymer migration.

3.4.5 Particle Diffusivity in Polymer Solutions

In an unbound fluid, diffusion of dilute particles of radius a in a medium of viscosity η is described by the well-known Stokes-Einstein (SE) equation

$$D = \frac{kT}{6\pi\eta a} \tag{3.56}$$

This equation was derived based on the assumption that the medium can be treated as a continuum relative to the particle length scale. The SE equation can perfectly explain the diffusion of noninteracting spheres in a small-molecule solvent. In polymer solutions, it may appear that the SE equation can not be applied because the presence of large molecular size

117
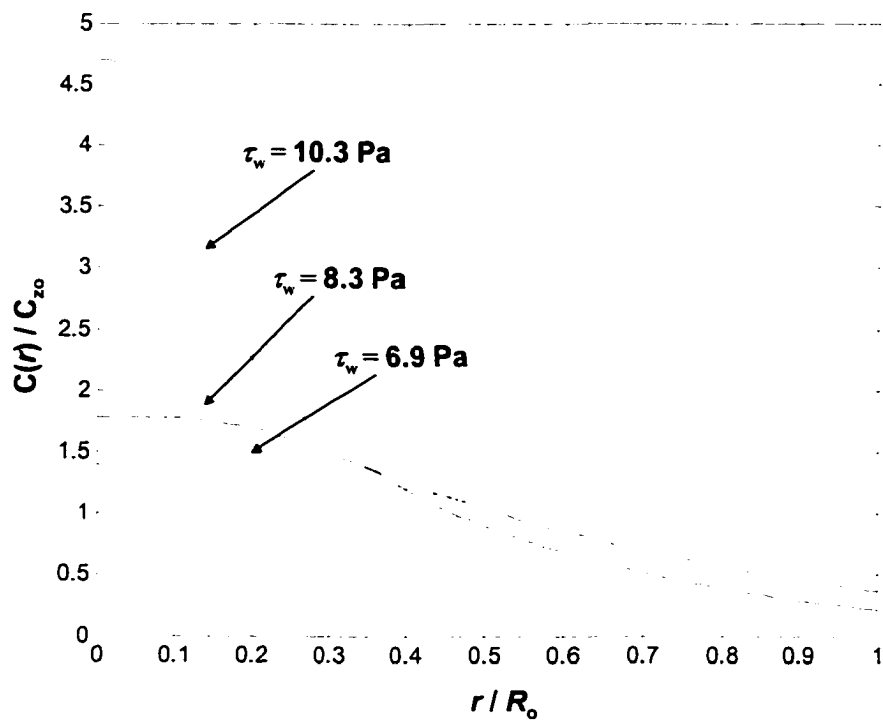
Figure 3-15: Fully-developed radial distribution of normalized concentration for the flow of PEO4 solution through the microcapillary associated with the polymer migration; capillary ID = 24.1 μm and length = 655.0 cm; concentration of PEO4 at the capillary entrance (C_{zo}) = 0.1 % w/w.
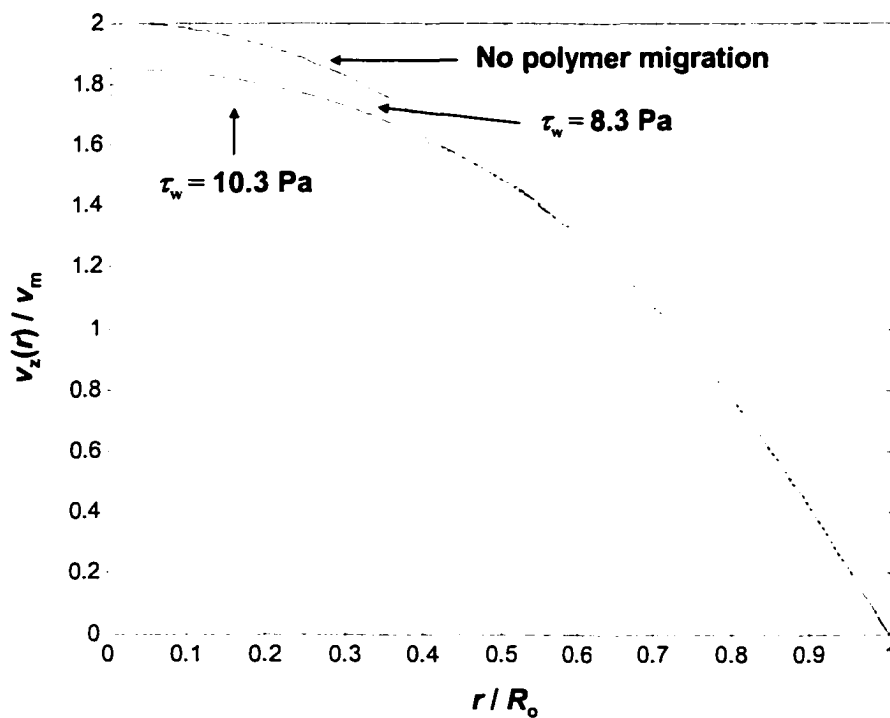
Figure 3-16: Fully-developed radial distribution of normalized velocity for the flow of PEO4 solution through the microcapillary associated with the polymer migration; capillary ID = 24.1 μm and length = 655.0 cm; concentration of PEO4 at the capillary entrance (C_{zo}) = 0.1 % w/w.

119

polymers (in solvent), which in some cases are comparable to the size of the particle, invalidates the assumption of the continuum medium.

According to deGennes' theory of polymer solutions [38], solution characteristics depend qualitatively on the polymer concentration C, with polymer solutions changing theirs properties as the concentration passes from one regime to the next. In a dilute polymer solution, the polymer molecules are appreciably separated, in which the interactions between molecules are insignificant, and their characteristic length is described in terms of the random coil size of polymer molecule in the solvent. For a semi-dilute solution, the polymer molecules start to overlap and form a transient mesh of polymer chains where the average distance between the chain contacting points ξ is smaller than the average size of a single molecule. In this regime, the characteristic length of polymer chains, which is ξ, is no longer dependant on the molecular weight of the polymer but rather be a function of the polymer concentration. This correlation length, ξ, is believed to be responsible for the dynamics of semi-dilute polymer solutions. The concentration which divides dilute solutions from semi-dilute solutions (C^*) can be estimated from $1/[\eta]$, where $[\eta]$ is the intrinsic viscosity. The values of C^* for various molecular weights of PEO in this study are shown in Table 3-3.

Table 3-3: Overlap Concentration (C^*) of PEO

Polymer	C^* (g/cm^3)
PEO1	0.070
PEO2	0.012
PEO3	0.005
PEO4	0.002

120

As the concentration of polymer increases, the SE equation predicts that the particle diffusivity will be decreased in accordance with the increasing viscosity of the polymer solution. Therefore, the ratio of $D\eta / D_o\eta_s$, where D_o and η_s are the particle diffusivity in pure solvent and solvent viscosity respectively, will be equal to 1. However, deviations from the SE equation have been observed by many investigators for the various systems of particles and polymer solutions in the range of polymer concentration from a dilute to semi-dilute regimes [98-104]. The maximum deviation has been found when the polymer concentration approaches C^*. A positive deviation where $D\eta / D_o\eta_s > 1$ corresponds to a diffusivity that decreases with increasing concentration less rapidly than the increase of viscosity or the diffusivity is higher than predicted by the SE equation. Ullmann et al. [98] studied the diffusion of probe latex particles in PEO solutions in which there was no adsorption of PEO on the particles. The adsorption of PEO was prevented by adding a small amount of nonionic surfactant (Triton X-100). In this nonadsorbing system, they observed a deviation from SE for small particles dispersed in solutions of high molecular weight PEO. The deviation was greater for higher concentrations of the PEO solutions. Ye et al. [99] investigated the validity of the SE equation for latex particles in polymer solutions in which the polymer chains were grafted on the particle surfaces. They found that the Stokes-Einstein equation can be applied even when the concentration of polymer was well above C^*. This is because of the fact that the polymer-coated particles always had a size larger than the correlation length of the polymer in solution due to the presence of the adsorbed polymer layer. Won et al. observed a maximum positive deviation from SE behaviors near C^* for the diffusion of polystyrene particles in the solution of poly(vinyl methyl ether). However, when the polymer concentration continued to increase to a sufficiently high value, SE behavior is recovered.

One model that relates the diffusion coefficient of a particle to the correlation length ξ was suggested by Langevin and Rondelez [105]:

$$\frac{D}{D_o} = \exp\left[-\left(\frac{a}{\xi}\right)^\varepsilon\right] + \frac{\eta_s}{\eta} \qquad (3.57)$$

where ε is the fitting parameter and η_s is the solvent viscosity. For $a \gg \xi$, the particle feels the medium as a continuum and the SE equation should be valid. If $a \ll \xi$, the particle actually passes through the mesh of entanglement polymer chains; the particle only experiences the polymer depletion area surrounding it, and thus the diffusion of a particle in the polymer solution should be controlled by the microscopic viscosity [106].

For concentrations ranging from dilute to semi-dilute regimes, the particle diffusivity often follows the hydrodynamic scaling model [107,108].

$$\frac{D}{D_o} = \exp\left(-\alpha C^v\right) \qquad (3.58)$$

Theoretically, v is equal to $1-1.5x$ with $x \sim 1/4$ for large chains in good solvents and $x \rightarrow 0$ for large chains in θ solvents [107]. The value $v = 5/8$ is predicted for a sufficiently large molecular weight of the polymer ($M \geq 1\times10^6$ g/mol) [109]. Apparently, the model predicts $\alpha \propto M^0 a^1$, while the experimental results follow roughly $\alpha \propto M^{0.8} a^0$ [98,107,108,110].

For most CHDF experiments in this study, the concentrations of PEO were considerably below the overlap concentration in which the SE relation should be applied because the overlapping chains are rare. Therefore, we did not attempt to obtain the fitting parameters by investigating the diffusion of particles in polymer solutions but instead, the scaling prefactor α and the scaling exponent v was obtained directly from the stretched exponential function of the viscosity shown in equation (3.54). The alteration of the particle diffusivity is assumed to depend only on the change of viscosity of the PEO solution.

122

3.4.5.1 Comparison with CHDF Experimental Results

The effect of particle diffusivity on the particle transport in CHDF was studied. As mentioned earlier, the diffusivity of a particle changes with the polymer concentration mainly because of the increasing viscosity of the polymer solution. Because of this, the transport behavior of latex particles dispersed in polymer solution is expected to be influenced by this change of polymer diffusivity.

The CHDF experimental results with PEO solutions as the eluants were compared with the CHDF simulations. The diffusivity of latex particles was calculated from equation (3.58). The problem was focused on the variation of the particle diffusivity due to the viscosity change of the eluants. We considered two cases; first, the case of no polymer migration (no PM) involved such that the viscosity of the PEO solution is radially uniform and second, the case in which there is polymer migration (PM) and thus the viscosity varies along the radial direction.

Figure 3-17 compares the experimental and predicted CHDF separation factors (R_f) and the theoretical plate heights (H_{TP}) for various sizes of PS latex particles pre-adsorbed with Brij35SP in the presence of 0.01 % w/w PEO4. The experimental results revealed a significant impact of PEO4 on improving R_f. The substantial increase of R_f and decrease of H_{TP} for PEO4 suggested that the particles suspended in PEO4 solution were excluded from the wall and resided close to the capillary center. The experimental H_{TP} first increased for the smaller particle sizes indicating the strong effect of axial convection due to the fluid velocity and because the particle diffusivity was reduced as the particle size increased. Hence, this would strengthen the effect of convection resulting in the increased degree of axial dispersion. As the particle sized increased further, the effect of inertia forces caused the particles to move toward the capillary center which eventually would reduce H_{TP}.

The experimental R_f and H_{TP} were compared with the ones predicted from the CHDF

123

Figure 3-17: Comparison of the experimental R_f and H_{TP} with the predicted results which incorporate the effect of polymer migration for transport of latex particles in 0.01 % w/w PEO4; capillary ID = 24.1 μm and length = 655.0 cm; eluant = 0.01 % w/w PEO4 with 4 mM NaCl content; average velocity of fluid = 2.8 cm/s.

124

dynamic model. For particle diameters less than 234 nm, the predicted R_f can match considerably well the experimental results. Under this condition of low PEO concentration, the predicted R_f in the case where polymer migration takes place was slightly higher than that without the radial migration of polymer. This is mainly because PEO4 solution is very dilute, so despite the occurrence of the polymer migration, a slight change of viscosity was created across the capillary radius. For larger particle sizes, the CHDF model predicted a much lower R_f than observed in the experiments. This implies that at these particle sizes, the change of particle diffusivity due to the increasing viscosity was not responsible for the enhancement of R_f. In addition, the predicted R_f for the case of polymer migration tended to coincide with R_f predicted without the polymer migration. The simulated H_{TP} does not compare very well with the experiments especially for larger particles. However, the predicted trend of H_{TP} with the particle size corresponded to the observed H_{TP}.

Figure 3-18 shows the experimental and predicted R_f and H_{TP} for various sizes of PS latex particles with a higher concentration of 0.1 % w/w PEO4. Evidently, the predicted R_f and H_{TP} failed to explain the separation of latex particles under this condition. The assumption of the alteration of particle diffusivity both with and without polymer migration could not account for the higher rate of increase of the experimental R_f specifically for the smaller particle sizes. Also, for the experimental observed H_{TP}, the rapid decrease could not be explained by the change of particle diffusivity alone.

The simulation results indicated that polymer migration could induce an enhancement of the separation factor. The migration of polymer generates an increase in the viscosity around the tube axis causing the diffusivity of the particles to decrease. As the particle diffusivity decreases, the particles take a longer time to migrate to the wall and as a result, the particle will stay close to the faster streamlines near the center of the tube.
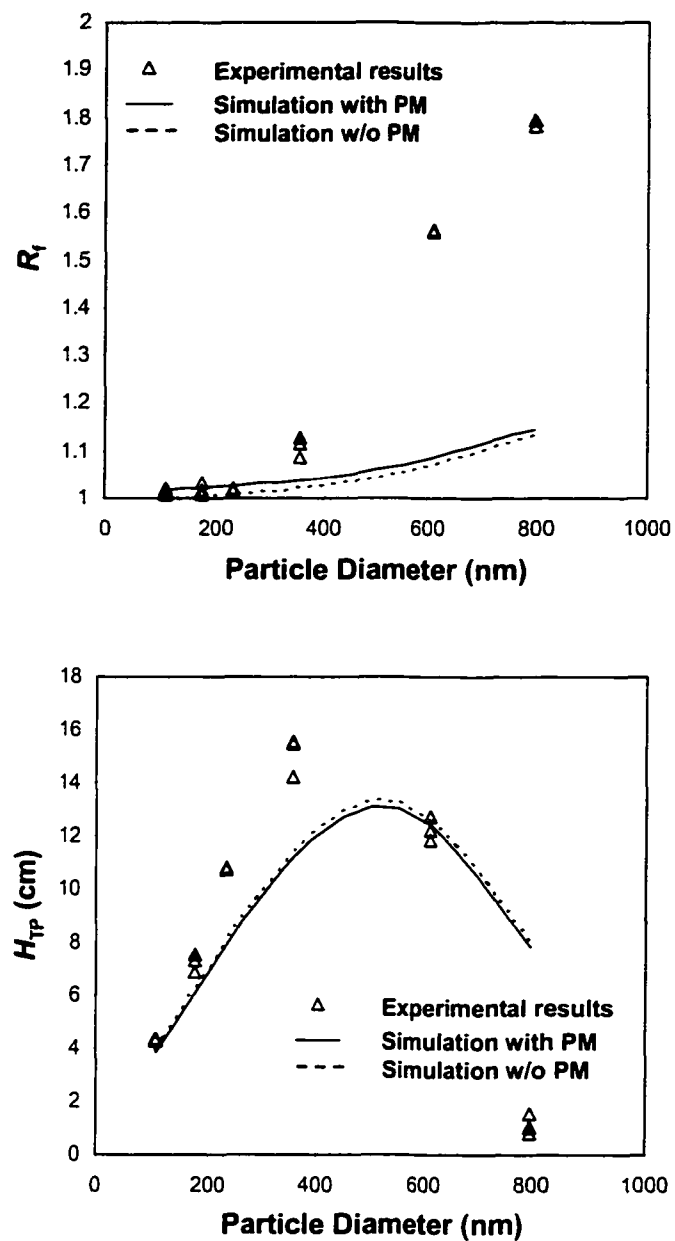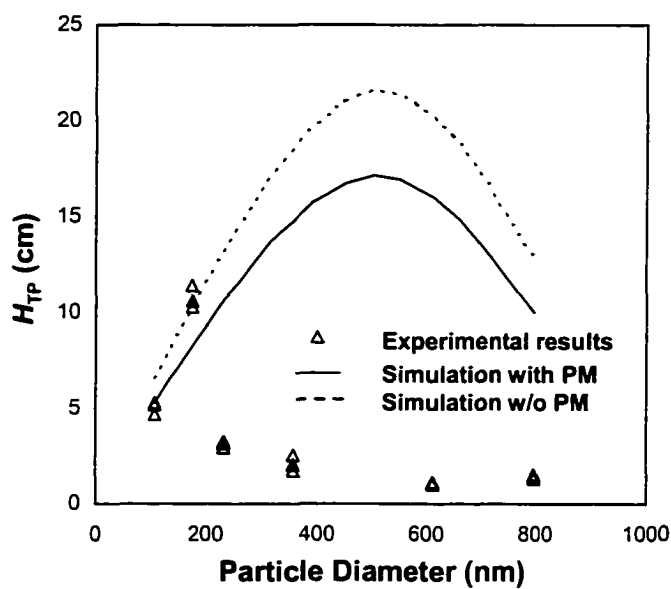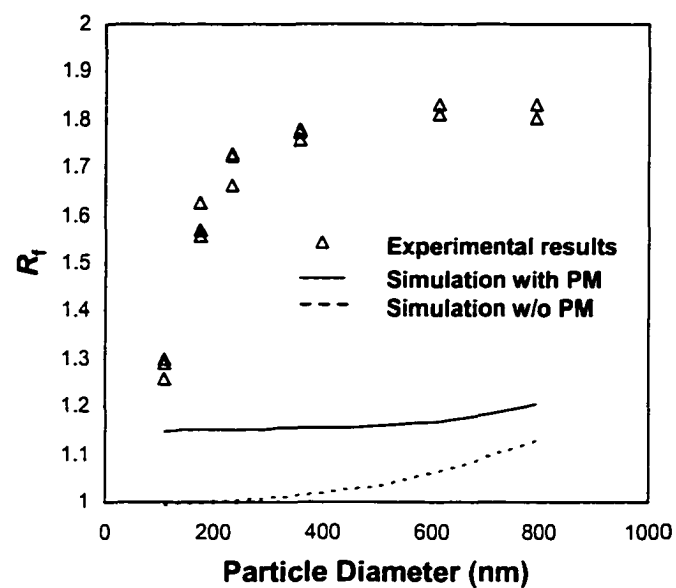
Figure 3-18: Comparison of the experimental R_f and H_{TP} with the predicted results which incorporating the effect of polymer migration for transport of latex particles in 0.1 % w/w PEO4; capillary ID = 24.1 μm and length = 655.0 cm; eluant = 0.1 % w/w PEO4 with 4 mM NaCl content; average velocity of fluid = 2.8 cm/s.

126

3.5 Viscoelastic Effect of PEO Solution

In a Newtonian fluid, the lateral migration of particles is the result of fluid inertia, which takes place at relatively high Reynolds numbers [47,48]. In viscoelastic fluids, the migration of particles can occur at low Reynolds numbers as been observed experimentally [14-20]. Karnis and Mason [14] found that neutrally buoyant solid spheres migrated toward the region of lower velocity gradient; that is, toward the outer cylinder wall in Couette flow and toward the center line in Poiseuille flow. The study of particle migration in cone-and-plate viscometer by Highgate and Whorlow [17,18] showed that the spheres in a viscoelastic fluid moved radially toward the outer edge. In plane-Poiseuille flow, Jefri and Zahed [20] investigated particle migration in three different types of fluids; Newtonian fluid, constant viscosity viscoelastic fluid, and shear thinning viscoelastic fluid. They observed that no migration took place for particles in Newtonian fluid whereas migration toward the upper and lower plates was seen for the shear thinning fluid. For particles in a viscoelastic fluid having constant viscosity, the particles were found to migrate toward the centerline.

Theoretical attempts to explain the migration phenomena of particles in a viscoelastic fluid were carried out by Leal et al. [69,111,112] and Brunn [113]. Ho and Leal [69] studied the migration of a single sphere in a second-order fluid for two-dimensional unidirectional flow and the theoretical results suggested that the migration of particles was the outcome of the lateral gradient of normal stress in the full velocity field.

It is known that a second-order fluid model is relevant for very slow flow and thus nearly Newtonian flow. The viscosities of PEO4 at various concentrations were measured as a function of shear rate using Bohlin viscometer with cone-and-plate geometry as shown in Figure 3-19. For 0.5 % w/w and 1.0 % w/w, PEO4 solutions showed a strong non-Newtonian behavior that can not be described by a second-order fluid. However, for the solutions at low concentrations (less than

127
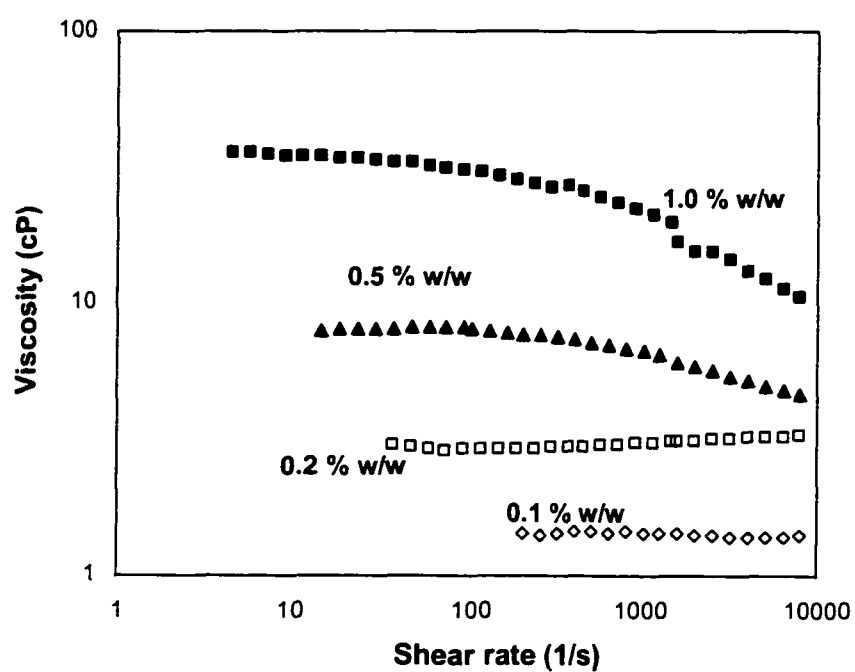
Figure 3-19: Viscosity as a function of shear rate for various concentrations of PEO4 at 25 ° C.

128

0.2 % w/w) nearly constant viscosities were observed. Therefore, it is justified to approximate the rheological behavior for low concentration PEO solutions using the second-order fluid model.

The theoretical treatment of Ho and Leal [69] was utilized in this section in order to explain at least qualitatively the increase of R_f and decrease of H_{TP} for the separation of latex particles in CHDF under the influence of the viscoelasticity of the PEO solutions.

The expression for the stress tensor of a second-order fluid is

$$\tau = -\eta \mathbf{A}_{(1)} + \phi_3(\mathbf{A}_{(1)} \cdot \mathbf{A}_{(1)}) + \phi_2 \mathbf{A}_{(2)} \qquad (3.59)$$

where $\mathbf{A}_{(1)} = \dot{\gamma} = \nabla \mathbf{v} + (\nabla \mathbf{v})^T$ which is the rate of strain tensor and

$$\mathbf{A}_{(2)} = \frac{\partial \mathbf{A}_{(1)}}{\partial t} + \mathbf{v} \cdot \nabla \mathbf{A}_{(1)} + \mathbf{A}_{(1)} \cdot (\nabla \mathbf{v})^T + \nabla \mathbf{v} \cdot \mathbf{A}_{(1)}$$ which is the second Rivlin-Ericksen tensor. η is the fluid (polymer solution) viscosity, ϕ_2 and ϕ_3 are the rheological parameters which can be estimated from the kinetic theory. Note that the first term of the right hand side of the equation represents the stress tensor for a Newtonian fluid.

If a polymer molecule is modeled as the linear elastic dumbbell, the parameters appearing in the second-order fluid model can be determined from:

$$\eta = \eta_s + nkT\lambda_H \qquad (3.60)$$

$$\phi_2 = nkT\lambda_H^2 \qquad (3.61)$$

$$\phi_3 = -2nkT\lambda_H^2 \qquad (3.62)$$

where n is the number of polymer molecules. The primary (ψ_1) and secondary (ψ_2) normal stress coefficients are given by:

$$\psi_1 = -\phi_3 \qquad (3.63)$$

$$\psi_2 = 2\phi_2 + \phi_3 \qquad (3.64)$$

and the primary (N_1) and secondary (N_2) normal stress differences are defined by

129

$$N_1 = \psi_1 \dot{\gamma}^2, \quad N_2 = \psi_2 \dot{\gamma}^2 \tag{3.65}$$

Clearly, this second-order fluid model cannot predict the shear rate dependence of viscosity and normal stress coefficients. Additionally, a second-order fluid always predicts a zero secondary normal stress difference.

Figure 3-20 shows the viscosity of PEO4 solutions compared with the estimation from equation (3.60). It is obvious that the very broad molecular weight distribution of PEO4 gave rise to the difference in predicted viscosity due to the uncertainty in calculating the number of polymer molecules, which is based on the molecular weight. Note that in this case, a constant value of the intrinsic relaxation time was used for PEO4. Therefore, because of this broad molecular weight distribution of PEO4, the use of single relaxation time may not be appropriate for a more accurate quantitative comparison. In the absence of a more rigorous analysis to account for the effect of the molecular weight distribution, the estimation of the number of polymer molecules will be based on the weight-average molecular weight.

The lateral migration velocity arising from the gradient of normal stress of the second-order fluid is given as [69]:

$$v_{pr} = \left(\frac{5}{3}\right) \dot{\gamma} \left(\frac{d\dot{\gamma}}{dr}\right) \phi_3 \left(\frac{1}{3} + \frac{\phi_2}{\phi_3}\right) \left(\frac{a^2}{\eta}\right) \tag{3.65}$$

where in unidirectional capillary flow, $\dot{\gamma}$ can be represented by the velocity gradient of the unperturbed velocity field. This expression can be easily incorporated into the CHDF dynamic model.

Figure 3-21 and 3-22 compares the predicted R_f and H_{TP} with the experimental results for PS latex particles pre-adsorbed with Brij35SP in the presence of 0.01 % w/w and 0.1 % w/w PEO4, respectively. The simulation showed considerably good agreement with the experimental results especially for the prediction of R_f. This indicates that the enhancement of particle

130
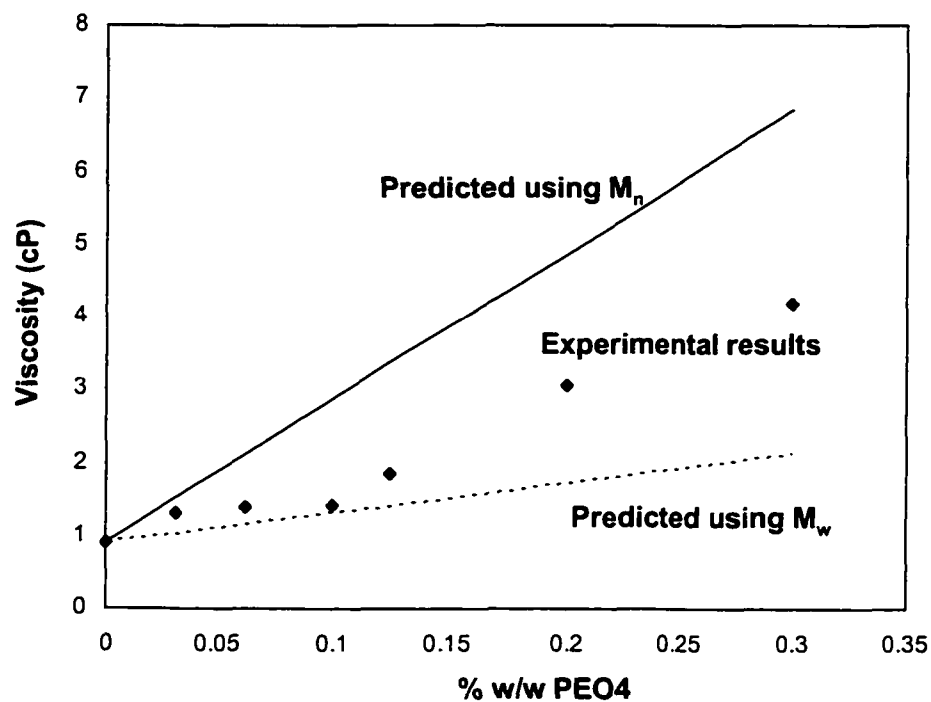
Figure 3-20: Comparison of the experimental viscosity of PEO4 solutions with the estimation from a linear elastic dumbbell model; the number of polymer molecules is calculated based on the number-average molecular weight (M_n) and the weight-average molecular weight (M_w) of PEO4; the intrinsic relaxation time of PEO4 molecule = 1.99×10^{-4} sec.

131

separation in CHDF was due to the dominant effect of the normal stress of PEO solutions in shear flow.

In the simulation, for both concentrations of PEO4, the capillary diamter was assumed to be reduced by the thickness of the adsorbed PEO4 on the capillary surface, which is aproximately 540 nm. However, this value of adsorbed layer thickness was obtained only for 0.1 % w/w PEO4. Clearly, for 0.1 % w/w PEO4, the presence of adsorbed PEO4 on the capillary surface does not cause any significant effect on the particle separation due to the more prominent effect fromm the normal stress of the PEO solution. For 0.01 % w/w PEO4, the effect of adsorbed PEO4 on the simulation was more distinct especially for particle diameters less than 357 nm. Nonetheless, the use of adsorbed PEO4 layer obtained from 0.1 % w/w for this case seems to give predicted values greater than those experimentally determined.

In fact, since the source of particle migration in a viscoelastic fluid arises from the gradient of normal stress, for a neutrally buoyant particle in slow Poiseuille flow, this lateral force is balanced by the Stokes drag force on the particle, that is [114]

$$6\pi a \eta v_{pr} \propto a^3 \frac{\partial N_1}{\partial r} \qquad (3.66)$$

or in term of v_{pr}

$$v_{pr} \propto \frac{a^2}{\eta} \psi_1 \dot{\gamma} \frac{\partial \dot{\gamma}}{\partial r} \qquad (3.67)$$

If we can obtain ψ_1 experimentally by measuring the normal stress difference of the polymer solution as a function of shear rate, the lateral migration velocity can be estimated based on the actual rheological properties of the polymer solution.
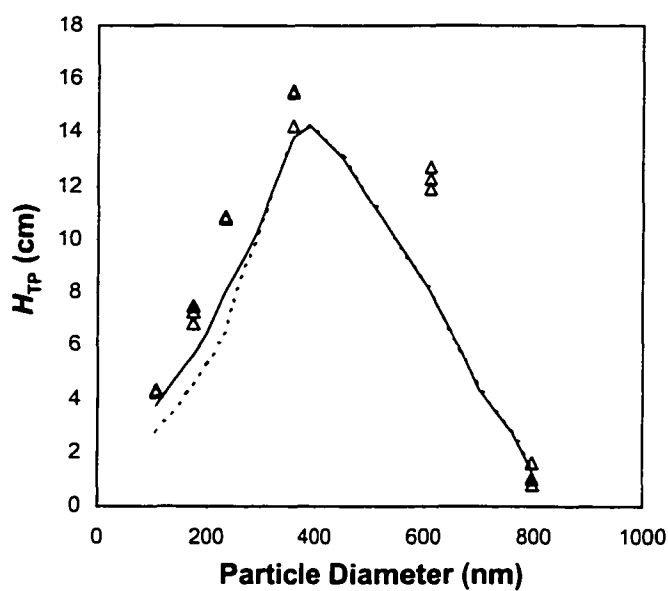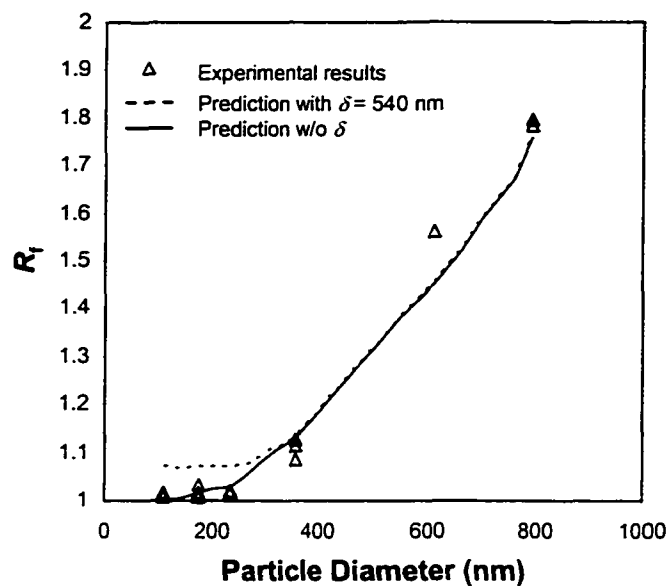
Figure 3-21: Comparison of the experimental R_f and H_{TP} with the predicted results which incorporate the effect of lateral particle migration due to the viscoelastic effect of PEO4 solution for transport of latex particles in 0.01 % w/w PEO4; capillary ID = 24.1 μm and length = 655.0 cm; eluant = 0.01 % w/w PEO4 with 4 mM NaCl content; average velocity of fluid = 2.8 cm/s; adsorbed PEO4 layer (δ) on the capillary surface = 540 nm.

133
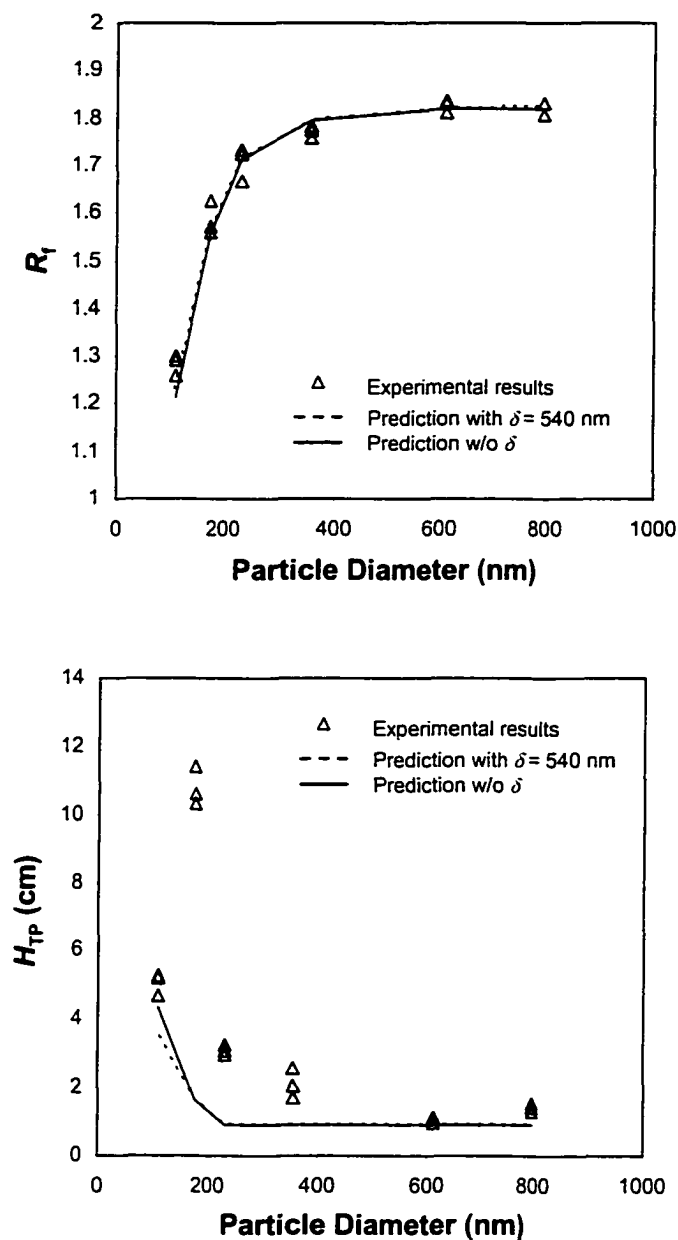
Figure 3-22: Comparison of the experimental R_f and H_{TP} with the predicted results which incorporate the effect of lateral particle migration due to the viscoelastic effect of PEO4 solution for transport of latex particles in 0.1 % w/w PEO4; capillary ID = 24.1 μm and length = 655.0 cm; eluant = 0.1 % w/w PEO4 with 4 mM NaCl content; average velocity of fluid = 2.8 cm/s; adsorbed PEO4 layer (δ) on the capillary surface = 540 nm.

134

3.6 Conclusions

Separation of latex particles in CHDF could be improved dramatically if PEO solutions are used as the eluant. The significant enhancement of R_f and rapid decrease of H_{TP} indicated that the particles migrated from the capillary wall toward the center. Despite the use of high ionic strength PEO solutions, R_f and H_{TP} still showed strong improvements suggesting that the migration was not due to the electrokinetic interaction between the particles and wall.

The flow of PEO solutions through the microcapillary was found experimentally to be associated with the surface phenomena of slip and adsorption. Low molecular weight PEO (PEO1 and PEO2) showed the dominant effect of the slip. Whereas the adsorption of PEO can be observed for PEO3 and PEO4 and the thickness of the adsorbed layer was found to be larger than the molecular coil size of the PEO molecules in the solvent.

The presence of the PEO adsorbed layer was accounted for in the CHDF dynamic simulation. The simulations revealed the enhancement of the particle separation with the increased thickness of the adsorbed layer. However, the experiments indicated a higher rate of particle separation enhancement which could not be explained by the effect of PEO adsorption alone.

Polymer migration was also considered. Theoretically, the rate of radial migration of polymer in a capillary flow depends upon the intrinsic relaxation time of the polymer and the shear rate. The polymer migration causes the variation of polymer concentration in the radial direction, which leads to a change of viscosity of the polymer solution while flowing through the microcapillary. Since for the same particle size, the change in particle diffusivity is induced by the increasing of viscosity due to the presence of PEO, the occurrence of polymer migration will affect the particle separation in CHDF. The CHDF simulation showed an increasing R_f and decreasing H_{TP} for transport of latex particles in a PEO solution when accompanied by polymer

135

migration compared to the simulations without polymer migration. Nonetheless, the comparison with the experimental results indicated that the enhancement of particle separation was not the result of the change in the particle diffusivity due to the polymer migration.

Migration of latex particles in PEO solution could be attributed to the viscoelastic behavior of the polymer solution. For the slow flow, the gradient of the normal stresses of PEO solution causes the particles to migrate from a high shear rate toward a low shear rate region. In the capillary flow, this will lead to the migration of particles from the capillary wall to the center of the capillary. The lateral particle migration velocity in a second-order fluid [44] was incorporated into the dynamic CHDF model. The simulation results showed better agreement with the experiments indicating that the separation of latex particles in PEO solution was mainly dominated by the viscoelastic properties of the PEO solution.

136

Chapter Four

Transport of Latex Particles through a Microcapillary in the

Presence of Polymer Solutions

4.1 Introduction

As demonstrated in the previous two chapters, PEO can adsorb onto the PS particles resulting in a size enhancement; also the transport of particles through a microcapillary using PEO solution as the eluant will be affected by the viscoelastic properties of the fluid such that the normal stress gradient of a PEO solution in a flow field will induce the migration of particles toward the capillary center. In this chapter, these two effects are considered together (adsorption and viscoelastic properties). To conduct the experiments, samples containing a mixture of PS latex particles and PEO (after equilibrating for at least 12 hours) were introduced into the CHDF system with the use of aqueous solution of PEO as the eluant.

The objective of this chapter is to demonstrate experimentally the effect of PEO on the separation of latex particles in CHDF. Many important factors are considered; i.e. the molecular weight of the PEO, the average velocity of the fluid and the ionic strength of the PEO solution.

4.2 Separation of Colloidal Particles in the Presence of PEO

CHDF separation factor (R_f) and theoretical plate height (H_{TP}) of various size PS latex particles using 0.1 % w/w PEO4 solution as eluant are compared with those of particles in DI water (low ionic strength) in Figure 4-1. The ionic strength of 0.1 % w/w PEO4 was adjusted by adding NaCl in order to diminish the effects from electrostatic and electrokinetic repulsive forces. The colloidal samples were prepared by mixing the standard PS latex particles into cleaned 0.1 %

137

w/w PEO4 (no salt added); therefore, colloidal stability could be imparted by both the electrostatic and steric effects.

Evidently, the impact of PEO present in the eluant was very significant and this was mainly due to the lateral particle migration induced by the gradient of normal stress of PEO solution in shear flow. For low ionic strength eluant (DI water with an estimated ionic strength of 1.5×10^{-6} M), the dominant repulsion between the particles and the wall comes from the electrokinetic lift force, which is significant for eluants with ionic strength smaller than 1 mM [5]. Therefore, the larger enhancement in R_f for particles in the PEO solution compared to DI water, particularly for small particle diameters, indicated a stronger migration effect due to the normal stresses of polymer solution compared to the repulsion from electrokinetic lift.

The pronounced migration effect in the PEO solution also can be observed from H_{TP}, which reflects the degree of particle axial dispersion. As the particle size increases, the diffusivity of the particles will be reduced resulting in an increased H_{TP} and this can be evident from the particles in DI water when the particle size is smaller than 400 nm. For particles in the presence of PEO, the enlargement of the particle size due to PEO adsorption and the increase of viscosity of the PEO solution can enhance the effect of axial dispersion; without the migration effect, the H_{TP} would be larger when compared to H_{TP} of the same particle size dispersed in DI water. Moreover, the decrease of H_{TP} with the particle size (instead of increasing for particles smaller than 400 nm) indicated that the rate of migration due to the viscoelastic effect increases more rapidly with particle size than the particle-wall repulsion arising from the electrokinetic lift force in DI water.

For larger particles in PEO solution, R_f and H_{TP} reached a plateau. This is because the strong viscoelastic effect of the PEO solution caused the particles to reside near the center of the capillary where the profile of fluid velocity is flatter compared to the profile close to the wall.

138

Figure 4-1: Experimental separation factor (R_f) and theoretical plate height (H_{TP}) of various size PS latex particles in the presence of 0.1 % w/w PEO4 solution and DI water; capillary ID = 24.1 μm and length = 655.0 cm; eluants = 0.01 % w/w PEO4 with 4 mM NaCl ($K \sim 470$ μS/cm) and DI water ($K \sim 1$ μS/cm); average fluid velocity = 3.4 cm/s.

139

Since the particles sampled the region where the fluid velocity difference is small, the particles experienced similar velocities despite their size differences. Because of this, R_f and H_{TP} showed the constant values even though the particle size increased. Under this condition, the CHDF will lose the ability to resolve the particle according to size.

4.3 Effect of Molecular Weight of PEO

CHDF experiments were conducted with different molecular weight of PEO. The PEO solutions were used at high ionic strength in order to eliminating any additional repulsion from the electrokinetic effect. The samples were the mixture of latex particles and low ionic strength PEO solutions.

Figure 4-2 shows the plot of R_f and H_{TP} for various molecular weights of PEO as a function of particle size. Clearly, the enhancement of particle separation (increase of R_f while H_{TP} decreases) in CHDF increased with the molecular weight of PEO. The main contribution to this enhancement was the increase of the lateral migration velocity of particles due to the normal stresses of PEO solutions. Higher molecular weights provide a longer relaxation time, which will result in higher values of the normal stresses of polymer solution. Additionally, the adsorption of larger molecular weight of PEO on the particles also contributed to the enhancement of particle separation. The particle size of PEO-adsorbed particles would be increase with the molecular weight which would induce faster migration compared to particles without adsorption.

Figure 4-3 compares the experimental R_f for particles in the presence of various molecular weight PEO solutions with the predicted ones obtained from the CHDF dynamic model. The particle migration velocity due to the viscoelastic effect of PEO solutions was calculated using equation (3.65) and incorporated into the CHDF model. In the simulation, the enlargement of particle diameter due to PEO adsorption also accounts for the thickness of PEO

140

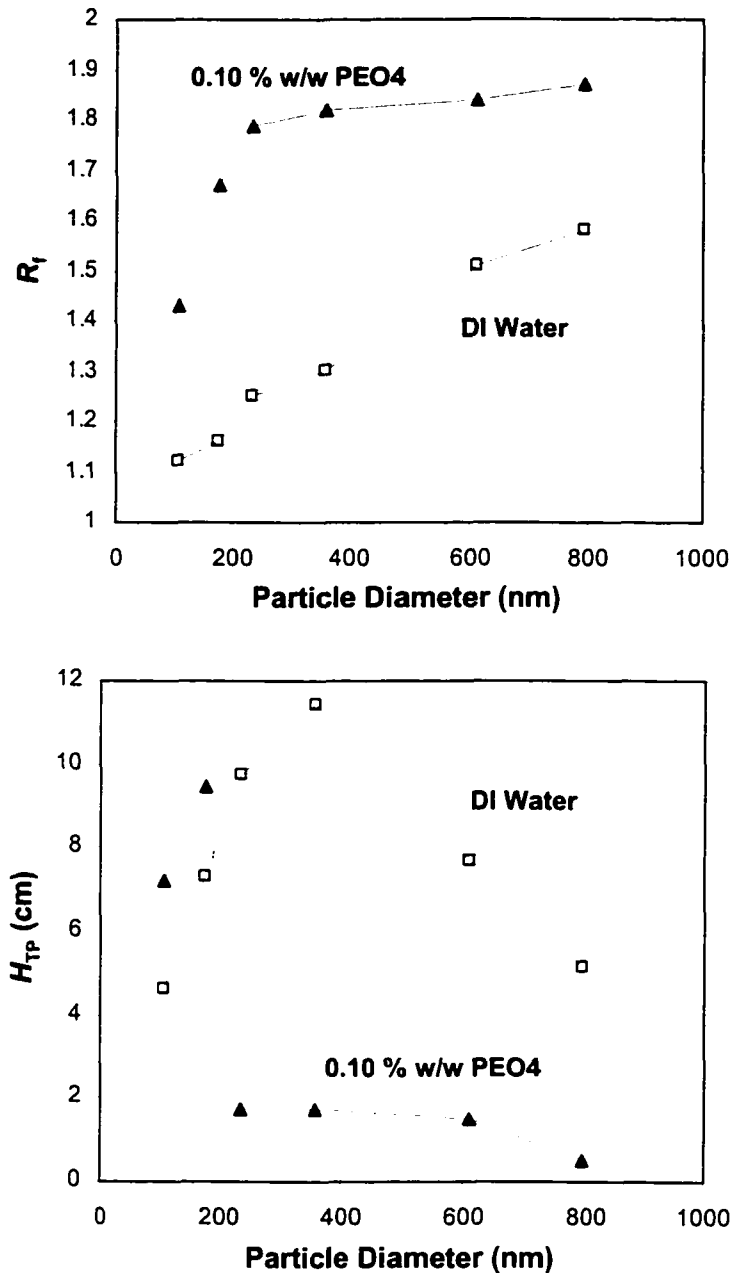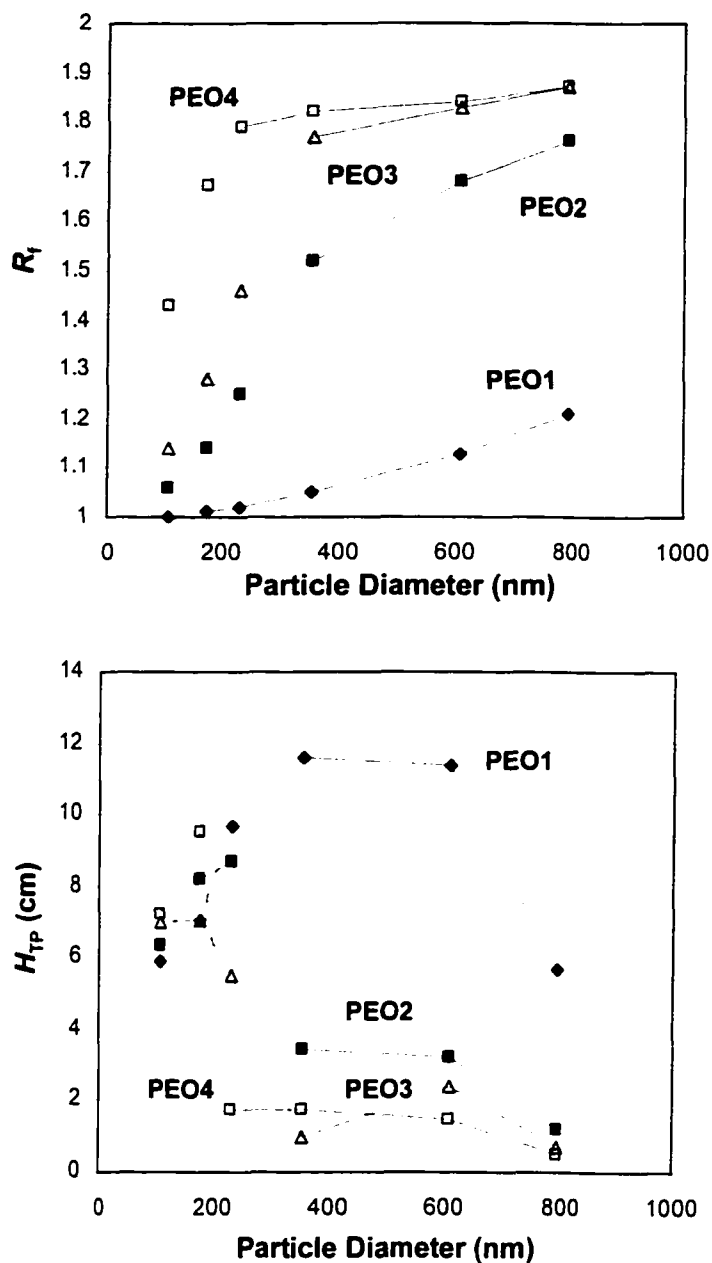**Figure 4-2:** Experimental separation factor (R_f) and theoretical plate height (H_{TP}) of various size PS latex particles in the presence of different molecular weight PEO solutions; capillary ID = 24.1 μm and length = 655.0 cm; eluants = 0.1 % w/w PEO1, 0.1 % w/w PEO2, 0.1 % w/w PEO3 and 0.1 % w/w PEO4, all PEO solutions contain 4 mM NaCl; average fluid velocity = 3.4 cm/s.

141
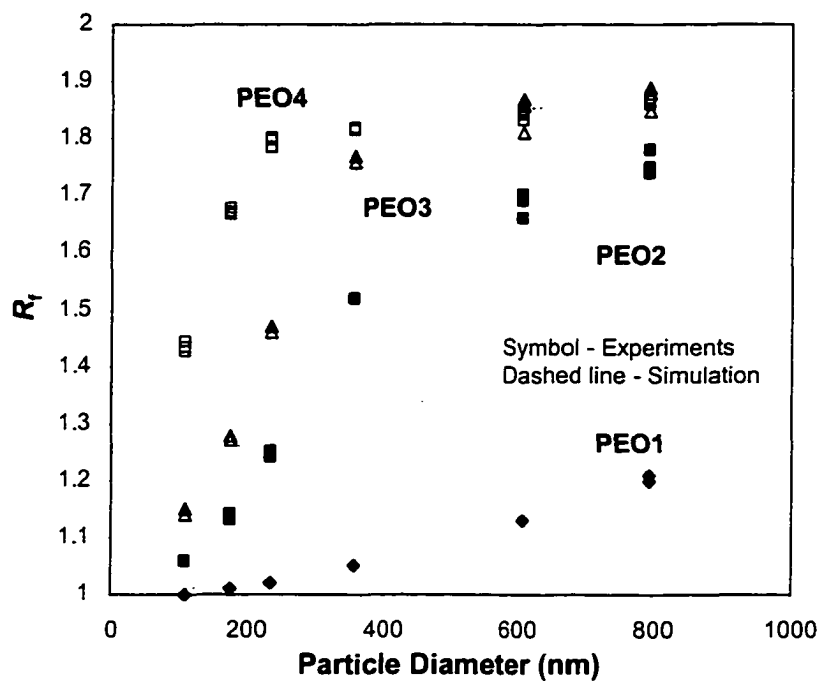
Figure 4-3: Comparison of the experimental R_f with the predicted results which incorporate the effect of lateral particle migration due to the viscoelastic effect of PEO solutions for transport of latex particles in different molecular weight PEO solutions; capillary ID = 24.1 μm and length = 655.0 cm; eluants = 0.1 % w/w PEO1, 0.1 % w/w PEO2, 0.1 % w/w PEO3 and 0.1 % w/w PEO4, all PEO solutions contain 4 mM NaCl; average fluid velocity = 3.4 cm/s. Simulation: adsorbed PEO layer on the capillary surface (δ); PEO1 and PEO2 = 0 nm, PEO3 = 180 nm and PEO4 = 540 nm.

142

adsorbed layer for each molecular weight of PEO which was estimated based on the power-law relationship described by equation (2.120). The calculated thickness of the PEO was scaled from the experimental thickness of adsorbed PEO4. The PEO adsorbed layer thickness on each particle size was estimated using equation (2.122) by assuming that the thickness of PEO4 on a flat surface ($\bar{d}$) is equal to 67 nm. This value of $\bar{d}$ was calculated based on the adsorbed PEO4 thickness on the largest diameter particle as shown in Table 2-3. The value of $\bar{d}$ should reach a constant value as the particle size increases due to the decreasing effect of curvature. The thicknesses of the adsorbed PEO layer on various diameters of particles are shown in Table 4-1.

For the case of PEO3 and PEO4, the simulation was performed by also taking into consideration the reduction of capillary diameter due to the presence of the PEO adsorbed layer on the capillary surface. The thickness of the PEO adsorbed layer was obtained experimentally as demonstrated in chapter 3 and is approximated as 180 nm for PEO3 and 540 nm for PEO4.

A comparison of predicted R_f with experimental R_f matched qualitatively. This indicates that the enhancement of particle separation in CHDF when PEO solutions are used as the eluant arises from the lateral particle migration due to the normal stresses of PEO solutions. The rate of migration increases with the molecular weight of the PEO because of the increase of the molecular relaxation time and this induces a stronger normal stress gradient across the capillary radius. The migration of particles is also a strong function of particle size as can be observed by the substantial increase of R_f with the particle diameter.

In the calculation of the particle migration, the adsorbed-PEO particle is assumed to be a rigid sphere with an adsorbed layer thickness equal to the hydrodynamic layer thickness (L_H). L_H is equivalent to the impermeable layer surrounding the particles which provides the same resistance to flow as an adsorbed polymer layer δ. Therefore, the permeability of the adsorbed polymer layer is related to the value of L_H whereby a low permeability will result in a large

143

Table 4-1: Estimated Adsorbed PEO Layer Thickness (δ) for Various Molecular Weight of PEO and Particle Sizes of Adsorbing Particles

Adsorbing Particle Diameter (nm)	δ PEO1 (nm)	δ PEO2 (nm)	δ PEO3 (nm)	δ PEO4 (nm)
109	1.0	4.2	8.5	18.1
176	2.5	11.1	22.3	47.4
234	2.6	11.4	22.8	48.4
357	2.8	12.2	24.5	52.1
610	3.0	13.2	26.4	56.0
794	3.1	13.6	27.3	58.0

144

thickness of the hydrodynamic layer. L_H is given by equation (2.36) and the permeability of the adsorbed polymer was estimated by assuming that the volume fraction of polymer segments is described by an exponential function.

The migration due to the fluid inertia was also included in the simulation. The particle diameter of a PEO-adsorbed particle was assumed to be that of a solid sphere with the additional thickness of L_H. Figure 4-4 compares the lateral migration velocity of a 234 nm particle induced by the normal stresses of PEO solutions with the lateral velocity arising from the inertia force of the fluid. In the figure, a positive migration velocity indicates the movement from the capillary wall toward the centerline. For the inertia effect, the migration velocity contains both positive and negative signs indicating that the particles would migrate from the capillary wall as well as the capillary center and the equilibrium point, where the migration velocity is zero, is known as the turbular pinch point.

For low molecular weight PEO1 and PEO2, the fluid inertia effect is comparable to the normal stress effect of PEO solution. Nevertheless, as the molecular weight increased such as in the case of PEO3 and PEO4, the effect of the inertial force was negligible when compared to the effect of normal stress of polymer solution.

For PEO2 as the eluant, the predicted R_f deviated noticeably from the one obtained experimentally. There are many factors which may contribute to the deviation. One of those is the neglecting of the adsorbed PEO2 layer on the capillary surface, which can cause the underestimation of predicted R_f. In the case of PEO2, the determination of the adsorbed layer is unlikely because the dominant effect is from the slip. As mentioned in chapter 3, besides the PEO adsorption, the flow of PEO solution in the capillary can be associated with the slip effect as well. These two phenomena can take place concurrently [13]. Even though the presence of the PEO2 adsorbed layer on the capillary wall can enhance the R_f, because of the thin adsorbed layer of

145
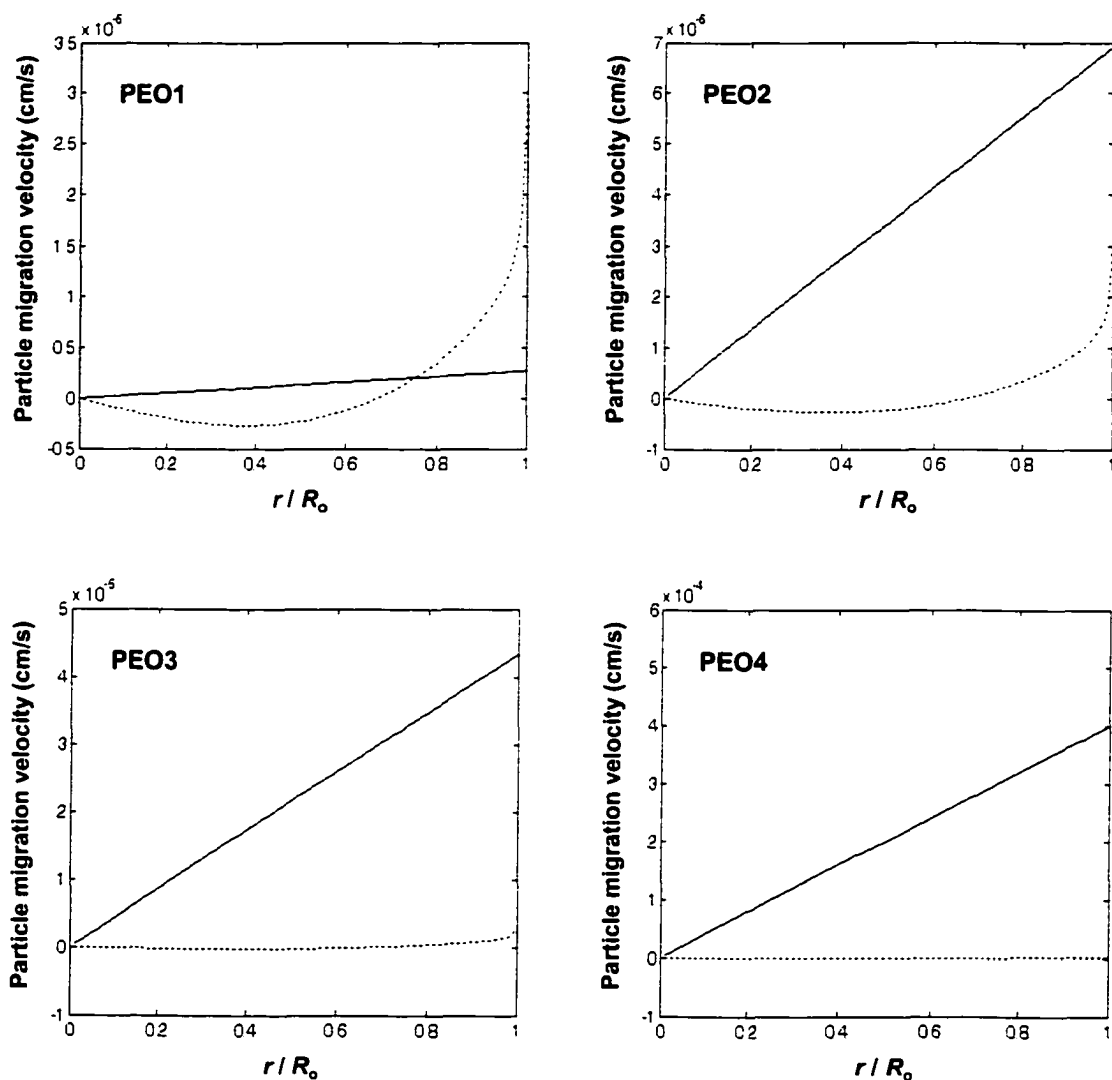
Figure 4-4: Migration velocity due to the viscoelastic effect of PEO solutions (solid line) and inertial effect (dotted line) as a function of normalized radial position for transport of 234 nm latex particles in different molecular weight PEO solutions; capillary ID = 24.1 μm and length = 655.0 cm; eluants = 0.1 % w/w PEO1, 0.1 % w/w PEO2, 0.1 % w/w PEO3 and 0.1 % w/w PEO4, all PEO solutions contain 4 mM NaCl; average fluid velocity = 3.4 cm/s.

146

Figure 4-5: Comparison of the experimental R_f and H_{TP} (open symbol) with the predicted results (line) taking into account the effect of different adsorbed PEO thicknesses on the capillary (δ) for transport of latex particles in 0.1 % w/w PEO2; capillary ID = 24.1 μm and length = 655.0 cm; eluant = 0.1 % w/w PEO2 with 4 mM NaCl content; average velocity of fluid = 3.4 cm/s.

147

PEO2, the enhancement effect is expected to be small as shown in Figure 4-5.

Another factor is the underdetermination of the migration velocity. The migration velocity of particles in polymer solution is a function of both the particle size and relaxation time. Nonetheless, the comparison with the experiments indicates that the deviation is most likely the result of underestimated relaxation time of the polymer molecule because almost all of the predicted points of R_f shifted to lower values. The relaxation time is calculated based on the linear elastic dumbbell in which the molecular weight distribution is assumed to be narrow. The molecular weight of the PEOs in this study has a very broad distribution; therefore the calculation of the migration relying on a single average value of the molecular weight relaxation time may cause the deviation of the prediction. The effect of the relaxation time of a PEO2 molecule on the R_f is shown in Figure 4-6. Evidently, by increasing the molecular relaxation time of PEO2 from 6.71×10^{-6} to 1.80×10^{-5}, a better agreement between the prediction and experiments was obtained.

Figure 4-7 shows the comparison of predicted H_{TP} with the experimental results. The agreement between the predictions and the experiments is qualitatively adequate confirming the existence of particle migration due to the normal stress of PEO solutions. Moreover, this indicates that the axial diffusion in the microcapillary of adsorbed-PEO particles in PEO solutions can be approximated by the Stokes-Einstein (SE) equation together with the visualization of the absorbed-PEO particle as a composite sphere.

H_{TP} for 109 nm and 176 nm particles in various molecular weights PEO shows an increase with the molecular weight. If the SE equation is valid, this increase of H_{TP} is the result of the reduced particle diffusivity due to the particle enlargement and increasing PEO solution viscosity. However, for particles in PEO4 solution, the prediction of H_{TP} seemed to overestimate the experimental results (presumably the particle-wall interaction is well characterized) indicating the deviation from the SE equation for small particles in this high molecular weight PEO. This
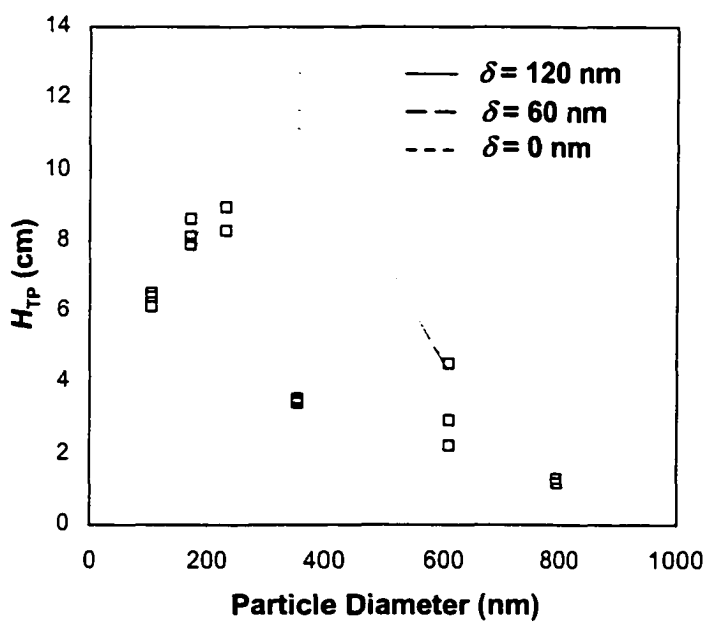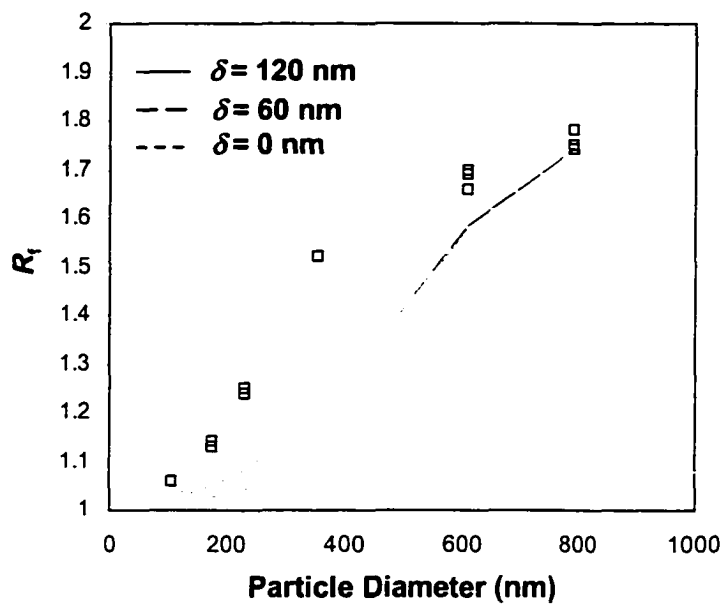
148
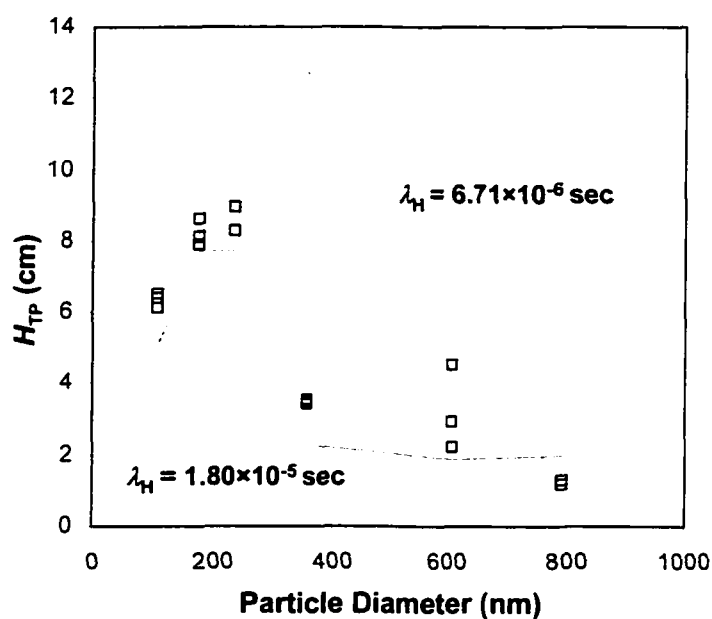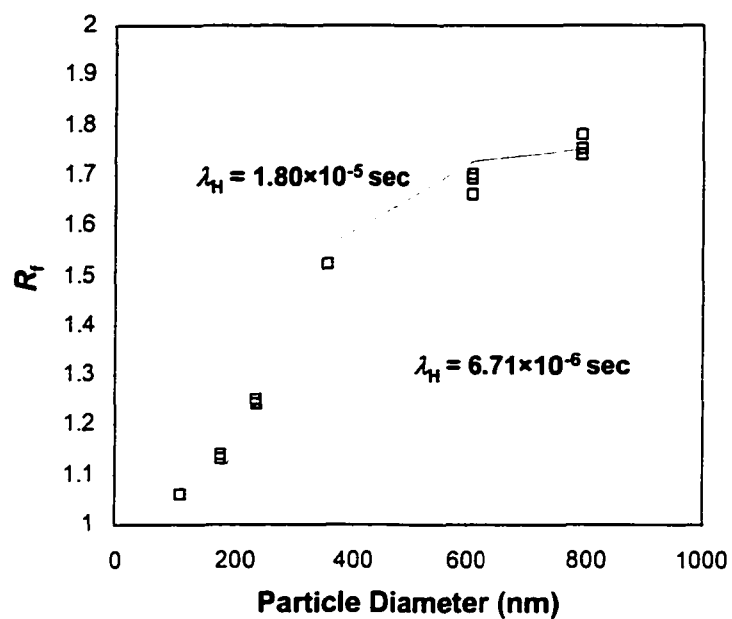
Figure 4-6: Comparison of the experimental R_f and H_{TP} (open symbol) with the predicted results (line) taking into account the effect of different molecular weight relaxation times (λ_H) for the transport of latex particles in 0.1 % w/w PEO2; capillary ID = 24.1 µm and length = 655.0 cm; eluant = 0.1 % w/w PEO2 with 4 mM NaCl content; average velocity of fluid = 3.4 cm/s.

149
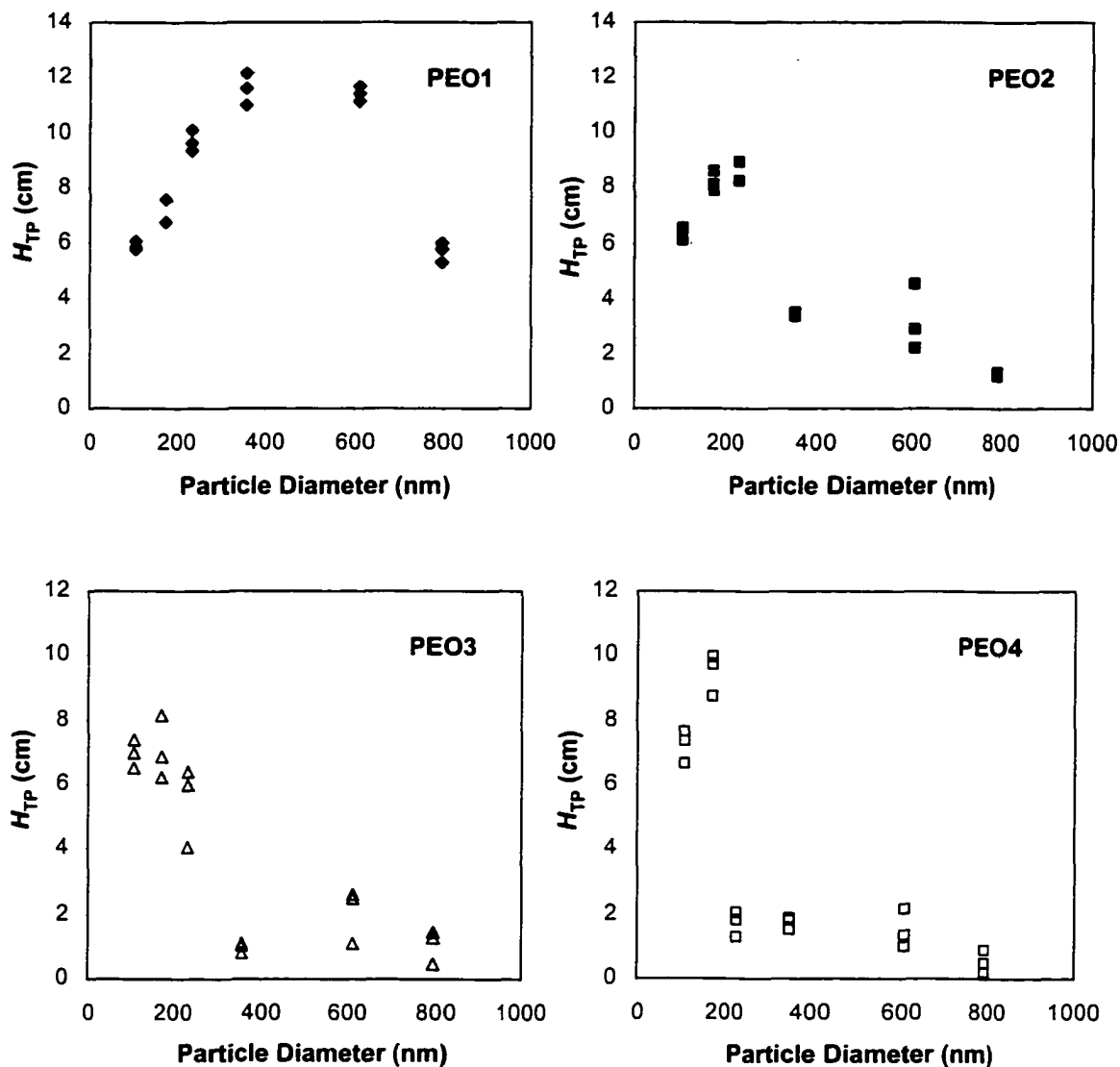
Figure 4-7: Comparison of the experimental H_{TP} (symbol) with the predicted results (dotted line) incorporating the effect of lateral particle migration due to the viscoelastic effect of PEO solutions for transport of latex particles in different molecular weight PEO solution; capillary ID = 24.1 μm and length = 655.0 cm; eluants = 0.1 % w/w PEO1, 0.1 % w/w PEO2, 0.1 % w/w PEO3 and 0.1 % w/w PEO4, all PEO solutions contain 4 mM NaCl; average fluid velocity = 3.4 cm/s. Simulation: adsorbed PEO layer on the capillary surface (δ); PEO1 and PEO2 = 0 nm, PEO3 = 180 nm and PEO4 = 540 nm.

150

corresponds to the negative deviation from the SE behavior in which the actual particle diffusivity D is decreased with the viscosity faster than predicted from the SE equation or the ratio of $D\eta / D_0\eta_s$ is less than 1 where D_0 is the particle diffusivity in pure solvent and η_s is the solvent viscosity.

Negative deviations for the diffusion of particles in polymer solutions have been previously observed [102,103,104,115] in light scattering measurements and the cause of deviation has usually been ascribed to the adsorption of free polymer from the medium. Moreover, the formation of aggregates by the bridging of particles through the dangling chain ends of the adsorbed polymer may combine with the adsorption in causing the negative deviation from the SE equation [116]. As the concentration of polymer approaching the overlap concentration C^*, it is likely that the adsorbed polymer, which extend into solution become entangles with the free polymer chains. As a result, this would further increase the drag experienced by the polymer-adsorbed particles leading to a decreasing particle diffusivity [115]. Furthermore, one might expect that a consequence of free polymer is that chain entanglement with the adsorbed polymer will cause the microscopic viscosity felt by the particles to exceed the macroscopic viscosity and thus the deviation from the SE equation would be increased [115,117].

4.4 Effect of Fluid Velocity

The effect of the average flow velocity of the PEO solution in the microcapillary on the particle separation was studied. The plot of R_f as a function of particle diameter for two different average velocities is shown in Figure 4-8. It is evident that by increasing the fluid velocity, the rate of particle migration increases resulting in the enhancement of R_f. Since the particle migration velocity caused by the gradient of normal stress of PEO solution is proportional to the velocity gradient (cf. equation 3.65) of the flow, increasing the fluid velocity will cause the

151
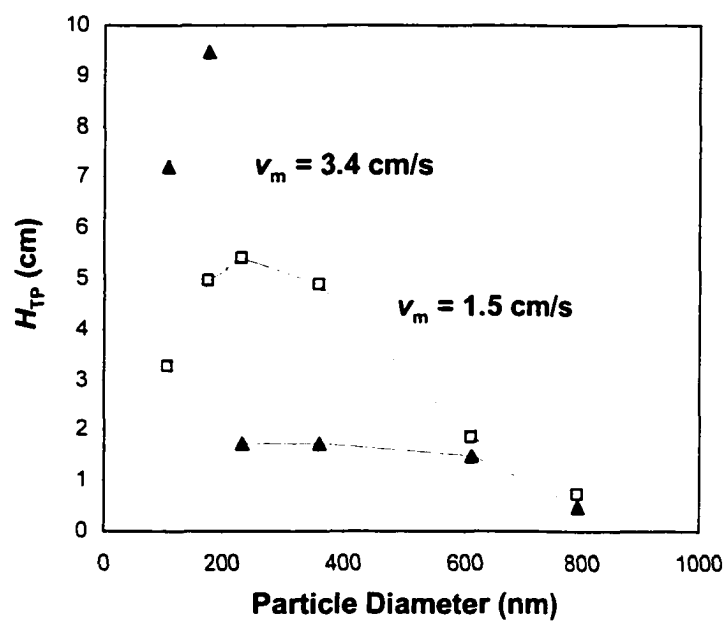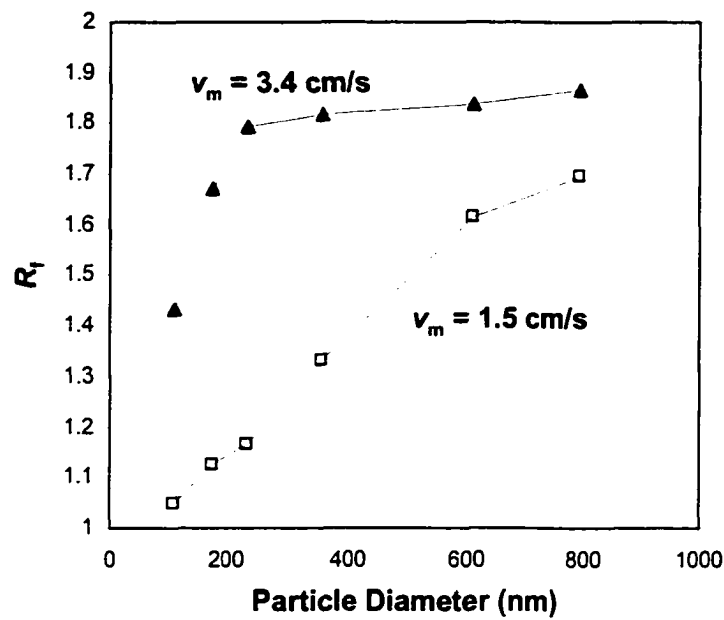
Figure 4-8: Effect of average fluid velocity on the experimental separation factor (R_f) and theoretical plate height (H_{TP}) for various sizes of PS latex particles in the presence of PEO4 solution; capillary ID = 24.1 μm and length = 655.0 cm; eluants = 0.1 % w/w PEO4 with 4 mM NaCl; average fluid velocity = 3.4 and 1.5 cm/s.

152

velocity gradient across the capillary radius to increase causing the particles to migrate faster from the capillary wall toward the center.

Fluid velocity also affects the axial dispersion (H_{TP}) of particles in CHDF. For weak particle-wall interaction, the H_{TP} of particles will depend primarily on the convective effect caused by the velocity distribution of the fluid flow field, providing that the particles possess the same diffusivity. Therefore, if the velocity of the fluid increases, H_{TP} will also increase and this can be observed for the H_{TP} of 109 nm and 176 nm latex particles. However, as the particle size and the fluid velocity increased, the effect from the normal stress of PEO solution will be more significant causing the particles to migrate closer to the capillary center. As a result, the particles will sample the small velocity difference around the center of the capillary and this will generate the lower H_{TP} of the larger particles in the faster fluid velocity.

4.5 Effect of Ionic Strength

CHDF experiments using low ionic strength PEO solutions (conductivity ~ 1 μS/cm and estimated ionic strength is 1.5×10^{-6} M) as eluant were performed in order to investigate the effect of ionic strength on the particle separation in the presence of PEO solution. Figure 4-9 presents the plots of R_f as a function of particle diameter for particles in the presence of low and high (conductivity ~ 470 μS/cm and ionic strength is 4×10^{-3} M) ionic strength of various molecular weights of PEO solution. The separation factor of particles in low ionic strength PEO solutions exhibits higher values compared to that of particles in high ionic strength solutions. The R_f values show the most difference for the lowest molecular weight (PEO1) and the discrepancy decreases as the molecular weight of PEO increased. For PEO3 and PEO4, the difference in R_f for low and high ionic strength PEO solutions is slight. The increase of R_f for particles in low ionic strength PEO solutions suggests that under this condition, there is an additional repulsive force is involved

153

besides the effect from the normal stress of PEO solution. This can be confirmed from the H_{TP} for particles in low ionic strength PEO solution shown in Figure 4-10, which revealed a lower H_{TP} compared to that in high ionic strength solutions. The stronger particle-wall interaction in low ionic strength PEO solutions will repel the particles to stay closer to the capillary axis where the fluid velocity difference is small. This will decrease the convective effect resulting in a lower H_{TP}. Similar to R_f, the discrepancy of H_{TP} between low and high ionic strength solutions is more distinct as the molecular weight of the PEO decreased.

It is known that for particles transported through a low ionic strength fluid in the presence of a stationary wall, the primary source of particle-wall repulsion is the electroviscous force known as electrokinetic lift [5]. When a small electrically-charged sphere translates through a quiescent polar fluid such as an aqueous electrolyte solution in close proximity and parallel to a charged surface, the convection of charge within the diffuse layer of the EDL (electrical double layer) surrounding the particle and wall surfaces induces a streaming potential profile between the surfaces. The streaming potential imposes an electrical stress on the charged interface and integration of the normal component of the Maxwell stress yields the electrokinetic lift [118,119].

The electrokinetic lift force F_{ek} expression for translational motion of a spherical particle near a planar surface has been derived by Bike and Prieve [120]. For a cylindrical geometry, the appropriate expression is [5]:

$$F_{ek} = \left(\frac{\varepsilon_o \varepsilon_r}{4\pi}\right)^3 \left(\frac{27\pi}{16}\right)\left(\frac{v_{pz}a}{KR_o^2}\right)^2 \left[1 - \left(\frac{r}{R_o}\right)\right]^{-4} \zeta_2(\zeta_2 + 2\zeta_1) \qquad (4.1)$$

where ε_r and ε_o are the relative permittivity of the medium and the permittivity of a vacuum, v_{pz} is the local axial particle velocity, a is the particle radius, R_o is the capillary radius, r is the radial position, ζ_1 and ζ_2 are the zeta potentials of the wall and particle respectively, and K is the fluid conductivity.

154
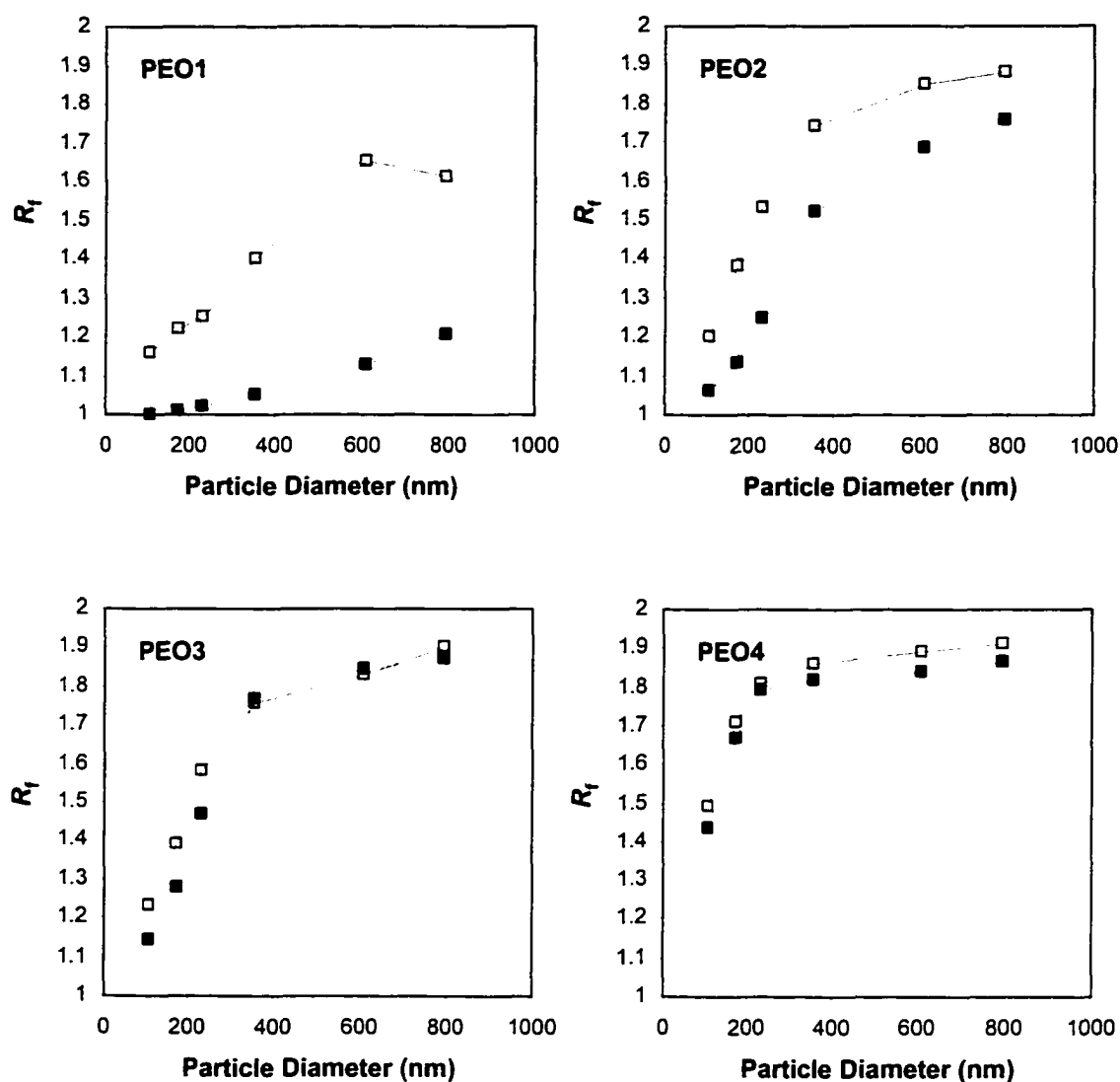
Figure 4-9: Effect of ionic strength on the experimental separation factor (R_f) for various size PS latex particles in the presence of different molecular weight PEO solutions; high ionic strength (open symbol and solid line) PEO solutions have $K \sim 470$ μS/cm and estimated ionic strength = 4×10^{-3} M, low ionic strength PEO solutions (closed symbol and dotted line) have $K \sim 1$ μS/cm and estimated ionic strength = 1.5×10^{-6} M; capillary ID = 24.1 μm and length = 655.0 cm; eluants = 0.1 % w/w PEO1, 0.1 % w/w PEO2, 0.1 % w/w PEO3 and 0.1 % w/w PEO4; average fluid velocity = 3.4 cm/s.

155
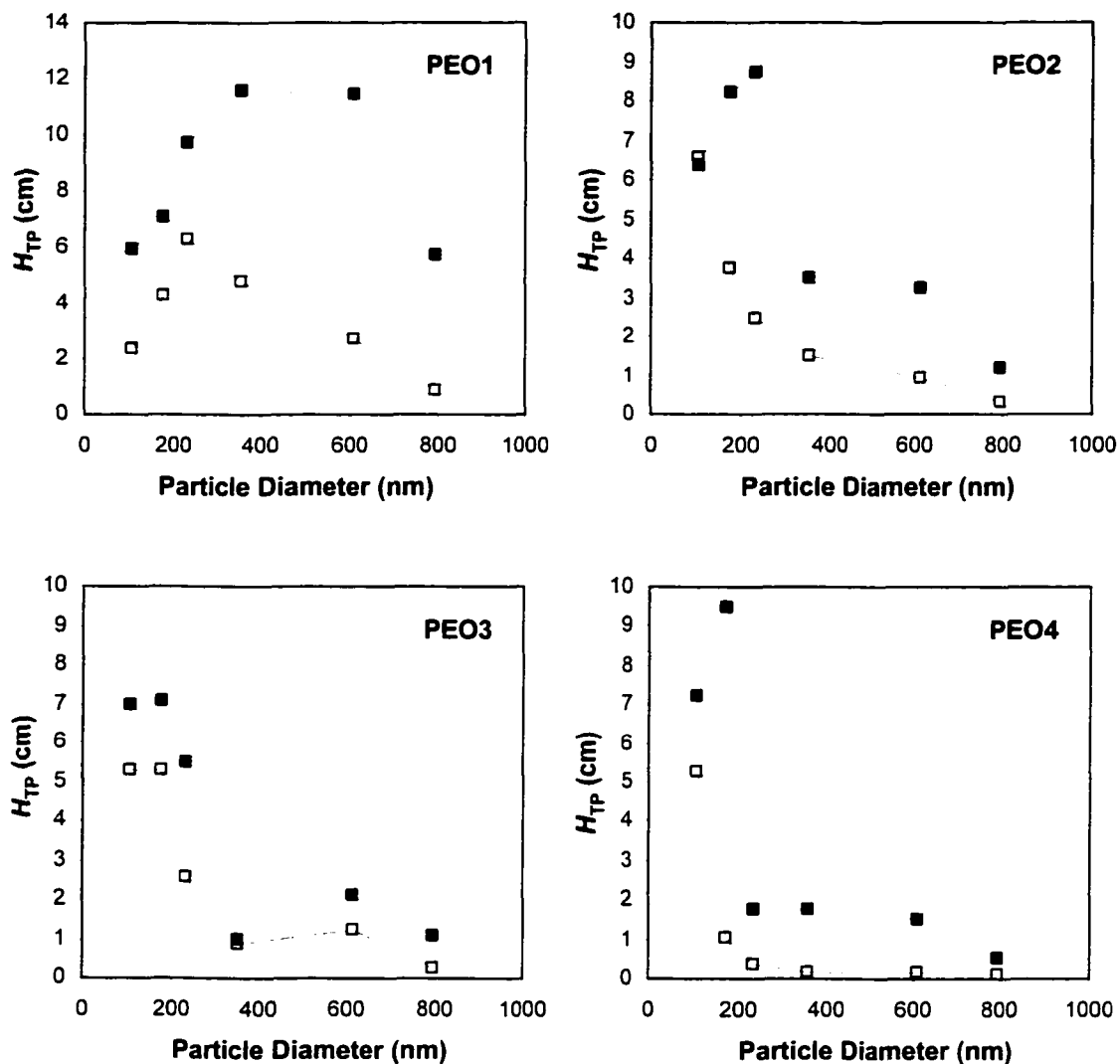
Figure 4-10: Effect of ionic strength on the experimental theoretical plate height (H_{TP}) for various size PS latex particles in the presence of different molecular weight PEO solutions; high ionic strength (open symbol and solid line) PEO solutions have $K \sim 470$ μS/cm and estimated ionic strength = 4×10^{-3} M, low ionic strength PEO solutions (closed symbol and dotted line) have $K \sim 1$ μS/cm and estimated ionic strength = 1.5×10^{-6} M; capillary ID = 24.1 μm and length = 655.0 cm; eluants = 0.1 % w/w PEO1, 0.1 % w/w PEO2, 0.1 % w/w PEO3 and 0.1 % w/w PEO4; average fluid velocity = 3.4 cm/s.

156

To obtain the particle migration induced by the electrokinetic lift v_{ek}, the F_{ek} is equated

with the Stokes drag force of a particle in a flow field to yield:

$$v_{ek} = \left(\frac{\varepsilon_o \varepsilon_r}{4\pi}\right)^3 \left(\frac{9a}{32\eta}\right)\left(\frac{v_{pz}}{KR_o^2}\right)^2 \left[1-\left(\frac{r}{R_o}\right)\right]^{-4} \zeta_2(\zeta_2 + 2\zeta_1) \qquad (4.2)$$

Since under this low ionic strength conditions (the estimated ionic strength $= 1.5\times10^{-6}$ M), the

Debye length (κ_D^{-1}) surrounding the particle is roughly equal to 250 nm, which is far exceeds the

PEO adsorbed layer thickness (for PEO4, $\delta \sim$ 50 nm), the presence of adsorbed PEO poses

presumably a negligible effect on the electrokinetic lift. In other word, the distribution of ion

species inside and outside the polymer adsorbed layer is expected to be similar; however this is

not necessarily true for an adsorbed polyelectrolyte.

Figure 4-11 shows the comparison between experimental R_f and the predicted ones from

CHDF dynamic model for particles in low ionic strength PEO1 and PEO4 solutions. The particle

migration due to the electrokinetic lift and the normal stress of PEO solution are considered here

In the calculation of electrokinetic lift, the zeta potentials of the wall and particle surfaces are

assumed to be -100 mV and -50 mV, respectively [5]. Clearly, in low molecular weight PEO1,

better agreement between the prediction and experiment is obtained when the electrokinetic lift is

included, suggesting the stronger and prevailing effect of the electrokinetic lift force over the

normal stress effect of PEO1 solution. However, for PEO4, despite the strong repulsion generated

by the electrokinetic lift, the incorporation of the particle migration due to the normal stress of

PEO solution provided a better prediction implying that for higher molecular weight PEO, the

dominant migration effect arises from the viscoelastic property of polymer solution.

157
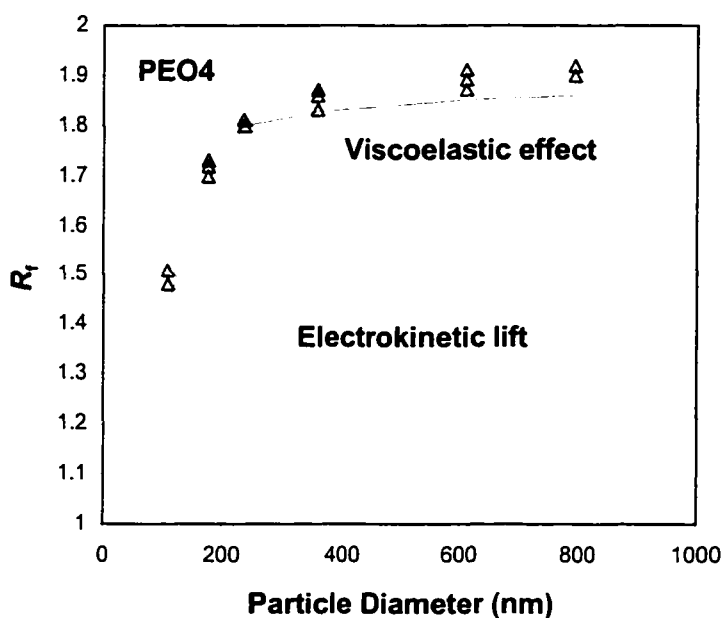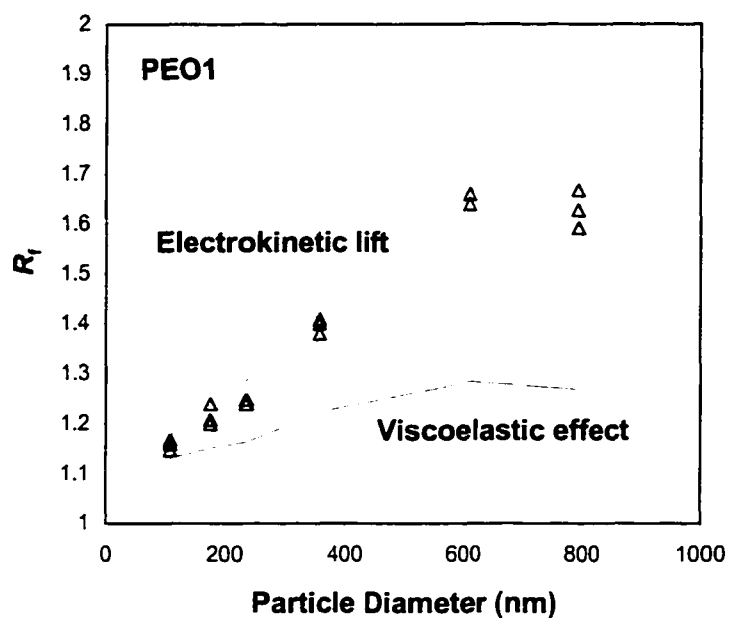
Figure 4-11: Comparison of the experimental R_f(open symbol) with the predicted results (line) which taking into account the effect of particle migration due to the viscoelastic and electrokinetic effect for transport of latex particles in 0.1 % w/w PEO1 and PEO4; capillary ID = 24.1 μm and length = 655.0 cm; eluant = low ionic strength 0.1 % w/w PEO1 and PEO4; average velocity of fluid = 3.4 cm/s.

158

4.6 Conclusion

CHDF experiments using PEO solution as the eluant revealed a significant impact of PEO on the transport of colloidal particles through the microcapillary. The increasing of R_f and decreasing H_{TP} indicates the migration of particles from the capillary wall toward the center, which primarily arises from the normal stress (viscoelastic effect) gradient of PEO solution in the flow field. This effect is strongly dependent on the molecular weight of the PEO; that is, the higher the molecular weight of the PEO, the closer the particles will migrate to the capillary center.

The change of the velocity of PEO solutions through the microcapillary also affects the separation of particles. For higher fluid velocity, experimental R_f showed larger values. This is mainly because the particle migration, which arises from the normal stress of PEO solution, is proportional to the shear rate and thus, by increasing the velocity, the shear rate will be increased resulting in a higher migration velocity.

The CHDF experiments using low ionic strength PEO solutions as eluant showed a higher R_f and lower H_{TP} compared to high ionic strength PEO solution. The difference increased as the molecular weight of the PEO decreased. The simulation considering both the effect of electrokinetic lift and the viscoelastic property of PEO solutions suggested that for low molecular weight PEO, the particle-wall interaction is dominated by the electrokinetic lift, whereas for high molecular weight PEO, the viscoelastic effect is the primary source of particle migration.

159

Chapter Five

Conclusions and Recommendations for Further Research

5.1 Final Conclusions

In the present study, transport of PS latex particles through a microcapillary in the presence of PEO solutions was investigated. PEO present in the eluant as well as the dispersed medium of the latex samples was observed to significantly affect the separation mechanism of latex particles in CHDF. The experiment using high ionic strength PEO4 solution (molecular weight ca. 1,000,000 g/mol) was found to produce a substantial increase in the particle separation factor and a rapid decrease in the theoretical plate height (degree of axial dispersion) when compared to the experiment where the eluant was DI water. Thus, in PEO4 solutions, particles migrate closer to the capillary center. This migration is not due to the contribution from the electrokinetic effect which is significant in low ionic strength eluants (ionic strength less than 1 mM).

Using dynamic light scattering, latex particles dispersed in PEO solutions were observed to have larger effective particle sizes due to the adsorption of PEO molecules on particle surfaces. The thickness of the adsorbed PEO increased with PEO molecular weight. The log-log plot between the molecular weight of PEO and the layer thickness of the adsorbed PEO showed a straight line with a slope of 0.63, indicating a power law relationship.

The adsorbed layer thickness of PEO was also affected by the particle size of the latex sample. It was found to increase as the size of the adsorbing particle increased.

Furthermore, CHDF experiments using 4 mM NaCl as eluant revealed the enlargement of latex particles due to PEO adsorption when the concentration of PEO used in the dispersed medium of the latex sample was near the saturation surface concentration of PEO on PS particles.

160

The model describing the transport of adsorbed-PEO particles in CHDF was developed by visualizing the adsorbed-PEO particle as a composite spheres consisting of a rigid core surrounded by a permeable adsorbed polymer layer. The drag force exerted on the composite sphere depends upon the thickness and permeability of the adsorbed layer. CHDF simulations showed that the composite sphere provides a lower degree of axial dispersion compared to a rigid sphere of the same diameter.

Flow of PEO solutions through the microcapillary was also considered. It was found experimentally that the flow of PEO solutions can be accompanied by the slip and adsorption effects which take place in the vicinity of the capillary wall.

Theoretically, the slip effect is the result of polymer migration arising from the change of chain conformations in the inhomogeneous stress field. This gives rise to a gradient of polymer concentration leading to the radial variation of polymer solution viscosity. As a result of the changing viscosity, the particle diffusivity will be altered.

The adsorbed PEO layer reduces the size of the capillary. The layer will deter the particles from experiencing the slow-moving fluid close to the capillary wall. The CHDF dynamic model was performed taking into account these surface effects. However, the mathematical prediction did not agree with the experimental results. Because of this, the effect of the viscoelasticity of the PEO solutions was focused on.

PEO solutions were modeled as a second-order fluid. This model is applicable only for low concentrations of PEO where the solution shows a nearly constant viscosity. The migration of particles in PEO solution at low Reynolds number was induced by the gradient of normal stresses of PEO solution in the shear flow. Lateral migration velocity of a particle in the second-order fluid shear flow [69] was incorporated into the CHDF model. Better agreement with experimental results was observed, suggesting the primary effect of normal stress of PEO solution

161

on the particle separation in CHDF.

CHDF experiments using PEO solutions as the eluant and disperse medium of the colloidal sample revealed the significant increase of the separation factor and dramatic decrease of the theoretical plate height as the particle size increased. Two important effects are come into play; the enlargement of particle size due to PEO adsorption and the particle migration due to the viscoelastic property of PEO solutions. However, the comparison of the experimental results with the prediction from CHDF dynamic model by incorporating the aforementioned effects suggested that the improvement of particle separation in CHDF is primarily due to the viscoelastic property of PEO solutions.

5.2 Recommendations for Further Research

Despite the significant amount of information obtained from this study, this dissertation can not address all the important aspects involved with developmental research of this kind. The following are the recommendations that could be further explored:

- Fundamentally, the degree of polymer migration depends upon the molecular weight of polymer. Applying this principle, CHDF can be utilized for the molecular weight determination of flexible to semi-flexible polymers. By using UV-absorbed polymers for example, polyacrylamide or using some other means of detection method such as reflective index, the rate of polymer migration can be measured experimentally using CHDF. Once the rate of migration, which can be characterized by the separation factor, is known, this can be related to the molecular weight of the polymer. The feasibility of using CHDF as a tool for detecting the polymer migration has been realized by the work of Chun and his co-workers [121,122]. Further research should focus on parametric study such as the suitable range of capillary diameter that can

162

provide a good resolution for a wide spectrum of polymers. The capillary surface should be treated in order to prevent polymer adsorption.

- In this study, it was shown experimentally that the particle separation was improved significantly when high molecular weight polymer solution was used as the eluant. The plot between the separation factor and particle diameter showed a steep increase in the slope. It is interesting to further explore the feasibility of CHDF to measure very small particle (< 100 nm) using polymer solution as the eluant. A parametric study should be conducted to determine the optimum conditions such as the capillary diameter, the molecular weight, and the concentration of polymer.

- It is known that a larger capillary provides a poor particle separation. However, by using high molecular polymer solution as the eluant, separation could be improved. Thus, by using larger capillary, CHDF could be utilized for measuring larger particle sizes (> 2 μm).

- The effect of non-Newtonian behavior of the polymer solution on particle transport in CHDF should be explored further. The shear thinning which is normally found in polymer solution can affect the velocity profile of the flow and cause a change in dispersion characteristic of particles in CHDF.

- Mathematical prediction of the particle migration in polymer solutions can be improved by selecting a more realistic kinetic model representing the polymer molecule. In this study, the simplest model, which is the linear elastic dumbbells, was used which only provide a crude prediction of the experimental results. Models such as the finitely extendable nonlinear elastic (FENE) dumbbells or even chainlike models of Rouse and Zimm [85] could allow a more quantitative analysis.

163

References

1. Silebi, C. A., and DosRamos, J. G., *J. Colloid Interface Sci.*, **130**, 14 (1989).

2. DosRamos, J. G., and Silebi, C. A., *J. Colloid Interface Sci.*, **133**, 302 (1989).

3. Silebi, C. A., and DosRamos, J. G., *AIChE J.*, **35**, 1351 (1989).

4. Venkatesan, J., *Ph.D. Dissertation*, Lehigh University, Bethlehem, PA (1992).

5. Hollingsworth, A. D., *Ph.D. Dissertation*, Lehigh University, Bethlehem, PA (1997).

6. Hollingsworth, A. D., and Silebi, C. A., *Langmuir*, **12**, 613 (1996).

7. Klein, J., and Luckham, P.F., *Macromolecules*, **17**, 1041 (1984).

8. Cohen, Y., and Metzner, A.B., *J. Rheol.*, **29**, 67 (1985).

9. DosRamos, J. G., *Ph.D. Dissertation*, Lehigh University, Bethlehem, PA (1988).

10. Van De Ven, T. G. M., *Colloidal Hydrodynamics*, Academic Press Inc.: San Diego, 1989.

11. Kato, T., Nakamura, K., Kawaguchi, M., and Takahashi, A., *Polymer J.*, **13**, 1037 (1981).

12. Polverari, M., and van de Ven, T.G.M., *Colloids and Surfaces A,* **86**, 209 (1994).

13. Kozicki, W., Kuang, P.Q., Aragaki, T., Yim, S.P., *Can. J. Chem. Eng.*, **71**, 347 (1993).

14. Karnis, A., and Mason, S.G., *Tran. Soc. Rheol.*, **10**, 571 (1966).

15. Gauthier, F., Goldsmith, H.L., and Mason, S.G., *Trans. Soc. Rheol.*, **15**, 297 (1971).

16. Gauthier, F., Goldsmith, H.L., and Mason, S.G., *Rheol. Acta*, **10**, 344 (1971).

17. Highgate, D.J., and Whorlow, R.W., *Rheol. Acta*, **9**, 569 (1970).

18. Highgate, D.J., and Whorlow, R.W., *Rheol. Acta*, **8**, 142 (1969).

19. Prieve, D.C., John, M.S., and Koenig, T.L., *J. Rheol.*, **6**, 637 (1985).

20. Jefri, M.A., and Zahed, A.H., *J. Rheol.*, **33**, 691 (1989).

21. Brinkman, H.C., *Appl. Sci. Res,* **A1**, 27 (1947).

22. Anderson, J.L., and Kim, J., *J. Chem. Phys.*, **86**, 5163 (1987).

23. Debye, P., and Bueche, A.M., *J. Chem. Phys.*, **16**, 573 (1948).

24. Koplik, J., Levine, H., and Zee, A., *Phys Fluids*, **26**, 2864 (1983).

25. Bird, R.B., Stewart, W.E., and Lightfoot, E.N., *Transport Phenomena*, John Wiley and Son, Inc.: New York, 1960.

26. Vanni, M., *Chem. Eng. Sci.*, **55**, 685 (2000).

27. Masliyah, J.H., Neale, G., Malysa, K., and Van de ven, T.G.M., *Chem. Eng. Sci.*, **42**, 24 (1987).

28. Keh, H.J., and Kuo, J., *Colloid Polym Sci.*, **275**, 661 (1997).

29. Happel, J., and Brenner, H., *Low Reynolds Number Hydrodynamics*, Prentice-Hall, Inc.: Englewood Cliffs, 1965.

30. Anderson, J.L., and Solomentsev, Y., *Chem Eng. Comm.*, **148-150**, 291 (1996).

31. Cohen Stuart, M.A., Waajen, F.H.W.H.,Cosgrove, T., Vincent, B., and Crowley, T.L., *Macromolecules*, **17**, 1825 (1984).

32. Misra, S., and Varanasi, S., *J. Colloid Interface Sci.*, **146**, 251 (1991).

33. Ploehn, H.J., Russel, W.B., and Hall, C.J., *Macromolecules*, **21**, 1075 (1988).

34. Misra, S., and Fogler, H.S., *Langmuir*, **9**, 1306 (1993).

35. Vincent, B., *J. Colloid Interface Sci.*, **42**, 270 (1973).

36. Vincent, B., Edwards, J., Emmett, S., and Jones, A., *Colloids Surfaces*, **18**, 261 (1986).

37. de Gennes, P.G., *Macromolecules*, **14**, 1637 (1981).

38. de Gennes, P.G., *Scaling Concepts in Polymer Physics*, Cornell University Press: Ithaca, 1979.

39. Jeon, S.I., Lee, J.H., Andrade, J.D. and de Gennes, P.G., *J. Colloid Interface Sci.*, **142**, 149 (1991).

40. Brenner, H., and Gaydos, L.J., *J. Colloid Interface Sci.*, **58**, 312 (1977).

41. Bell, G.M., Levine, S., and McCartney, L.N., *J. Colloid Interface Sci.*, **33**, 335 (1970).

42. Ohshima, H., Healy, T.W., and White, L.R., *J. Colloid Interface Sci.*, **90**, 11 (1982).

43. Ohshima, H., and Ohki, S., *Biophys J.*, **47**, 673 (1985).

44. Ohshima, H., Nakamura, M., and Kondo, T., *Colloid Polym. Sci.*, **270**, 873 (1992).

45. Hamaker, H.C., *Physica*, **4**, 1059 (1937).

46. Gregory, J., *J. Colloid Interface Sci.*, **83**, 138 (1981).

47. Segre, G. and Silberberg, A., *J. Fluid Mech.*, **14**, 136 (1962).

48. Segre, G., and Silberberg, A., *Nature (London)*, **194**, 1269 (1962).

49. Cox, R.G., and Brenner, H., *Chem. Eng. Sci.*, **23**, 147 (1968).

50. Ishii, K., and Hasimoto, H., *J. Phys. Soc. Jpn.*, **48**, 6, 2144 (1980).

51. Villadsen, J., and Michelsen, M.L., *Solution of Differential Equation Models by Polynomial Approximation*, Prentice-Hall, Inc.: Englewood Cliffs, 1978.

52. Finlayson, B.A., *The Method of Weighted Residuals and Variational Principles with Application in Fluid Mechanics, Heat and Mass Transfer*, Academic Press: New York, 1972.

53. Baker. J.A., and Berg, J.C., *Langmuir*, **4**, 1055 (1988).

54. Flory, P.J., and Krigbaum, W.R., *J. Chem. Phys.*, **18**, 1086 (1950).

55. Flory, P.J., *Principles of Polymer Chemistry*, Cornell University Press: Ithaca, 1953.

56. Killmann, E., Maier, H., Kaniut, P., and Gutling, N., *Colloids Surfaces*, **15**, 261 (1985).

57. Cosgrove, T., Vincent, B., Crowley, T.L., and Cohen-Stuart, M.A., in *Polymer Adsorption and Dispersion Stability*, Goddard, E.D., and Vincent, B., eds.; ACS Symp. Series No. 240, American Chemical Society: Washington, D.C., 1984.

58. Grosberg, A.Y., and Khokhlov, A.R., *Statistical Physics of Macromolecules*; AIP Press: New York, 1994.

59. Wolff, C., *Can. J. Chem. Eng*, **58**, 634 (1980).

60. Boils, D., and Hair, M.L., *J. Colloid Interface Sci.*, **157**, 19 (1993).

61. Polverari M., and van de Ven, T.G.M., *J Phys. Chem.*, **100**, 13687 (1996).

62. Garvey, M.J., Tadros, Th.F., and Vincent B., *J. Colloid Interface Sci.*, **55**, 440 (1976).

63. Faers. M.A., and Luckham, P.F., *Colloids Surfaces A*, **86**, 317 (1994).

64. Greenwood, R., Luckham, P.F., and Gregory, T., *Colloids Surfaces A*, **98**, 117 (1995).

65. Killmann, E., Maier, H., and Baker, J.A., *Colloids Surfaces*, **31**, 51 (1988).

66. Baker, J.A., Berg, J.C., and Pearson, R.A., *Langmuir*, **5**, 339 (1989).

67. Chang, S.H., and Chung, I.J., *Macromolecules*, **24**, 567 (1991).

68. Churaev, N.V., Sergeeva, I.P., and Sobolev, V.D., *J. Colloid Interface Sci.*, **169**, 300 (1995).

69. Ho, B.P., and Leal L.G., *J. Fluid Mech.*, **76**, 783 (1976).

70. Kozicki, W., and Tiu, C., in *Encyclopedia of Fluid Mechanics*, vol. 7, Cheremisinoff, N.P., eds.; Gulf Publishing Co.: Houston, 1988.

71. Mooney, M., *J. Rheol.*, **2**, 210 (1931).

72. Kozicki, W., Parasi, S.N., Rao, A.R.K., and Tiu, C., *Chem. Eng. Sci.*, **25**, 41 (1970).

73. Varoqui, R., and Dejardin, P., *J. Chem. Phys.*, **66**, 4395 (1977).

74. Cohen, Y., and Metzner, A.B., *Macromolecules*, **15**, 1425 (1982).

75. Rowland, F.W., Bulas, R., Rothstein, E., and Eirich, F.R., *Ind. Eng. Chem.*, **57**, 46 (1965).

76. Rowland, F.W., and Eirich, F.R., *J. Polym Sci.*, *Part A-1*, **4**, 2033 (1966).

77. Anderson, J.L., McKenzie, P.F., and Webber, R.M., *Langmuir*, **7**, 162 (1991).

78. Cohen, Y., and Metzner, A.B., *AIChE Symp. Ser. No. 212*, **78**, 77 (1982).

79. Metzner, A.B., Cohen, Y., and Ranjel-Nafaile, C., *J Non-Newtonian Fluid Mech.*, **5**, 449
    (1979).

80. Tirrell, M., and Malone, M.F., *J. Polym. Sci.*, *Part B*, **15**, 1569 (1977).

81. Vrentas, J.S., and Duda, J.L., *AIChE J.*, **25**, 1 (1979).

82. Scholtan, W., *Makromol. Chem.*, **14**, 169 (1954).

83. Russel, W.B., Saville, D.A., and Schowalter, W.R., *Colloidal Dispersions*, Cambridge
    University Press: Cambridge, 1989.

84. Peterlin, A., *Pure Appl. Chem.*, **12**, 563 (1966).

85. Bird, R.B., Curtiss, C.F., Armstrong, R.C., and Hassager, O., *Dynamics of Polymeric Liquids*,
    Vol. 2, *Kinetic Theory*, 2 nd ed.; Wiley: New York, 1987.

86. Prakash, J.R., and Mashelkar, R.A., *J. Chem. Phys.*, **95**, 3743 (1991).

87. Kirkwood, J.G., and Riseman, J., *J. Chem. Phy.*, **16**, 565 (1948).

88. Öttinger, H.C., *J. Chem. Phys*, **83**, 6535 (1985).

89. Öttinger, H.C., *J. Chem. Phys.*, **90**, 463 (1989).

90. Wedgewood, L.E., *J. Non-Newtonian Fluid Mech.*, **31**, 127 (1989).

91. Prakash, J.R., and Mashelkar, R.A., *J. Rheol.*, **36**, 789 (1992).

92. Aubert, J.H., and Tirrell, M., *J. Chem. Phys.*, **72**, 2694 (1980).

93. Stockmayer, W.H., and Fixman, M., *J. Polym Sci.*, *Part C*, **1**, 137 (1963).

94. Kurata, M., and Tsunashima, Y., *Polymer Handbook*, 3 rd ed., Brandup, J., and Immergut, E.H., eds.; John Wiley and Son Inc.: New York, 1989.

95. Yamagawa, H., *Modern Theory of Polymer Solution*, Harper and Ron Inc.: New York, 1971.

96. Phillies, G.D.J., *Macromolecules*, **28**, 8198 (1995).

97. Dutta, A., and Mashelkar, R.A., *J. Non-Newtonian Fluid Mech.*, **16**, 279 (1984).

98. Ullmann, G.S., Ullmann, K., Lindner, R.M., and Phillies, G.D.J., *J. Phys. Chem.*, **89**, 692 (1985).

99. Ye, X., Tong, P., and Fetters, L.J., *Macromolecules*, **31**, 5785 (1998).

100. Won, J., Onyenemezu, C., Miller, W.G., and Lodge, T.P., *Macromolecules*, **27**, 7389 (1994).

101. Cheng, Y., and Prudhomme, R.K., *Macromolecules*, **35**, 8111 (2002).

102. Lin, T., and Phillies, G.D.J., *J. Phys. Chem.*, **86**, 4073 (1982).

103. Lin, T., and Phillies, G.D.J., *Macromolecules*, **17**, 1686 (1984).

104. Gorti, S., and Ware, B.R., *J. Chem. Phys.*, **83**, 6449 (1985).

105. Langevin, D., and Rondelez, F., *Polymer*, **19**, 875 (1978).

106. Gold, D., Onyenemezu, C., and Miller, W.G., *Macromolecules*, **29**, 5700 (1996).

107. Phillies, G.D.J., *Macromolecules*, **20**, 558 (1987).

108. Phillies, G.D.J., *Macromolecules*, **21**, 3101 (1988).

109. Phillies, G.D.J., *J. Phys. Chem.*, **93**, 5029 (1989).

110. Phillies, G.D.J., and Clomenil, D., *Macromolecules*, **26**, 167 (1993).

111. Chan, P.C.H., and Leal, L.G., *J. Fluid Mech.*, **82**, 549 (1977).

112. Leal, L.G., *J. Non-Newtonian Fluid Mech.*, **5**, 33 (1979).

113. Brunn, P., *Rheol. Acta*, **15**, 40 (1976).

114. Tehrani, M.A., *J. Rheol.*, **40**, 1057 (1996).

115. Douglas, G., Onyenemezu, C., and Miller, W.G., *Macromolecules*, **29**, 5700 (1996).

116. Russo, P.S., Mustafa, M., Cao, T., and Stephens, L.K., *J. Colloid Interface Sci.*, **122**, 120 (1988).

117. Cooper, E.C., Johnson, P., and Donald, A.M., *Polymer*, **32**, 2815 (1991).

118. Prieve, D.C., and Bike, S.G., *Chem. Eng. Comm.*, **55**, 149 (1987).

119. Bike, S.G., and Prieve, D.C., *J. Colloid Interface Sci.*, **136**, 95 (1990).

120. Bike, S.G., and Prieve, D.C., *J. Colloid Interface Sci.*, **154**, 87 (1992).

121. Chun, M.S., Park, O.O., and Yang, S.M., *J. Colloid Interface Sci.*, **161**, 247 (1993).

122. Seo, Y.H., Park, O.O., and Chun, M.S., *J. Chem. Eng. Jpn.*, **29**, 611 (1996).

Vita

Sittipong Amnuaypanich, the eldest son of Supat and Anongnuch Amnuaypanich, was born on June 22, 1972 in Songkhla, Thailand. He received his primary education from Hadyaiwittayalai School where he graduated in 1989. That year, he went to Prince of Songkhla University where he spent four years pursuing a Bachelor degree in Chemical Engineering. Promptly after graduating from Prince of Songkhla University in 1993, he joined Siam Cement Public Company and worked as a production engineer in Saraburi, Thailand. In December 1996, he was granted a scholarship from the Royal Thai Government to pursue a Doctorate degree in Chemical Engineering. In the Fall of 1997, Mr. Amnuaypanich left Thailand and started his graduate study in the Department of Chemical Engineering at Lehigh University. He joined the Emulsion Polymers Institute where he conducted research on particle transport phenomena in capillary hydrodynamic fractionation. He obtained a Masters degree in Chemical Engineering in the Spring of 2000 and continued his Ph.D. study at the same university. After graduating with a Doctor of Philosophy in Chemical Engineering, he will return to Thailand and serve as a lecturer at KhonKaen University.

Reproduced with permission of the copyright owner. Further reproduction prohibited without permission.